Effect of Sample Disturbance in Opalinus Clay Shales

by

Jianyong Pei

B.S., Hydraulic Engineering, Tsinghua University, China (1996)
M.S., Geotechnical Engineering, Tongji University, China (1999)

Submitted to the

Department of Civil and Environmental Engineering
in partial fulfillment of the requirements for the degree of
Master of Science in Civil and Environmental Engineering

at the

MASSACHUSETTS INSTITUTE OF TECHNOLOGY
[February 2004]
September 2003

Signature of Author .....
Department of Civil and Environmental Engineering, August 15, 2003

Certified by .....
Prof. Herbert H. Einstein
Thesis Superviser

Certified by .....
Dr. John T. Germaine
Thesis Superviser

Accepted by .....
Heidi Nepf
Chairman, Departmental Committee on Graduate Studies

Effect of Sample Disturbance in Opalinus Clay Shales

by

Jianyong Pei

Submitted to the
Department of Civil and Environmental Engineering on August 15, 2003
in partial fulfillment of the requirements for the degree of
Master of Science in Civil and Environmental Engineering

ABSTRACT

The sample disturbance problem for different geomaterials is reviewed in this thesis. A general discussion on the disturbance sources and complexities of the disturbance problem is followed by detailed reviews on disturbance mechanisms and effects in soil and rock. This investigation leads to the conclusions that the combination of theoretical and physical modeling is an effective way to study the disturbance problem. Following the discussion of sample disturbance in soil and rock, the main aspects of shale behavior and shale sample disturbance are introduced in order to evaluate the applicability of theoretical and physical modeling in shale. It is shown that the coupled chemical – thermal – poromechanical effects of shale behavior may be a major barrier to a successful application of these modeling methods and to a better handling of sample disturbance.

Thesis Supervisor: Prof. Herbert H. Einstein
Title: Professor of Civil Engineering

Thesis Supervisor: Dr. John T. Germaine
Title: Principle Research Associate

Table of Contents

List of Figures

List of Tables

1. Introduction

This thesis deals with the disposal of radioactive wastes in shale formation in Switzerland. Radioactive substances are widely used in power production, medicine, research and industry. However, the use of radioactive substances produces a substantial amount of nuclear waste each year. During the operation of a nuclear power plant, highly active substances are generated in the fuel elements. The so-called "spent fuel" has to be replaced after a period of around four years in the reactor. For instance, the operation of the nuclear power plants in Switzerland for a 40 year lifetime will produce around 3000t of spent fuel (Geological Problems in Radioactive Waste Isolation: Second Worldwide Review, 1996). These radioactive wastes must be properly disposed so that they won't endanger the environment and people's health.

Disposing the nuclear waste in deep geological repository has been found to be an attractive solution. To ensure that the radioactive waste does not pollute the groundwater, and does not transfer into the groundwater, geological formations with low permeability are attractive for repositories of radioactive waste disposal. Therefore, shale formations have been found to be good candidates for such disposal repository.

Based on the previous investigations made by the Swiss NAGRA (National Cooperative for the Disposal of Radioactive Waste), the Opalinus shale which exists in northern Switzerland is a potential host formation for nuclear wastes. In order to

further assess the suitability of Opalinus shale formation to be the host rock of the waste repository, different in-situ and field tests are necessary to characterize the formation. Among the many parameters characterizing Opalinus clay shale, permeability is probably the most important. However, it has been found that it is extremely hard to measure the in-situ permeability of Opalinus shale or to back figure it from laboratory tests. The reason why laboratory tests do not work well is sampling disturbance. When samples are taken from rock formation, various disturbance effects can be introduced by the sampling process. For example, the existing cracks in the sample may be opened, and new cracks may be created. Therefore, the measured permeability can be much larger than the in-situ permeability.

In view of this fact, NAGRA sponsored this research project to study the sources, mechanisms and effects of sample disturbance in Opalinus shale. This thesis presents a preliminary study on this topic. It summarizes the knowledge on sample disturbance in general (including sample disturbance in soft soil and rock), and provides possible ways of specifically studying sample disturbance in Opalinus shale.

2. Overview of Sample Disturbance

Sampling disturbance is a very important problem, and it has long been a research topic for the geotechnical profession. It is so important because reliable application of any analytical or numerical methods requires reliable parameters, but the parameters of a geomaterial measured in the lab usually deviate from the in-situ parameters due to sample disturbance. Therefore, the ultimate objective of studying the sample disturbance problem is to find a way either to eliminate sampling disturbance, or to back-calculate the in-situ parameters based on the disturbed behavior or state. However, it has also been realized that sample disturbance is a very complex problem, and the ultimate objective may not be achievable. This section will offer an overview of the disturbance problem and current research on it. Before further discussions on this topic, some terms need to be defined, and some concepts need to be clarified.

2.1. Definition of Terms

Geomaterials refer to various natural materials that are involved in geotechnical engineering. Being natural materials, they are quite often multi-phase materials that have many different components. Usually, geomaterials have porous structures. The pores in a geomaterial are often filled with liquid or gas.

The *State* of a sample is a collection of properties that describe the current internal conditions of the sample. To completely define the state of a sample, the

number of necessary properties can be very larger. However, only some of them are important for the problem of sample disturbance. These important properties can be categorized as follows:

- Compositional Properties: This refers to the properties that describe the type, quantity, distribution and geometry of different components of the sample. For example, if a soil sample is composed of the solid, liquid and gas phases, then the compositional properties of this soil sample may include: grain size distribution, pore size distribution, fabric of soil particles, porosity, water and gas content, degree of saturation, void ratio, etc.
- Mechanical Properties: These properties describe the mechanical interactions between the different components of the sample. For a soil sample, the mechanical properties may include: total stresses, effective stresses, true stresses in soil grains, pore liquid pressure, pore gas pressure, etc.

When the sample is located in the ground before any sampling process has been performed, its state is called the *In-situ State*. At its in-situ state, the sample is in balance with its environment. For example, the stress within the sample is in equilibrium with the external load from the surrounding materials; the volume of liquid that flows into the sample in a period of time equals the volume that flows out; the ion concentrations inside the sample equals to the ion concentrations outside of the sample. If the environment of the sample is changed, then this balance will be

disturbed and the state of the sample will be changed. The *Behavior* of a sample is defined as the collection of many different parameters that describe how the state of the sample changes with the variation of its environment.

During the sampling process, the environment of the sample are changed by the sampling operations, the balance is disturbed and the state of the sample is changed. The factors that cause the disturbance are called the *Sources of Disturbance.* The state of the sample after being changed by disturbance is called the *Disturbed State.* Each disturbance source may change the balance in a different way and cause the sample's state to change differently. The change of state caused by a particular disturbance source is called the *Mechanism of Disturbance* of the disturbance source. The *Severity of Disturbance* is defined as the extent to which the in-situ state is changed by the disturbance.

The behavior of a sample also changes with its state. The behavior of the sample after disturbance is called the *Disturbed behavior.* The difference between the disturbed behavior and the in-situ behavior shows how the disturbance changes the behavior of the sample, and this is called the *Effects of Disturbance.*

2.2. General Description of Disturbance Sources

This section will give a step by step description of the sampling process in the most general sense. The possible sources of disturbance will be identified based on this description. It should be noted that the disturbance sources listed here are by no means a complete set. During sampling, many factors may change the state of the

sample, some of which we may not even know. On the other hand, some of the sources listed here may only be applicable when particular conditions are met. These conditions will be pointed out in the following description.

Disturbance starts from the in-situ state of the sample, which is shown schematically in Figure 2.1. As has been said previously, the state of the sample is determined by all the properties that describe the current conditions of the sample.

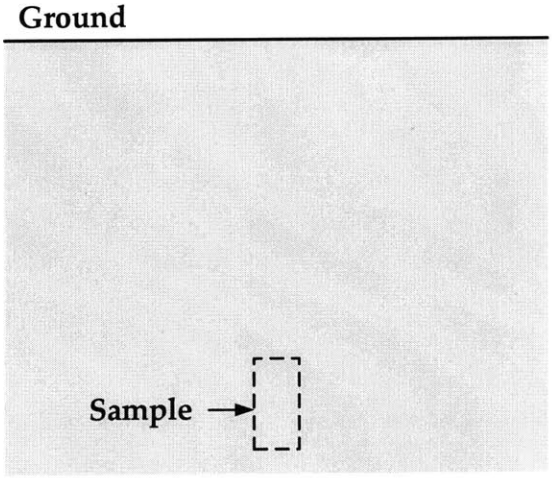

Figure 2.1 The In-situ State of the Sample

2.2.1. Making a Borehole

Usually the geomaterial to be sampled is located at some depth in the ground, as shown in Figure 2.1. Therefore, it is necessary to make a borehole to the elevation of the sample. In essence, this is achieved by breaking and taking the material away. In order to prevent the borehole wall from caving in, a borehole fluid and/or borehole casing are typically used to support the borehole wall. The most frequently used borehole fluid is drilling mud. In rare cases, compressed air may be used as the borehole fluid.

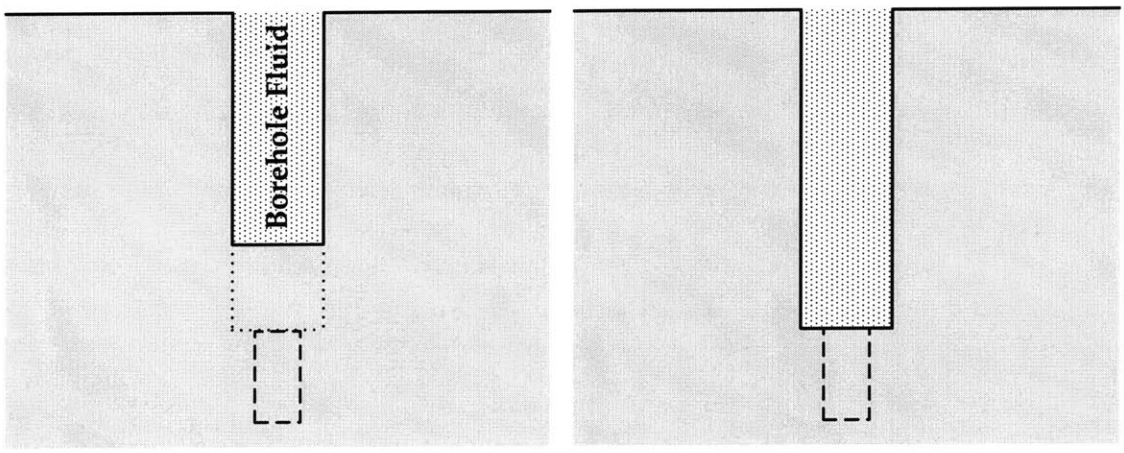

(a) Advancing of Borehole (b) Bottom of Borehole Reaches the Sample

Figure 2.2 Making a Borehole in the Ground

Several possible disturbance sources may be introduced at this step:

1. Drilling Machinery:

- Vibration by Drilling Machine: Drilling machines will cause vibration of the material in the sample.
- Loading by Drilling Machine: When the machine touches the surrounding material, it exerts forces on the material. This load will change the stress field near the contact area. If the sample is within the range of influence, it will be disturbed.
- Heat Generation: During drilling, heat can be generated by the friction between the drilling tool and the material being sampled. The temperature of the sample can be changed.

2. Remove of Original Material

- Contact with Borehole Fluid: As the material on top of the sample is removed, the sample will be in contact with the borehole fluid (Figure 2.2

(b)). This may cause disturbance in the following ways:

- ✧ Stress Change: At the boundary where the sample is in contact with the borehole fluid, the stress will be changed to the pressure of the borehole fluid, which is usually different from the in-situ stress.
- ✧ Temperature Change: The temperature of the borehole fluid is usually not the same as the in-situ temperature. Therefore, the temperature of the sample will be changed by heat conduction.
- ✧ Capillary Effects: This only occurs if the borehole fluid is air, and the sample contains free water. Negative pore pressure can develop at the liquid-air interface.
- ✧ Composition Change: If drilling mud is used as the borehole fluid, the composition of the sample can be changed by pore liquid exchange and mud penetration. Pore liquid exchanged between the mud and the sample is caused by the hydraulic gradient between the mud and the sample. Mud penetration occurs when the pore size of the sample is large enough. If compressed air is used as the borehole fluid, the composition change will mainly be caused by pore liquid evaporation and air entry.
- ✧ Chemical Change: The sample originally is at chemical balance with its surrounding material. When it is in contact with borehole fluid, this balance will be disturbed and chemical reactions may

occur between the sample and the borehole fluid. If drilling mud is used as the borehole fluid, then ion exchange may occur due to the different ion concentrations in drilling mud and in the sample; water migration may occur due to osmotic pressure. If compressed air is used, then oxidation may occur.

- Stress Relief: When the material originally in the borehole is taken away, the wall and the bottom of the borehole are unloaded. The stresses that originally acted on the sample will also be relieved. This unloading may be partly compensated by the pressure of borehole fluid. The stress relief at the wall and bottom of the borehole will cause the stress field around the borehole to change, which also affects the stress state of the sample.

2.2.2. Taking Samples with Samplers

After the borehole is made to the depth of the sample, the sample can then be cut out from the surrounding material and detached from it (Figure 2.3). This is usually achieved by using samplers with suitable cutting devices. Some of the cutting devices may remove the surrounding material (Figure 2.3 (a)). These devices are often used to sample very hard materials. Some of the cutting devices may simply penetrate into the bottom of the borehole, and isolate the sample from the surrounding material. This is usually applied in soft material sampling.

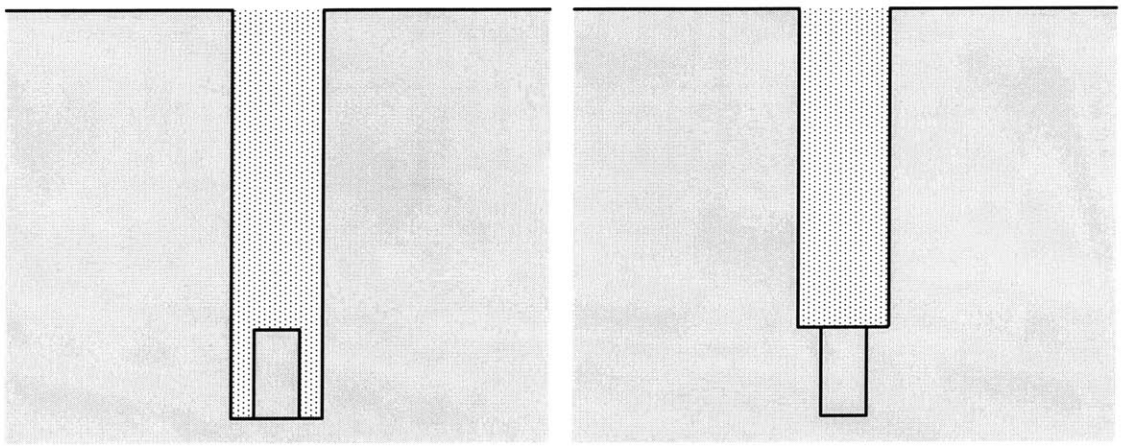

(a) Cut by Removing Material (b) Cut by Displacing Material

Figure 2.3 Cutting out the Sample from the Material Body

During the cutting of the sample, the sample is isolated from the original material surrounding it. The possible disturbance sources during the cutting are:

1. The Cutting Process

The cutting process can be a very important source of disturbance since it is conducted very close to the surface of the sample. The sample might be disturbed in the following ways during the cutting process:

- Vibration: The cutting process may cause vibration in the sample and the surrounding material.
- Loading by Cutting Tools: When the cutting tool touches the side of the sample, it directly exerts forces on the sample surface.
- Heat Generation: The breakage of the surrounding material and the abrasion of the cutting tool may generate heat, which will change the temperature of the sample.
- Contact with Borehole Fluid or Sampler: Depending on the sampling

method, the sample may be in contact with the borehole fluid or the sampler during the cutting process. Again, the possible disturbance may include Stress Change, Temperature Change, Capillary Effects, Composition Change, and Chemical Change. The details of these changes have been listed in Section 2.2.1. When the sample is in contact with the sampler, stress changes in the sample will be mostly affected by the force exerted by the sampler, while the temperature and chemical changes of the sample will be dependent on the temperature and the material of the sampler.

- Stress Relief: If an opening is cut around the sample (Figure 2.3(a)), the stresses on the boundary of the opening will be relieved. Again, this changes the stress field around the opening and affects the stress state of the sample. If no opening is left behind the cutting tool (Figure 2.3(b)), the stresses in the sample will be determined by the force exerted by the sampler (see above).

2. Detaching the Sample

When the sample is cut out, it is then broken at the bottom so that the sample can be detached completely from the native formation. This is usually achieved by applying a torque or an extraction force on the sample. The possible disturbance sources are:

- Torsion or Tension at the Bottom: It is clear that in this process, the bottom

of the sample will be disturbed.

- Forces on the Sample: In order to generate the torsion or tension at the end of the sample, some force must be applied on the sample. This also acts as a possible disturbance source.

2.2.3. Move the Sample to the Ground Surface

When the sample is detached, it will be taken out of the borehole to the ground surface (Figure 2.4).

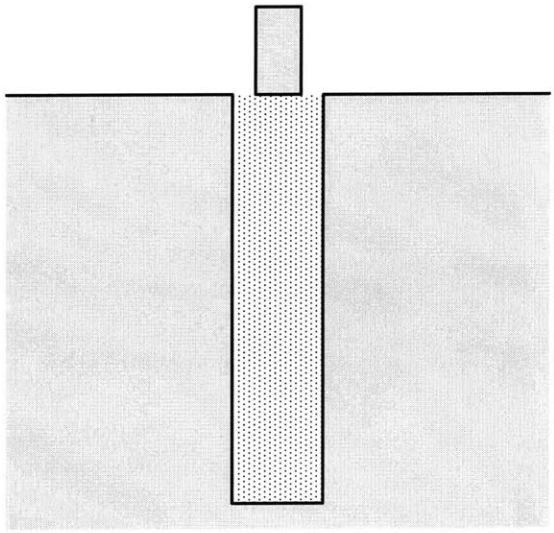

Figure 2.4 Taking the Sample to Ground Surface

During this step, disturbance may occur if the sample is at least partly exposed to the fluid, which is usually the case. The possible sources of disturbances are:

- Contact with Borehole Fluid: The sample is still in contact with the borehole fluid when it is pulled out from the borehole. Therefore, possible disturbances still include: Stress Change, Temperature Change, Capillary

Effects, Composition Change and Chemical Change. However, in this step the sample is rising in the borehole and its depth is constantly changing. The change of depth may affect sample disturbance in the following aspects:

- ✧ Stress Change: When the sample is rising in the borehole, the pressure of borehole fluid becomes smaller and smaller, which means that the sample is experiencing stress relief. This stress relief is very significant when drilling mud is used as the borehole fluid and the borehole is very deep.
- ✧ Temperature Change: Due to geothermal effects, the temperature of borehole fluid may vary with depth. The temperature of the sample thus will also be affected when it is rising in the borehole.
- ✧ Composition Change: In case that drilling mud is used as the borehole fluid, its composition may vary with depth due to gravity. Hence the composition of the sample may be changed differently with decreasing depth. In addition, the amount of mud that penetrates into the sample may decrease as the mud pressure decreases with decreasing depth.
- ✧ Chemical Change: Since the composition of drilling mud may vary with depth, different chemical reactions may occur when the sample is at different depths.

2.2.4. Sample Transportation and Storage

When the samples are taken to the ground, they usually will be put into special containers (or in samplers) and properly sealed. Then they are transported to the laboratory where they will be stored up until they are tested.

The possible sources of disturbance during transportation and storage of the sample are listed below:

- Random Bumping: During the transportation, the sample may be subject to random bumping.
- Temperature Change: During transportation and storage, the temperature of the sample will be affected by the environmental temperature.
- Contact with Air: If the sample is not properly sealed, it may be in contact with air. The sample will then be affected by the properties of the air. The following disturbances are possible:
  - ✧ Stress Change: Where the sample is in contact with the air, the pressure on the sample will be the atmospheric pressure.
  - ✧ Temperature Change: The temperature of the sample will be affected by the air temperature.
  - ✧ Capillary Effects: Negative pore pressure may be generated at the interface of pore liquid and air.
  - ✧ Moisture Loss and Air Entry: The water in the sample may evaporate. When the moisture of the sample is lost, air enters the pores of the sample to occupy the space originally occupied by water.

- ✧ Chemical Change: Chemical reactions may occur between the sample and the air.

- Time Dependent Effects: The state change of the sample caused by the disturbance sources may not be completed immediately. The sample's state will continue to change during the time of storage although the source of disturbance may not be present already.

2.2.5. Sample Preparation

When the samples are ready for different kinds of tests, they must be extruded from the sampler (or other containers) in which they were stored, and be prepared into suitable geometry for the testing apparatus. The possible sources for this step are:

- Stress Relief: During this process, any stresses that were locked in the sample container will be relieved. The pressure that is acted upon the sample will be the atmospheric pressure.

- Cutting of the Sample: The sample must have suitable geometry to fit in the testing apparatus. This is usually done by cutting. For example, soft materials are usually cut by wire saws or cutting rings; hard materials are usually cut by a lathe or a laboratory core drill. The cutting process may disturb the sample through vibration, loading by cutting tools, heat generation, etc (refer to Section 2.2.2).

- Contact with Air: Cutting creates new surfaces on the sample, and the

material on the new surfaces is then in contact with air. Again, Stress Change, Temperature Change, Capillary Effects, Moisture Loss and Air Entry, and Chemical Change may occur. The details have been described in Section 2.2.4.

- Installation of Sample: After cutting, the sample must be installed in the testing apparatus. This installation process can be very complicated for some tests, for example, in triaxial tests. Specific disturbance sources are quite different for different tests. Therefore, the details will not be presented in this general outline.

2.3. Complexity of Sample Disturbance Problem

Based on the definitions of Section 2.1 and the description of Section 2.2, it is evident that sample disturbance is a complex problem with the following characteristics:

1. Disturbances seem to be unavoidable.

The purpose of taking a sample is to put the sample into the testing equipment and measure its behavior. In this process, it is inevitable that the surrounding material of the sample will be removed, and the balance between the sample and its environment will be disturbed. Therefore, sample disturbance seems to be unavoidable.

2. The state of the sample is difficult to determine.

The only way of determining the state of a sample is to measure its properties. However, some of the properties of the sample cannot be easily measured and quantified. In addition, the measurement of one property may introduce disturbances so that other properties are changed. Therefore, obtaining the state of the sample is still a formidable task. It has been said that the in-situ state is the starting point of the state change caused by disturbance. If this starting point is not clearly known, then how the sample's state is changed during the sampling process will be difficult to follow. The mechanism of disturbance is then very difficult to quantify.

3. Characterizing the disturbance sources may be a difficult task.

It is difficult first because the great variety of disturbance sources. This is evident simply by looking at the list of disturbance sources provided in Section 2.2. Besides this variety, many disturbance sources in the list involve large uncertainties. For example, while cutting the sample from its native formation, the cutting device of the sampler is very close to the sample. The disturbance on the sample is then greatly dependent on the operator's skills. When the temperature of the sample is affected by the environmental temperature, the disturbance is clearly dependent on weather conditions. As a result, the disturbance sources involve great uncertainty and it is very difficult to characterize them.

4. The disturbance mechanisms are different for different geomaterials.

Based on the definitions of Section 2.1, the behavior of a sample defines how the state of the sample changes when its environment is changed. Therefore, the change of the sample's state by disturbance is determined by the behavior of the sample. For example, during the stress relief in borehole drilling, if the material being sampled is soil, then the effective stress of the soil sample will be changed. This in turn will cause deformation and strain of the sample. However, if the material being sampled is rock, stress relief may cause the opening and propagation of cracks in the sample. This example clearly shows that for different materials, the mechanisms of disturbance may differ greatly for the same disturbance source. As a result, the understanding of the mechanism of disturbance is restricted by the understanding of the material behavior. However, since geomaterials are mostly multiphase natural materials, our understanding of their behavior is still quite limited. Therefore, a thorough understanding of disturbance mechanisms seems to be impractical.

5. The disturbance mechanisms and effects are always coupled.

According to the general list of disturbance sources in Section 2.2, several disturbance sources often affect the sample's state simultaneously. For example, during borehole drilling, the sample is simultaneously disturbed by temperature changes, chemical reactions, static stress state changes, and dynamic vibration. Given that the geomaterial is usually a porous material, it is then necessary to

understand the coupled porous, thermal, chemical, dynamical behavior of the geomaterial. This seems to be quite difficult with the current analytical and numerical methods.

Based on the discussion above, sample disturbance seems to be unavoidable. The sources of disturbance involve significant uncertainties and the mechanisms of disturbance are very difficult to quantify. Therefore, it is practically impossible to achieve the ultimate objective (eliminate disturbance or back-calculate in-situ behavior from measured behavior) based on our present level of understanding of sampling disturbance.

2.4. Status of Current Research

Realizing that the disturbance problem is so complicated, current research usually introduces various assumptions to simplify it. Based on the complexities described in the previous section, the assumptions are often used to:

- Simplify the characterization of disturbance sources;
- Simplify the behavior of the geomaterial;
- Decouple the simultaneous mechanisms and effects of disturbance sources.

With these simplifications, the mechanisms and effects of disturbance can be understood. The severity of disturbance can then be evaluated, and measures can be proposed to minimize disturbance.

This section outlines the common structure of current research, and describes

how the assumptions or simplifications are introduced. The structure of current research on the disturbance problem can be presented step by step:

Step 1. Understand the disturbance mechanisms, and identify the important disturbance sources.

A general list of possible disturbance sources has been presented in Section 2.2. In order to understand the mechanism of them, the disturbance sources must be characterized, and the state change caused by these disturbance sources can then be predicted based on the behavior of the material being sampled. As has been said, simplifications will be introduced regarding the characterization of disturbance sources and the material behavior. In addition, it is probably necessary to assume that different disturbance sources are not coupled.

With these simplifications, the state changes caused by some of the disturbance sources can be obtained. The mechanisms of other disturbance sources may remain unknown. However, with this understanding of the disturbance mechanisms, it may be possible to judge which disturbance sources account for the majority of the total state change, i.e. which disturbance sources are the most important ones and considering them is sufficient to approximate real disturbance.

Step 2. Understand the effects of disturbance.

Another important aspect of the sample disturbance problem is trying to understand how the behavior of the sample changes with disturbance, i.e. the effects

of disturbance. Based on the definition of Section 2.1, two methods can be used to obtain the disturbance effects:

1) Comparing the disturbed behavior with the in-situ undisturbed behavior. This actually requires the knowledge of the in-situ behavior. Since the in-situ behavior of natural materials is not readily obtained, this method can only be used with artificial materials whose "in-situ" behavior can be controlled.
2) Comparing slightly disturbed behavior with heavily disturbed behavior. In this case, the ability of producing different disturbance severities is necessary. This is only possible for the disturbance sources whose mechanisms are well understood. However, if the disturbance sources under consideration are the important disturbance sources, then the disturbance effects obtained may be a good approximation of the entire disturbance.

Step 3. Proposing measures to minimize the effects of disturbance.

With the knowledge of the mechanisms and effects of various disturbance sources, current research also seeks to propose measures that can be used to minimize the effects of disturbance.

Among all the geomaterials, the one that was most intensely researched regarding sample disturbance is probably soft soil. The disturbance sources in soft

soil sampling are relatively well known. Carefully devised theoretical models have been established and analytical methods have been applied to understand the disturbance mechanisms. Based on the results of these studies, it is even possible to simulate the effects of some disturbance sources in the laboratory. This has led to many recommendations on how to improve the design of the sampler, the sampling procedures and soil testing to minimize the effects of disturbance.

Some research has also been conducted on the sample disturbance in rock. The sampling process in rock has been analyzed and possible disturbance sources have been identified. In order to understand the mechanisms of disturbance in rock, numerical methods have been applied with simplified models. The effects of disturbance on the behavior of rock samples have also been examined, for example, how the P-wave velocity, Uniaxial Compressive Strength, Stiffness change with increasing disturbance. Based on these research results, some measures that can be used to minimize the disturbance effects in rock sampling and testing have been also proposed.

However, it seems that there is very little research performed on the sample disturbance in shale, the objective of this research. Compared with soil and rock, shale is a more intricate material. This is because it has two peculiar characteristics:

1) In terms of mechanical behavior, shale is a transitional material between soil and rock. Thus a thorough understanding of its mechanical behavior will require both Soil Mechanics and Rock Mechanics.
2) Shale usually has high clay mineral content, which makes it chemically

active. Its mechanical properties are significantly affected by various chemical effects. Therefore, the coupled chemical-mechanical effects may have to be considered.

These peculiarities make the problem of sample disturbance in shale even more complicated than in soil and rock. Therefore, a preliminary study is necessary to propose applicable methods to understand the disturbance mechanisms and effects in shale sampling, and to identify the important disturbance sources.

2.5. Outline of This Study

Eventually, one would like to study the sample disturbance problem in shale by following the structure that is described in Section 2.4. However, due to the scarcity of literature in shale sample disturbance, it is necessary to collect information from a wide range of sources. Thus the first step of this preliminary study is an extensive review of the literature of sample disturbance in general. Since shale is considered as a transitional material between soil and rock, it may bear some similarity with both soil and rock. As a result, the papers on the sample disturbance problem in soil and rock constitute an important part of the literature review.

In order to obtain an elementary understanding of the behavior of shale, technical reports from Mont Terri Project were reviewed, together with some past research performed at MIT. In addition, papers from the domain of borehole stability were also reviewed to understand the coupled chemical-mechanical behavior of shale.

Based on the behavior of shale and the general list of disturbance sources in Section 2.2, general predictions are made on the disturbance mechanisms in shale sampling. Also, rigorous methods that can be used to understand the disturbance mechanisms and effects in shale are proposed based on the information collected from soil and rock sampling.

2.6. Structure of the Thesis

This thesis will cover the information of sample disturbance in soil, in rock, and what we think is important in shale. For each of these geomaterials, we try to follow the structure presented in Section 2.4 but mostly focus on Step 1 and Step 2. Specifically, this thesis contains:

- Review of Sampling Disturbance in Soil:
  - ✧ Section 3 describes the disturbance sources in soil sampling and their mechanisms (Step 1 of Section 2.4). This section focuses on how disturbance changes the compositional properties and the mechanical properties of soil samples. Based on the understanding of disturbance mechanisms, tube sampling is found to be an important source of disturbance in soil sampling.
  - ✧ Section 4 presents the effects of disturbance on the behavior of soil samples concentrating on the mechanism of tube sampling disturbance (Step 2). Some of the methods that can be used to evaluate the severity of disturbance are also discussed.

- ✧ Section 5 describes a simple soil model, and shows how the mechanisms and effects of disturbance can be predicted by this simple soil model (both Step 1 and Step 2 of Section 2.4). Again, this analysis assumes that tube sampling is the only disturbance source.

- Review of Sampling Disturbance in Rock:
  - ✧ Section 6 first describes the sampling methods that are used in rock. The mechanisms of disturbances are then discussed with a numerical model. Numerical modeling is applied to help quantify the disturbance mechanisms. According to the results of numerical modeling, it is found that stress relief is an important disturbance source (Step 1). The mechanisms of stress relief indicate that deeper lying samples should be subject to more severe disturbance in a uniform rock formation, which is confirmed by the results of a research project involving laboratory and field testing (Step 2).

- Preliminary Research of Sampling Disturbance in Shale:
  - ✧ Section 7 of this thesis first describes shale behavior by comparing it with the behavior of soil and rock. Based on the behavior of shale and observations on shale sampling, predictions are made on the disturbance mechanisms in shale.
  - ✧ Section 8 summarizes the methodology that was used to understand disturbance mechanisms and effects in soil and rock is then summarized. Suggestions on how this methodology can be applied to

study shale sample disturbance are proposed.

3. Mechanism of Disturbance in Soil Sampling

This and the following several sections (Section 3, 4, and 5) will focus on the sample disturbance problem in soil. Since taking samples of sand without major disturbance is impossible, these sections will mostly focus on the sampling of soft clay. Hence the term soil in these sections will refer to soft clay if not otherwise specified. According to Leroueil and Vaughan (1990), the behavior of soil is only dependent on its fabric and stress history. Samples of soil are usually taken by tube sampling because of the low strength of soil.

According to the structure presented in Section 2.4, the first and most fundamental step in the study of the disturbance problem is to identify disturbance sources and understand their mechanisms. A general description of disturbance sources in sampling geomaterials has been given in Section 2.2, which also covers the disturbance sources in soil sampling. This section describes how these disturbance sources change the state of the soil. For each sampling procedure, the composition changes and the mechanical property changes will be discussed. The order in which these two types of state changes are described varies since sometimes one must be introduced first in order to understand the other.

Several points need to be noted before further discussion:

- The sampling process can be considered as undrained process if it is performed very quickly. This is because we are mostly focused on the

sampling of soft clay. With the very low permeability of clay, the sampling processes that are finished in minutes or hours are essentially undrained.

- It is practically impossible to discuss the change of all the composition and mechanical properties of the soil sample. Therefore, the following discussion only focuses on the most important properties of soil. For example, the void ratio, water content, and effective stresses.

The starting point of all the state changes is the in-situ state of the sample, which will be introduced first.

3.1. In-situ State of Soil

Before any sampling is performed, a soil element in the ground is in its intact state or in-situ state (Figure 3.1). The in-situ state of the sample is determined by the deposition history and loading history of the soil formation.

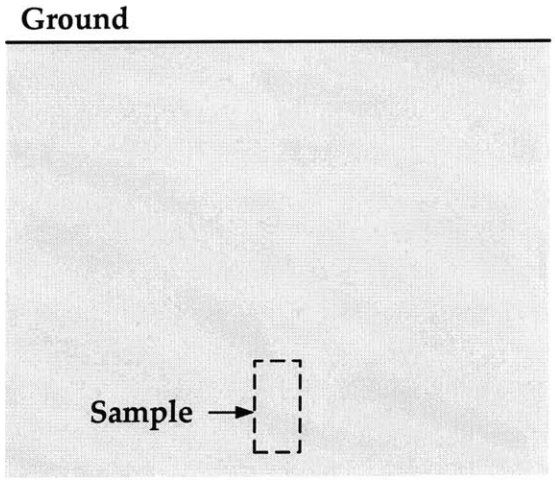

Figure 3.1 The In-situ State of the Sample

Among all the in-situ properties of the sample, the most important yet intricate one is the in-situ stress state. Suppose a soil element is subject to the in-situ

total stresses σ_{h0} and σ_{v0} (Figure 3.2). If we denote the in-situ pore pressure to be u_0, the effective stresses can be obtained by the effective stress principle:

$$\sigma'_{v0} = \sigma_{v0} - u_0; \sigma'_{h0} = \sigma_{h0} - u_0$$

It follows that if the total stress state is isotropic, then the effective stress must also be isotropic, and vice versa.

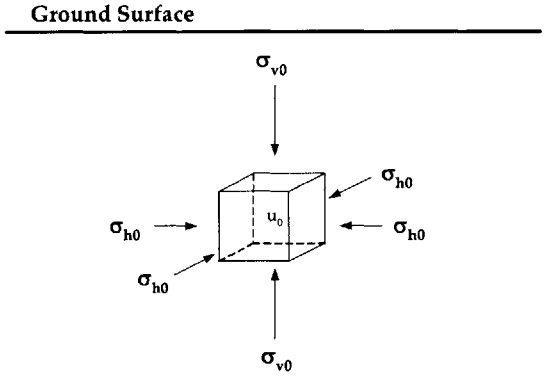

Figure 3.2 In-situ Stress State (Total Stress)

Due to the depositional characteristics of natural soil, usually the vertical stress σ_{v0} is a principal stress. The other two principal stresses are in the horizontal direction and usually have the same magnitude σ_{h0}. Therefore, any horizontal direction is also a principal direction and this stress state is axi-symmetric. This property of soil's stress state is very important since it makes it possible to model the behavior of soils with standard triaxial tests. According to the Effective Stress Principle, these statements are also true for effective stress σ'_{v0} and σ'_{h0}.

The vertical effective stress σ'_{v0} is imposed on the soil element by the overlying deposits. At the depth of the soil element, σ'_{v0} is usually uniformly distributed on a large area and the deformation of the element is restricted to the vertical direction with no lateral movement. In nature, the deposition goes on very

slowly and the soil element is compressed vertically without generating any excessive pore pressure. Therefore, the one dimensional compression of the soil element is also called one dimensional consolidation.

In one-dimensional consolidation, the ratio between the horizontal effective stress and the vertical effective stress is defined as K_0:

$$K_0 = \sigma'_{h0}/\sigma'_{v0}$$

The one-dimensional consolidation is also called "K_0 consolidation". It has been found that during one-dimensional consolidation, if σ'_{v0} increases monotonically, K_0 is roughly constant and the soil element is said to be "normally consolidated". The value of normally consolidated K_0 is different for different soil types but usually is less than 1. It ranges from 0.4 for low plasticity clayey silt to 0.7 for plastic clay.

If for some reason, e.g. erosion of overlying soil, σ'_{v0} is decreased, the element will extend or swell in the vertical direction. This swelling is still one-dimensional and it is termed "one dimensional swelling" or "K_0 swelling". The soil element is then called to be "over-consolidated". The ratio between the past maximum vertical effective stress σ'_p and the current vertical effective stress σ'_{v0} is defined as the Over Consolidation Ratio (OCR):

$$OCR = \sigma'_p/\sigma'_{v0}$$

σ'_p is often called "pre-consolidation pressure". During this unloading process, it is found that the rate of decrease of horizontal effective stresses is smaller than that of the vertical effective stresses, which means that K_0 value increases during swelling. Eventually, σ'_{v0} may become smaller than σ'_{h0} and K_0 becomes larger than 1 for

heavily over-consolidated soil.

It is apparent that the in-situ stress state is isotropic if $K_0 = 1$. This case is rare and the in-situ stress state is anisotropic for most natural deposits.

3.2. Making a Borehole

Before the sample located at a certain depth in the ground can be taken, a borehole must be made (Figure 3.3). Since the strength of soil is small, drilling mud is usually used as the borehole fluid to increase borehole stability. Therefore, the following description will assume that drilling mud is used as the borehole fluid. In Section 2.2.1, the known disturbance sources in borehole drilling have been listed. The state of the soil will be changed by these disturbance sources, and the changes are described in this section.

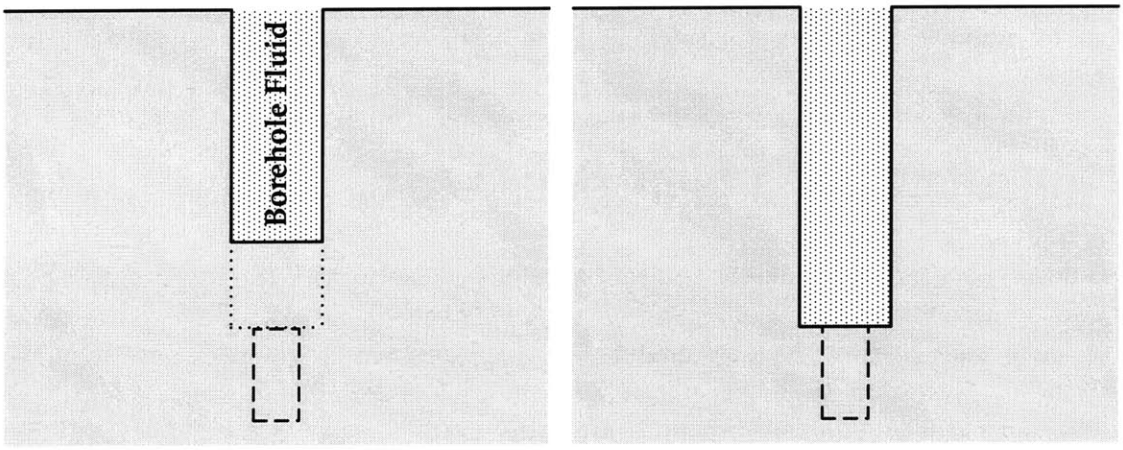

(a) Advancing of Borehole (b) Bottom of Borehole Reaches the Sample

Figure 3.3 Making a Borehole in the Ground

3.2.1. Change of Mechanical Properties

According to the definitions in Section 2.2, the mechanical properties of the

sample include total stresses, effective stresses, pore pressure, etc. These mechanical properties of soil are prone to change during the borehole drilling process. These changes may include:

1. The vibration of the drilling machine can cause excess pore pressure in the surrounding soil. The amount of excess pressure varies with the in-situ state of soil. For normally and slightly over-consolidated soil, the pore pressure may be increased. If total stresses remain unchanged, then the effective stress will be decreased. In addition, when the drilling machine is in contact with the wall or the bottom of the borehole, it exerts forces on the soil and directly changes the effective stresses and the pore pressure of the soil.
2. It has been shown that the temperature of the sample may be changed by the friction between the drilling bit and the soil, and by the temperature difference between the drilling mud and the sample. Since the thermal expansion factors of the soil matrix and the pore liquid are usually different, they have different thermal strains under the same amount of temperature change. As a result, excessive pore pressure may be generated and the effective stresses are changed.
3. When the soil above the sample is removed, the stresses on the wall and bottom of the borehole are relieved. With the presence of the drilling mud, the pressure on the wall and bottom of the borehole will finally become the mud pressure. Since the mud pressure is usually smaller than the

in-situ stress, the net effect of the stress change would still be a relief of stresses.

It has been found that stress relief may considerably change the effective stress of the soil sample. Therefore, the rest of this section will mainly focus on the quantification of the stress relief mechanism.

Since the soil sample is at the bottom of the borehole (Figure 2.2 (b)), the effect of stress relief will be the reduction of its vertical total stress σ_v. For normally and slightly over-consolidated soil, the in-situ vertical stress σ_v is larger than the in-situ horizontal stress σ_h. Therefore, decreasing the vertical total stress will reduce the deviatoric stress the sample is subjected to. The stress state of the sample then gradually approaches the $K_0 = 1$ line and may finally cross it. In order to quantify the effective stress change by this deviatoric total stress relief, Ladd and Lambe (1963) proposed the Perfect Sampling Approach (PSA) to conceptually represent this process.

3.2.1.1. Perfect Sampling Approach

PSA assumes that deviatoric stress relief is an undrained process, and that during deviatoric stress relief the minor principal total stress is kept constant while the major principle total stress decreases monotonically until the isotropic stress state is reached. For normally and slightly over-consolidated soil samples, σ_v is decreased until $\sigma_h = \sigma_v$ (Figure 3.4). Since this is an undrained process, the magnitudes of effective stresses are dependent on the pore pressure generated.

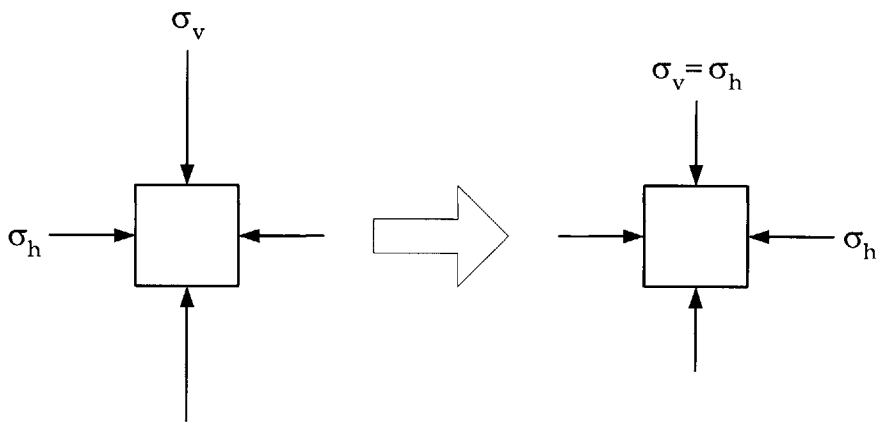

Figure 3.4 Assumption of Stress Change of Perfect Sampling Approach

If we suppose that the problem of borehole drilling can be treated as an axi-symmetrical problem, then a soil element located beneath the bottom of the borehole but on the axis of it also has an axi-symmetric stress state. In this case, the effective stress change of the soil element due to borehole drilling can be simulated in triaxial tests. However, before the simulation of deviatoric total stress relief can be described, some basic knowledge of triaxial tests and the interpretation of the test results must be introduced.

3.2.1.2. Triaxial Test and Interpretation

Triaxial tests are very widely used in the simulation of sample disturbance. This section offers a brief introduction of the apparatus and interpretation of triaxial tests, which is very important to understand the results of simulation. A typical triaxial cell is shown in Figure 3.5.

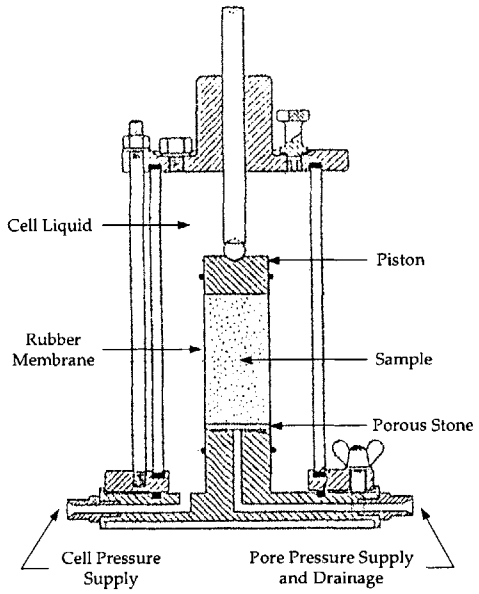

Figure 3.5 illustration of a Typical Triaxial Cell

The soil sample in triaxial tests is usually cylindrical. It is put on the pedestal above a porous stone. A piston is in contact with the sample and exerts the total axial stress σ_a on the sample. The sample is sealed by a rubber membrane that separates the liquid system of the sample from the liquid in the cell. During the test, the cell is filled with cell liquid. The cell liquid is pressurized so that the sample is acted upon by axi-symmetric horizontal pressure. This pressure is the total radial stress σ_r. Meanwhile, the pore pressure u in the sample can be controlled or measured.

It is clear that the radial pressure σ_r can be used to simulate the total horizontal stress σ_h, and the axial pressure σ_a can be used to simulate the total vertical stress σ_v. Correspondingly, the axial and radial effective stresses are obtained by:

$$\sigma'_a = \sigma_a - u;\ \sigma'_r = \sigma_r - u$$

Two quantities are defined for an axi-symmetric stress state, namely p′ and q:

$$p' = (\sigma'_a + \sigma'_r)/2;\ q = (\sigma'_a - \sigma'_r)/2$$

p′ and q can also be expressed in terms of vertical and horizontal effective stress:

$$p' = (\sigma'_v + \sigma'_h)/2;\ q = (\sigma'_v - \sigma'_h)/2$$

It can be seen that p′ is related to the magnitude of the true mean effective stress p'_m, which is defined as:

$$p'_m = (\sigma'_a + 2\sigma'_r)/3$$

Since p′ is very widely used, it is called "mean effective stress", and p'_m is called "true mean effective stress" to show the difference. The value of q stands for the magnitude of deviatoric stress.

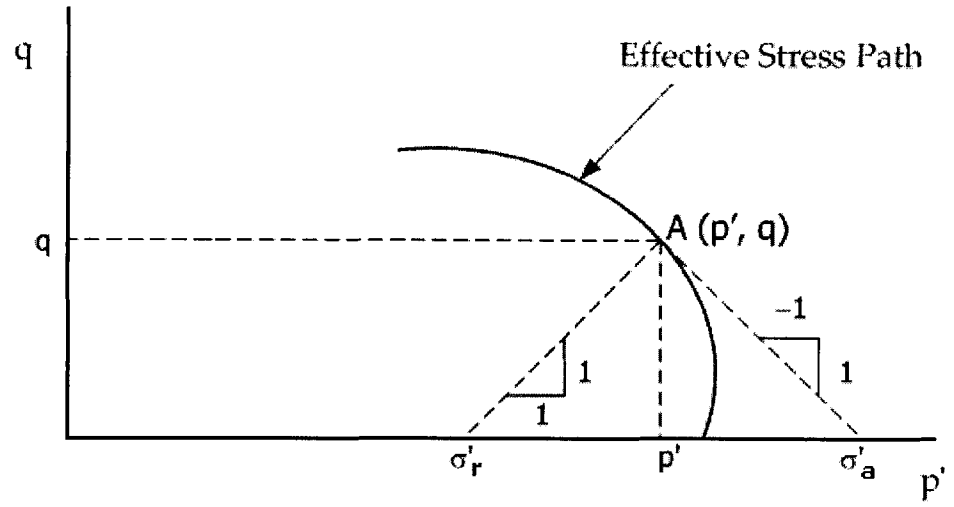

Figure 3.6 Plotting Effective Stress State in p' – q Space

A certain effective stress state (σ'_a, σ'_r) in a triaxial test corresponds to a point (p′, q) in the p′ – q stress space, for example, Point A in Figure 3.6. With the values of σ'_a and σ'_r, the values of p′ and q are readily obtained and Point A can be located. If only p′ and q are known for Point A, the σ'_a and σ'_r values can be obtained by drawing two lines from Point A with the slope of 1 and –1 respectively as shown in

Figure 3.6.

The results of triaxial tests are often shown in a $p' - q$ plot rather than in a $\sigma'_a - \sigma'_r$ plot. During a triaxial test, the effective stress state of a sample is constantly changing. The trace of corresponding (p', q) usually forms a curve in $p' - q$ stress space, which is called the "effective stress path". The curve shown in Figure 3.6 is an effective stress path starting from an isotropic stress state where $q = 0$ and $\sigma'_a = \sigma'_r$.

3.2.1.3. Simulation of PSA with Triaxial Tests

To simulate the deviatoric stress relief assumed by the PSA with a triaxial test, a soil specimen can be installed in the triaxial cell with certain amount of deviatoric stress imposed on it. The drainage boundary must be closed in order to simulate the undrained behavior. This state of the sample is defined as the "intact state". The deviatoric stress is then decreased by either decreasing σ'_r or σ'_a, whichever is larger, until they are equal to each other.

The total stresses and pore water pressure in the sample can be recorded during this process, so that the effective stress path of the sample can be obtained. The effective stresses in the sample after deviatoric stress relief can be compared with the effective stresses of the "intact state", and the change of effective stresses can be obtained. By performing this simulation, it has been found that the change of effective stresses caused by deviatoric stress relief is dependent on both OCR and the plasticity of the soil.

1. Effect of OCR on Effective Stress Path

The deviatoric stress relief has been simulated with triaxial tests on samples of a reconstituted low plasticity clay, the Lower Cromer Till, with different OCR (Hight, 2001). The results are shown in Figure 3.7, where σ'_{ac} stands for the axial effective stress when the specimen is normally consolidated (OCR = 1).

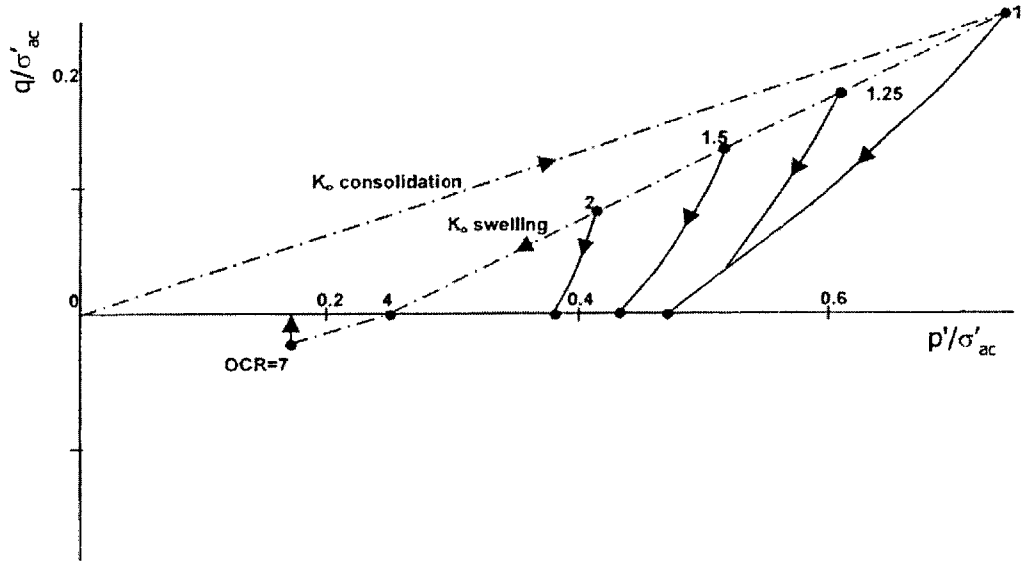

Figure 3.7 Effective Stress Paths Perfect Sampling Process vs. OCR (Hight, 2001)

Normally consolidated samples whose stress states are located on the K_0 consolidation line are first unloaded along the K_0 swelling line to generate different OCRs, which are marked along the swelling line. The deviatoric stress q is then relieved to zero. Figure 3.7 shows the effective stress paths followed by these samples during the perfect sampling process.

It can be seen that when the soil is normally or slightly over-consolidated, the relief of deviatoric stress causes the mean effective stress p′ to decrease from the K_0 stress state. With increasing OCR, the decrease of mean effective stress gets smaller.

For heavily over-consolidated samples, deviatoric stress relief causes a slight increase of the mean effective stress. For the soil tested (Lower Cromer Till), OCR = 4 separates the behavior with decreasing p′ from that with increasing p′. This value may be different for other soils.

2. Effect of Plasticity Index on Effective Stress Path

The effective stress path that a soil element follows during deviatoric stress relief is also dependent on its plasticity, as shown in Figure 3.8 (for normally consolidated or slightly over-consolidated soils). The deviatoric stress relief is simulated in triaxial tests on samples with different plasticity, and the corresponding effective stress paths are plotted in Figure 3.8.

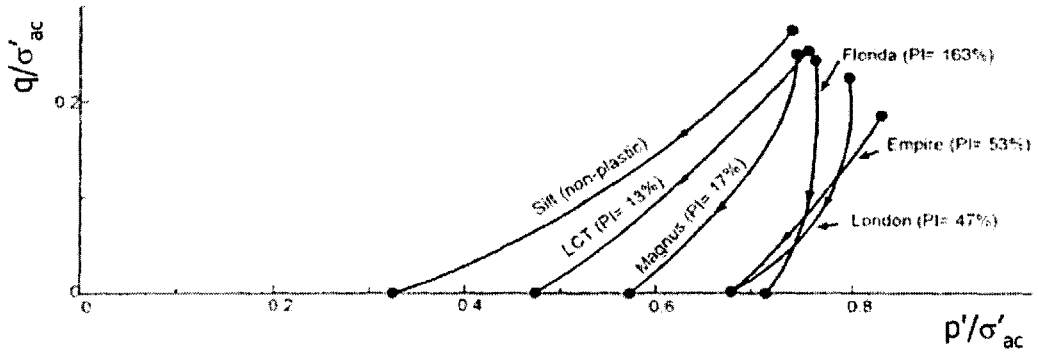

Figure 3.8 Effective Stress Change vs. Plasticity (Hight, 2001)

It is clear that the mean effective stresses for all the samples are decreased by deviatoric stress relief since all of them are normally or slightly over-consolidated. Soils with smaller plasticity have a larger decrease of the mean effective stress than soils with high plasticity. Therefore, after deviatoric stress relief the decrease of the mean effective stress in soils with high plasticity index is smaller.

From what has been said, we can see that the deviatoric stress relief assumed in the PSA can be simulated in laboratory tests. The change of effective stress during deviatoric stress relief can be quantified and better understood. Although PSA simplifies the real situation, the trends it predicts are reliable.

The above discussion about stress relief assumes that $\sigma_v > \sigma_h$ in the in-situ state of the sample, i.e. the sample is normally or slightly over-consolidated. For soil elements that are heavily over-consolidated, the horizontal stress may originally be larger than the vertical stress (as shown in Section 3.1). In this case, decreasing the vertical stress actually increases the deviatoric stress and the sample is sheared. According to soil mechanics, negative pore pressure is generated and the effective stress increases in heavily over-consolidated soil. In this case, PSA cannot be used since it only considers deviatoric stress relief.

3.2.2. Change of Composition

Based on the definitions of Section 2.1, the composition properties of soil include the void ratio, water content, fabric etc. Disturbance also changes these properties.

1. The vibration of the drilling machine can change the fabric of soil. For example, soil particles that are originally loosely packed may change their arrangement to become tightly packed. Since soil is a soft material, when it is loaded by the drilling machine excessive deformation will occur, which clearly changes the soil's composition properties.

2. The composition change of a soil sample is also caused by the pore liquid exchange between the sample and the drilling mud. The amount of liquid exchange is dependent on the hydraulic gradient in the soil sample and in the mud. Drilling mud penetration may occur if the pore size of the sample is large enough. Hence, the amount of mud penetration depends on the mud pressure and the pore size of the sample.

3. The composition of the soil sample may also be changed by various chemical effects. For a soil sample, the drilling mud is an alien material. When the sample is in contact with the drilling mud, chemical reactions may occur between the sample and the mud. For example, if the ion concentration of the liquid in the soil is not the same as that in the liquid of the drilling mud, ion exchange may occur. Water migration may occur due to the osmotic pressure. If the soil sample contains expansive clay minerals, then the sample may expand when the minerals are hydrated. In this case, the water content and void ratio of the sample will increase.

3.3. Tube Sampling

Since the strength of soil is usually small, the samples of soil are usually taken by tube samplers. A tube sampler is pushed into the bottom of the borehole to obtain a sample (Figure 3.9).

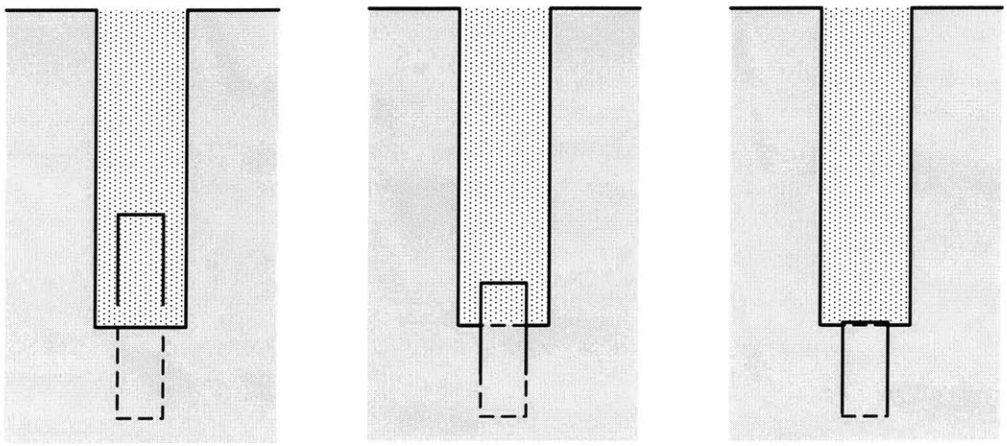

Figure 3.9 Taking Soil Sample with Tube Sampler

3.3.1. Change of Composition Properties

During the process of tube penetration and retrieving, very complex forces are exerted by the tube on the soil. As a result, very complex fabric distortion may take place. However, since the tube penetration process is performed very quickly, it can be considered an undrained process. Therefore, no change of void ratio and water content occurs during tube penetration.

Following the work of Hvorslev (1949), the fabric changes of soil samples can be described by the illustration in Figure 3.10.

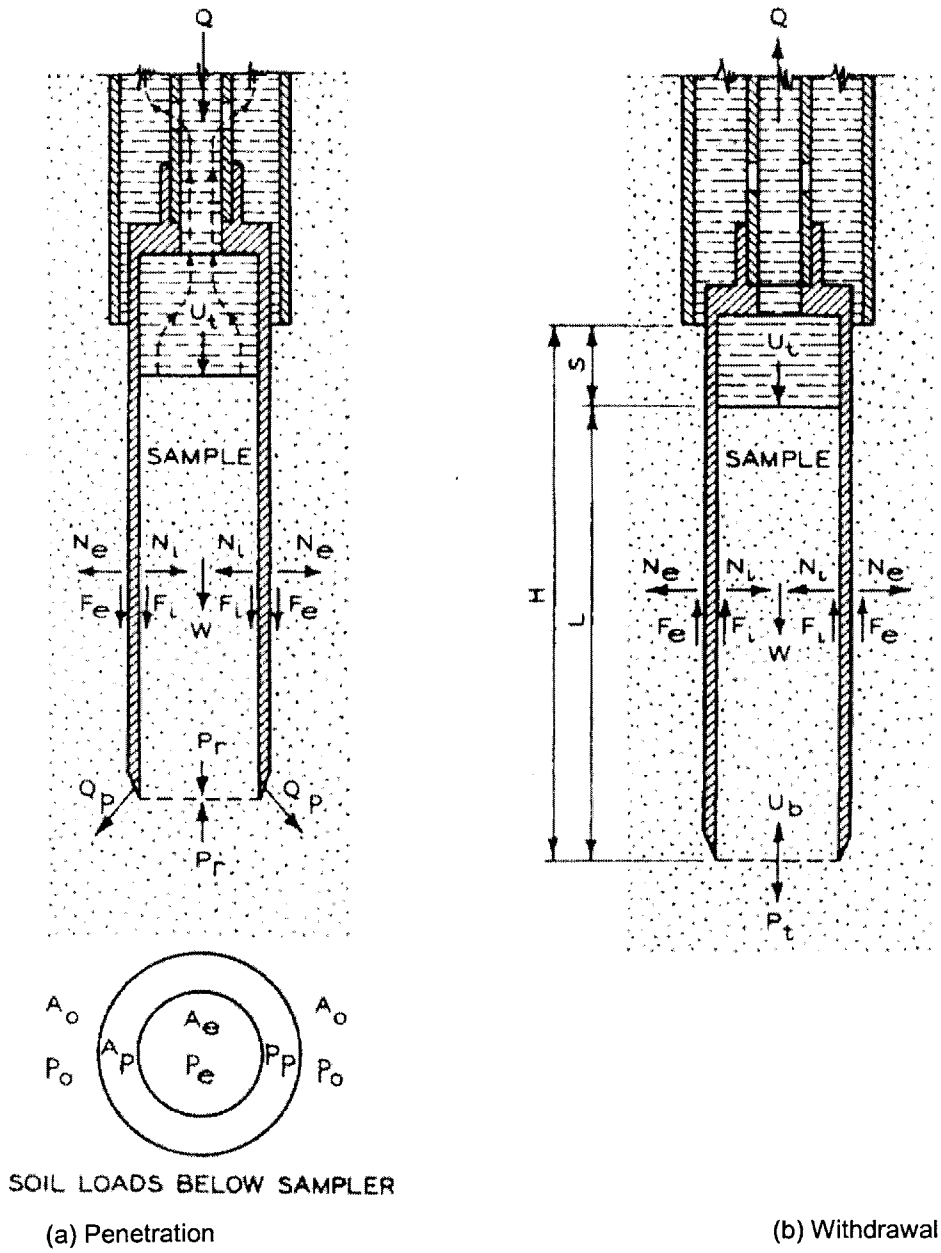

Figure 3.10 Interaction between Tube and Soil (Hvorslev, 1949)

According to Figure 3.10 (a), the sampler wall exerts forces on the soil during penetration, specifically the inner and outer normal force N_i, N_e and the inner and outer friction force F_i, F_e. The soil inside the sampler is also subject to the pressure of drilling fluid U_t on the top, the resistance P_r from the soil below, and its own weight W. During tube driving, the forces on the soil below the cutting edge and the areas

they act on are shown in the lower half of Figure 3.10 (a). P_e is the pressure on area A_e due to the reaction force P_r. P_p which acts on the ring area A_p is due to the pushing force Q_p. Finally, P_0 is the overburden pressure exerted by the overlying soil, which is the in-situ vertical effective stress.

At the beginning of penetration, the sample length inside the sampler L is small. The weight of sample W and the internal friction F_i are also small. Therefore, P_r and P_e must be small. However, since the cutting shoe is trying to displace the soil below it, P_p is generally large. Chances are that some soil under the cutting shoe is squeezed inside, which is called the entrance of excess soil. Figure 3.11 shows a picture of the fabric distortion on soils originally have horizontal thin layers.

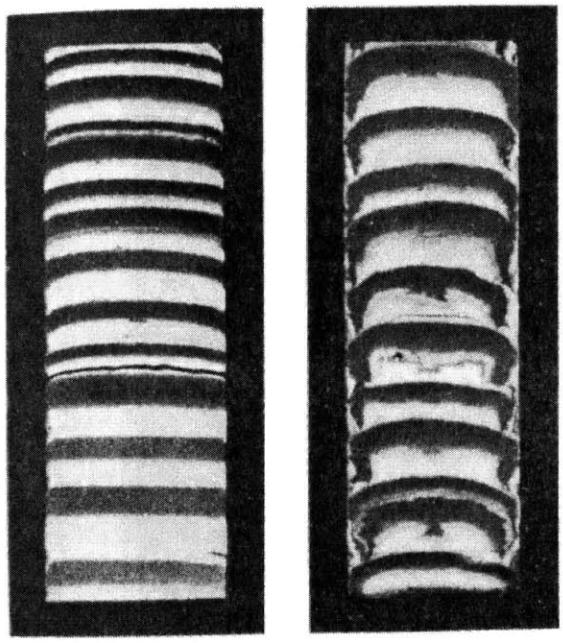

Figure 3.11 Fabric Distortion Caused by Entrance of Excess Soil (Hvorslev, 1949)

As more soil enters the sampler, P_e becomes larger and finally it reaches equilibrium with P_p. No entrance of excess soil occurs. At the end of sampling, W

and F_i may be very large to cause P_e to exceed P_p. The soil layers below the sampler will be compressed and deflected downward. This is called overdriving, and examples are shown in Figure 3.12 (a). In extreme cases when P_e exceeds the bearing capacity of soil, a permanent cone may form below the sampler, as shown in Figure 3.12 (b).

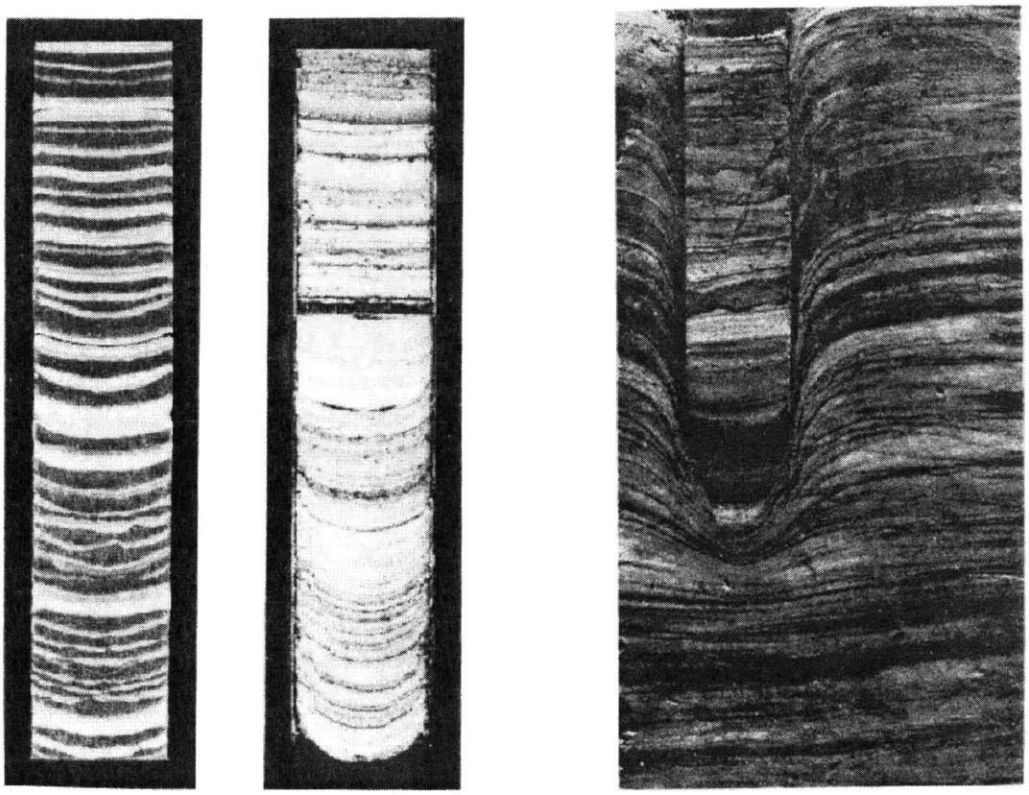

(a) Deflection of Soil Layers (b) Forming of Cone

Figure 3.12 Fabric Distortion Caused by Overdriving (Hvorslev, 1949)

The sample inside the sampler is subject to the inner friction F_i between the sampler wall and its boundary which may also cause fabric distortion of soil. Some examples are shown in Figure 3.13. The friction the soil sample is subject to can be so large that the periphery of the sample may be sheared to failure. To reduce this friction, most samplers are designed with an internal clearance and a very smooth

internal liner. It is clear that the internal clearance must not be too large to avoid excessive swelling of the sample.

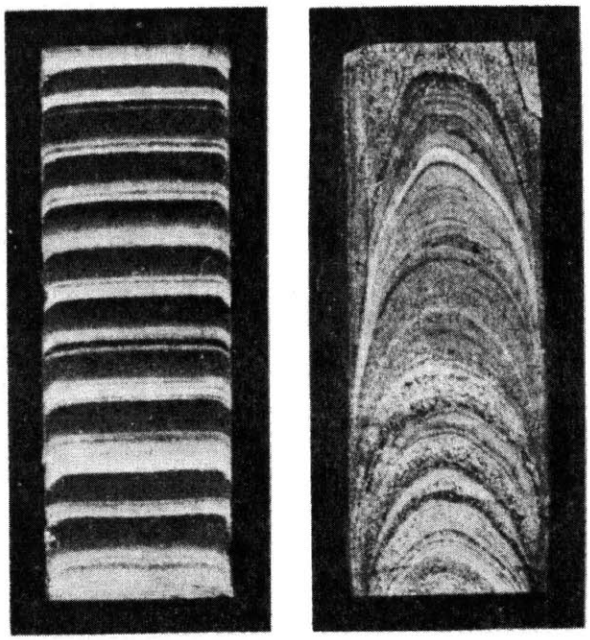

Figure 3.13 Fabric Distortion Caused by Internal Friction (Hvorslev, 1949)

When the sample is detached from the underlying soil, it is important that the sample be retained inside the tube. However, cohesion at the bottom of the sample may prevent the sample from being removed. Suction may also be generated when the sample is detached from the soil. These forces are denoted by force P_t in Figure 3.10 (b), and they must be overcome for the sample to be retrieved. On the other hand, the inner wall friction F_i is reversed during sampler withdrawal. There is also water or air pressure at the bottom of sample, which is denoted by U_b. When the force $F_i + U_b$ is large enough to overcome the force $U_t + W + P_t$, the bottom of the sample can be broken and the sample can be retrieved. Therefore, during sample retrieving a large internal friction F_i is desired in order to retain the sample. This is in

contrast to the requirement of a small internal friction during tube penetration. In practice, the operator always leaves the tube in the ground for several minutes after full penetration. This allows the sample to swell and in contact with the internal wall of the sampler to increase the friction.

As a result, during the sample detachment, the periphery of the sample is sheared in the reverse direction, and the bottom of the sample is subject to tension. Both of them may cause fabric change of the sample.

3.3.2. Change of Mechanical Properties

The forces exerted by the tube on the soil also change its mechanical properties. This section will focus on how the effective stress of the sample is changed by tube penetration.

It is well known that Baligh's Ideal Sampling Approach offers insight to understand the tube sampling process. With this approach, the strains of the sample that are caused by tube penetration can be quantified. This is a major improvement since it enables us to either simulate the effects of tube sampling in the laboratory or by numerical methods given a suitable soil model. The changes in effective stress can thus be obtained.

3.3.2.1. Ideal Sampling Approach

Due to the cutting of soil by the tip of the tube, and the friction caused by the wall of the tube, the soil sample is subject to very complicated stress boundary

conditions during the tube penetration. However, this problem can be considered as axi-symmetric. The possible deformation can be caused by the tubed penetration are shown in Figure 3.14:

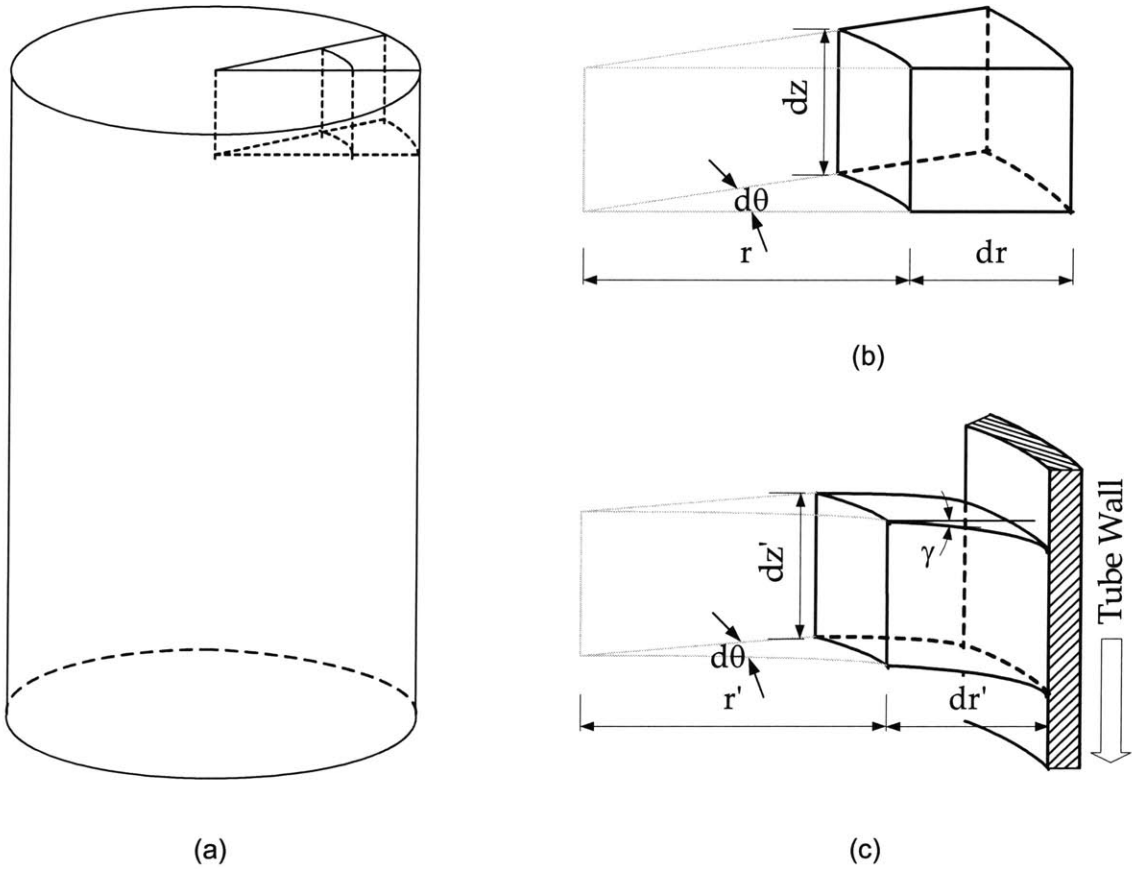

Figure 3.14 Possible Strains Caused by Tube Penetration

Figure 3.14 (a) shows the sketch of a soil sample. One element of it is taken out to show the different strain components in Figure 3.14 (b) and (c). Figure 3.14 (b) shows the original geometry of the element. When the tube penetrates the soil next to the element, the shape of the element is distorted, which is shown in Figure 3.14 (c). Since this is an axi-symmetrical problem, there are four possible strain components:

- Radial strain $\varepsilon_{rr} = \dfrac{dr - dr'}{dr}$;

- Tangential strain $\varepsilon_{\theta\theta} = \dfrac{rd\theta - r'd\theta}{rd\theta} = \dfrac{r - r'}{r}$
- Shear strain $\varepsilon_{rz} = \dfrac{1}{2}\gamma$
- Vertical strain $\varepsilon_{zz} = \dfrac{dz - dz'}{dz}$

With the Strain Path Method developed by Baligh (1985), the Ideal Sampling Approach is able to quantify the strain field around the tip of the tube. In the analysis of the ISA, the relative movement of soil to tube during tube penetration is equivalent to a uniform incompressible, inviscid, irrotational fluid flow. Therefore, the analysis is applicable to soft clay that is (Clayton et al, 1998):

- Saturated and undrained
- Homogeneous and isotropic
- With no shear strength

The geometry of the cutting edge of the sampler is modeled by a rounded tip, which is called a Simple Sampler (S-sampler). The penetration of the sampler is modeled by superimposing a single ring source on the soil flow.

For a sampler with external diameter (B) to wall thickness (t) ratio B/t = 40, the strain field in the surrounding soil during tube penetration can be summarized as shown in Figure 3.15, where the four strain components are shown:

(a) radial strain ε_{rr};

(b) tangential strain $\varepsilon_{\theta\theta}$;

(c) shear strain ε_{rz};

(d) vertical strain ε_{zz} (or axial strain since the axis direction of the sampler is vertical).

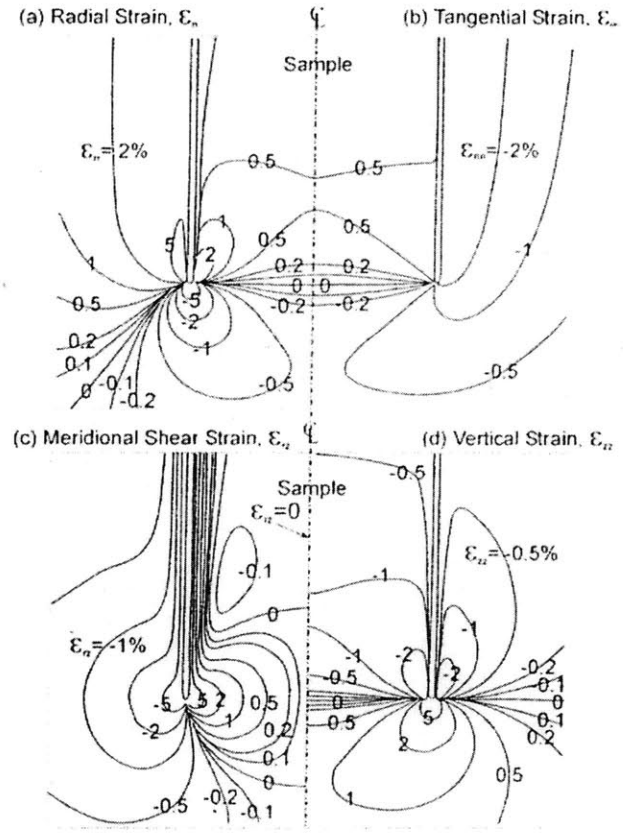

Figure 3.15 Strain Patterns at the Tip of Sampler (Baligh, 1987)
(a) Radial Strain ε_{rr} (b) Tangential Strain $\varepsilon_{\theta\theta}$ (c) Shear strain ε_{rz} (d) Vertical (Axial) Strain ε_{zz}

Clearly, large strains and strain gradients exist at the periphery of the sample. In the central part, the magnitudes of strains are smaller, and the axial strain ε_{zz} is the dominant strain component. For a soil element in the centerline of the sampler, the change of ε_{zz} during the tube penetration can be obtained based on Figure 3.15 and is shown in Figure 3.16. When the tube is advancing toward the soil, the strain is compressive until it reaches a maximum value $(\varepsilon_{zz})_{max}$. When the cutting edge passes the soil, the compression strain decreases to 0 and then extension strain develops. The extension strain continues until the total strain reaches $-(\varepsilon_{zz})_{max}$. Finally when the soil is inside the tube, a compressive strain brings the total strain back toward zero. The final axial strain of the soil element depends on the length the soil element

travels inside the tube. The magnitude of peak axial strain $(\varepsilon_{zz})_{max}$ is dependent on the ratio of B/t, and indicates the intensity of disturbance.

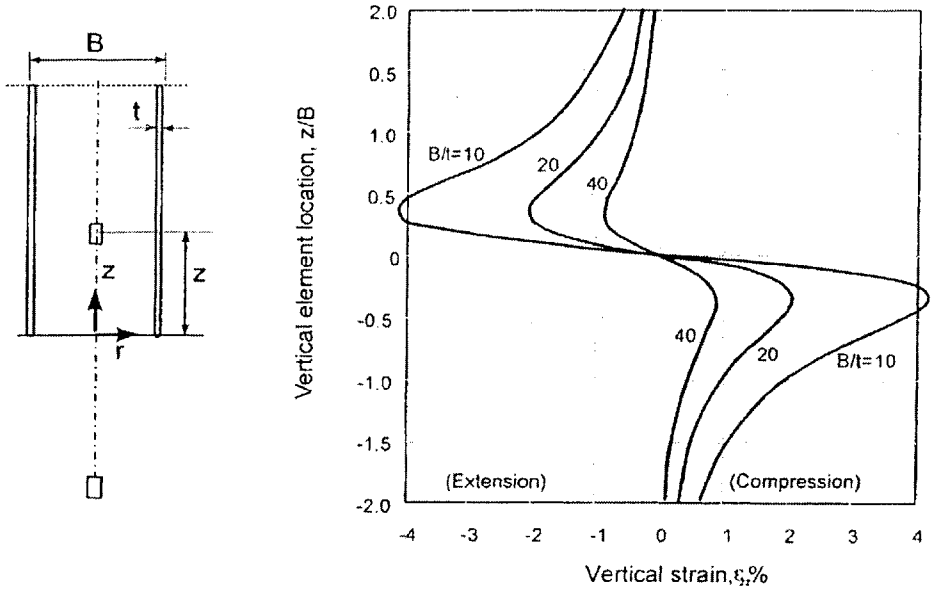

Figure 3.16 Strain History at Centerline of the Sampler (Baligh, 1985)

Baligh's Simple Sampler has a rounded tip which facilitates the analysis. However, real samplers often have a sharp cutting edge to minimize disturbance. Clayton et al. (1998) extended Baligh's solution and analyzed the variation of centerline strain ε_{zz} under different cutting edge geometry.

An illustration of a typical cutting edge is shown in Figure 3.17. The following parameters are defined to describe its geometric properties:

- Area Ratio AR = $\dfrac{R^2 - R_1^2}{R_1^2}$
- Inside Clearance Ratio ICR = $\dfrac{R_2 - R_1}{R_1}$
- Inside Cutting-Edge Angle ICA = $\arctan\left(\dfrac{R_2 - R_1}{H_1}\right)$

- Outside Cutting-Edge Angle OCA = $\arctan\left(\frac{R-R_1}{H_2}\right)$

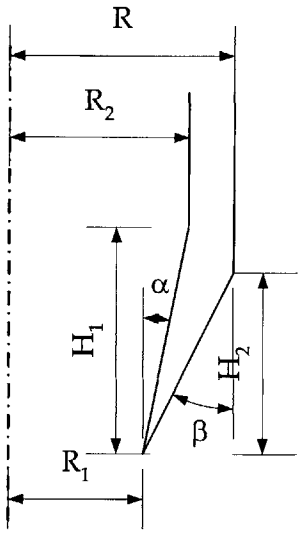

Figure 3.17 Tip Geometry of Real Tube Samplers (Clayton et al, 1998)

The research of Clayton et al. shows that the patterns of ε_{zz} variation for centerline soil element are roughly the same for different cutting edge geometries. Axial strain ε_{zz} always follows the compression – extension – compression strain cycle, although the maximum strain may not be the same for compression and extension. Varying the geometry of the cutting edge mainly changes the peak value of ε_{zz}. The influence of different geometry parameters on peak axial strain is shown in Figure 3.18. Please note that the Inside Cutting Angle is not shown in Figure 3.18 because the peak ε_{zz} hardly changes with variation of ICA.

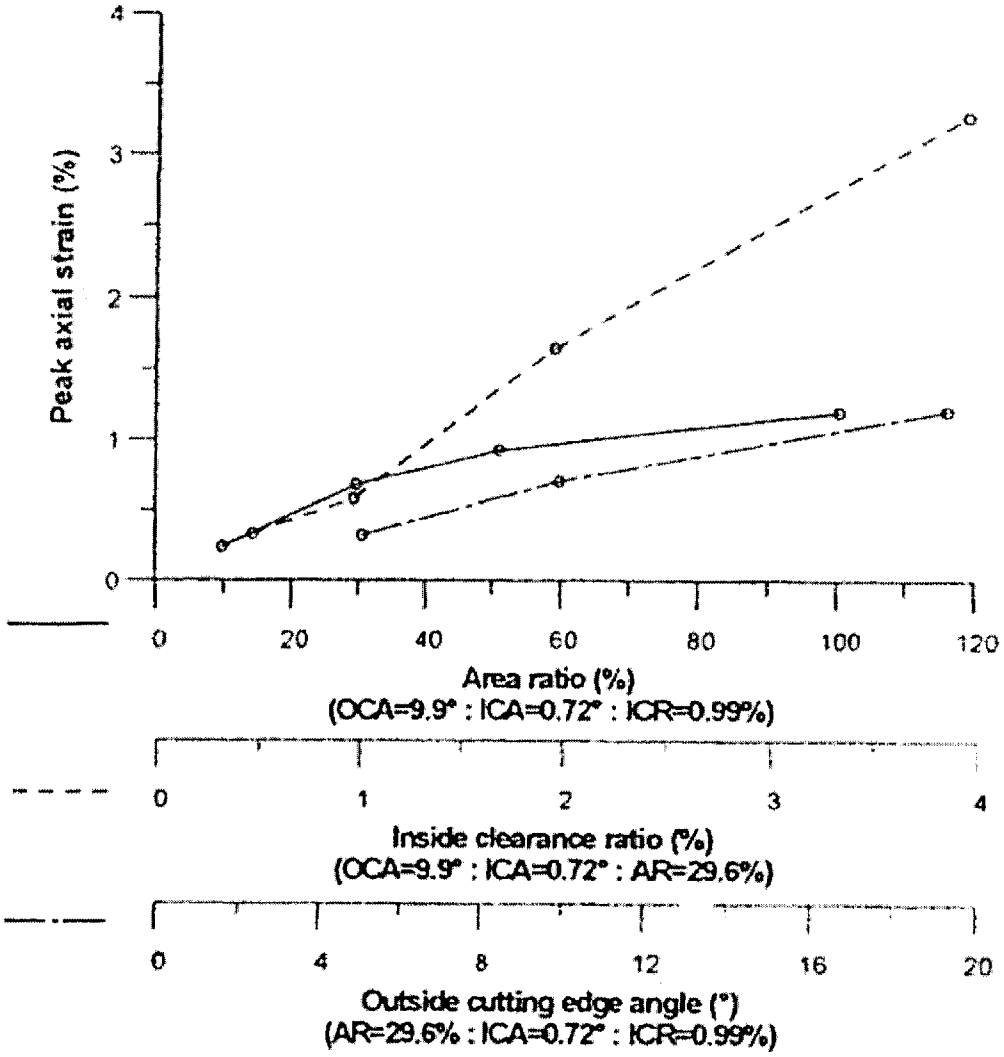

Figure 3.18 Change of Peak Centerline Axial Strain with Geometric Parameters (based on Clayton, 1998)

From the results shown in Figure 3.18, it can be concluded that to reduce the disturbance, the sampler geometry should be carefully designed so that:

- Area Ratio is minimized, which means that the diameter of the sampler should be large and its wall thickness should be small.
- Inside Clearance Ratio is reasonably small. According to Figure 3.18, smaller ICR will always give a smaller disturbance. However, if no

internal clearance is left, the sample may be subject to serious disturbance because of internal friction. Therefore, ICR should be controlled so that internal friction is effectively reduced while no excessive lateral swelling of the sample occurs.

- The Outside Cutting Edge Angle should be minimized, which means the cutting edge should be as sharp as possible.

3.3.2.2. From Strain to Stress

Uptill now, the results obtained with the ISA are the strain history of the sample during tube penetration. To obtain the effective stress history of the sample based on this strain history, two methods are possible.

The first method is to use a constitutive model to describe the behavior of the soil being sampled. Based on the strain history predicted from the ISA, the effective stress change in the sample can be obtained by the stress strain relationship of the constitutive model. Hight (1993a) actually has achieved this based on a simple soil model, which will be introduced in Section 5.

The other method is to simulate the strain history in the laboratory on an actual soil specimen and measure the effective stresses. This section introduces how to simulate the centerline strain history with triaxial tests and obtain the effective stress history of the sample during tube penetration. The basic knowledge of triaxial tests and the interpretation of its results have been introduced in Section 3.2.1.2. It should be noted that since triaxial tests can only create axi-symmetrical stress state,

they can only be used to simulate the disturbance of centerline soil elements.

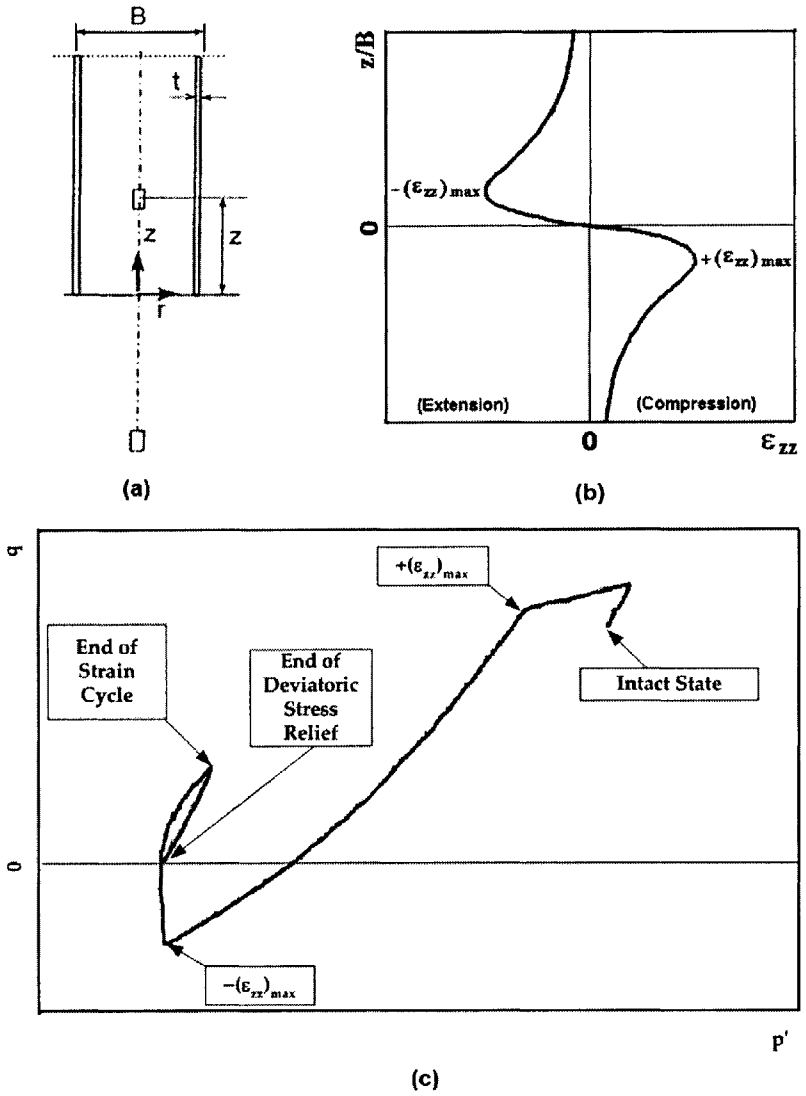

Figure 3.19 Triaxial Simulation of Tube Disturbance
(a) Definition of Geometry Parameters; (b) Strain Cycle Predicted by ISA; (c) Measured Effective Stress Path

Figure 3.19 shows the principles of simulating the centerline strain cycle with triaxial tests. A simplified version of centerline strain cycle is shown in Figure 3.19 (b). This strain cycle is then imposed on the specimen to simulate the tube sampling process as if the specimen were in the centerline of a tube sample. Different severities of disturbance can be modeled by different magnitudes of the peak axial

strain $(\varepsilon_{zz})_{max}$. After imposing this strain cycle, the specimen is supposed to be disturbed by tube sampling according to the ISA. The effective stress of the soil specimen subject to this "disturbance" can be measured to reveal the effective stress path the specimen follows. The effective stress path of a normally consolidated soil sample is shown in Figure 3.19 (c). Different stages of "disturbance" are clearly marked on the graph. The effective stress path starts from its "Intact State", and ends up at the "End of Strain Cycle".

Usually, a deviatoric stress relief is performed following the strain cycle to simulate the deviatoric stress relief caused by sample extrusion, which brings the effective stress path further to the End of Deviatoric Stress Relief. It must be noted that performing the deviatoric stress relief after imposing the strain cycle may not be very reasonable. The deviatoric stress relief aims at simulating the disturbance caused by sample extrusion. However, between tube sampling and sample extrusion, there is the transportation and storage period of the samples. During this period, the effective stress may be changed by bumping and shanking in transportation, or by pore pressure equalization in sample storage. Apparently, triaxial simulation does not take these factors into consideration.

3.3.2.3. An Example of Simulation and Its Results

The triaxial simulation of tube sampling disturbance and deviatoric stress relief has been performed at MIT on Resedimented Boston Blue Clay (RBBC) by Santagata (Santagata, 1994). RBBC is an artificial soil produced in the laboratory.

Since its condition of sedimentation and stress history can be well controlled, the effective stress at its "intact state" or "in-situ state" can be obtained with relatively small uncertainty. Part of the results of these simulations is presented here to show the change of effective stress during the tube sampling process and the following deviatoric stress relief.

It has been shown that the severity of disturbance by the centerline strain cycle is determined by the magnitude of peak axial strain $(\varepsilon_{zz})_{max}$. Therefore, $(\varepsilon_{zz})_{max}$ is varied in these simulations to get different levels of disturbance. The simulation with $(\varepsilon_{zz})_{max}$ = N% is denoted "ISA±N" in the following discussion. Based on what has been said, a larger N means more serious disturbance.

The effective stress paths of RBBC samples in the simulations are shown in Figure 3.20. Figure 3.20 (a) shows the effective stress paths of normally consolidated RBBC samples. Three different levels of disturbance, i.e. ISA±1, ISA±2 and ISA±5 are simulated. Figure 3.20 (b) shows the effective stress paths for OCR = 4 over-consolidated RBBC samples. Only the ISA±1 and ISA±2 cases are shown. In both plots, σ'_{vc} stands for the vertical effective stress of the "in-situ" stress state, i.e. of Point 1. The values of p′ and q plotted in Figure 3.20 are actually normalized by σ'_{vc}.

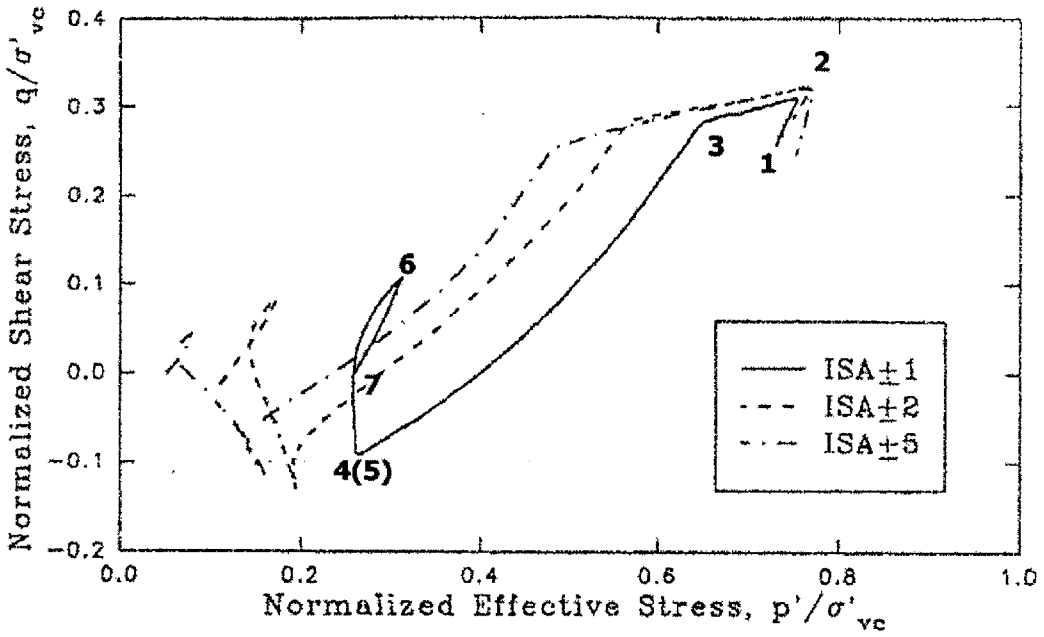

(a) Effective Stress Paths for OCR = 1

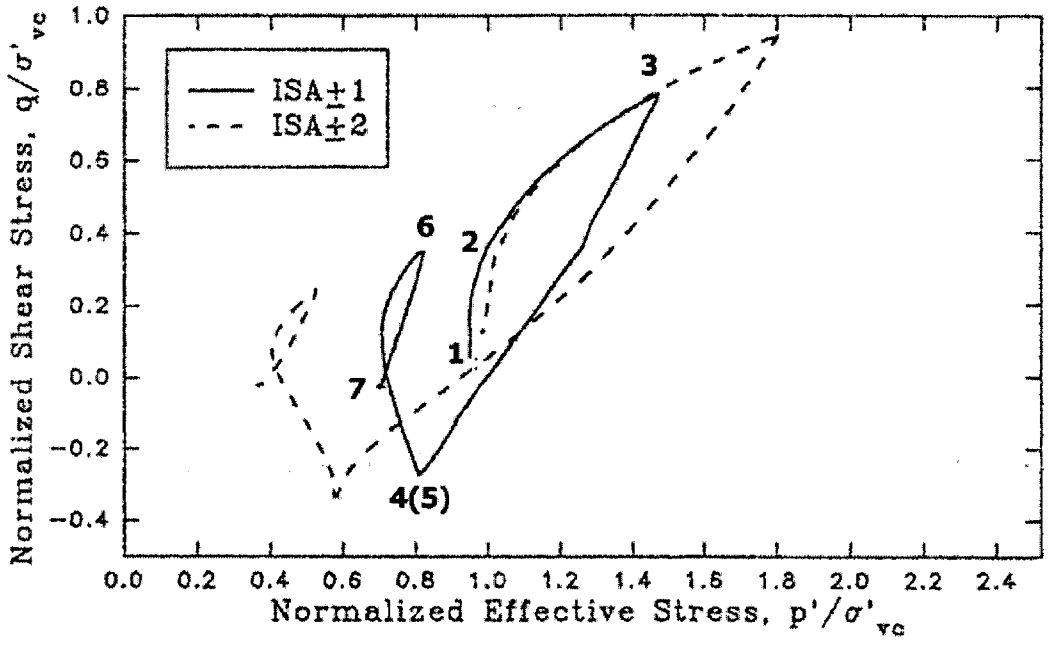

(b) Effective Stress Paths for OCR = 4

Figure 3.20 Effective Stress Path to Simulate Disturbance (Santagata, 1994)

In both graphs, the effective stress paths from 1 to 4 simulate the tube sampling strain cycle. 1→2→3 simulates the compressive strain when the cutting edge is approaching the soil element. At Point 3, the compressive strain reaches its

maximum $(\varepsilon_{zz})_{max}$. 3→4→5 simulates the extension strain when the cutting edge passes the soil element. At Point 5, the extension strain reaches $-(\varepsilon_{zz})_{max}$. 5→6 simulates the final compression when the soil element is inside the tube. The effective stress path from 6 to 7 simulates the final stress relief due to sample extrusion. Although Point 4 and Point 5 seem to be the same, this is not necessarily so. The details of this problem will be discussed later in Section 5. The numbers are only marked for the solid line for clarity. Equivalent points can be easily identified on other stress paths.

It is clear that the mean effective stress in the sample is reduced for normally consolidated (OCR = 1) RBBC samples. It is also shown that the reduction of mean effective stress increases with the severity of disturbance. More detailed simulations on normally consolidated RBBC have been performed, and the percentage loss of the true mean effective stress $\Delta p'_m/p'_{m0}$ is plotted in Figure 3.21 against the magnitude of $(\varepsilon_{zz})_{max}$ (shown as "strain cycle amplitude ε_c"). p'_m is the true mean effective stress which is defined by:

$$p'_m = (\sigma'_v + 2\sigma'_h)/3$$

and p'_{m0} is the value of p'_m at the "intact" stress state. Clearly, higher levels of disturbance cause larger decrease of the true mean effective stress.

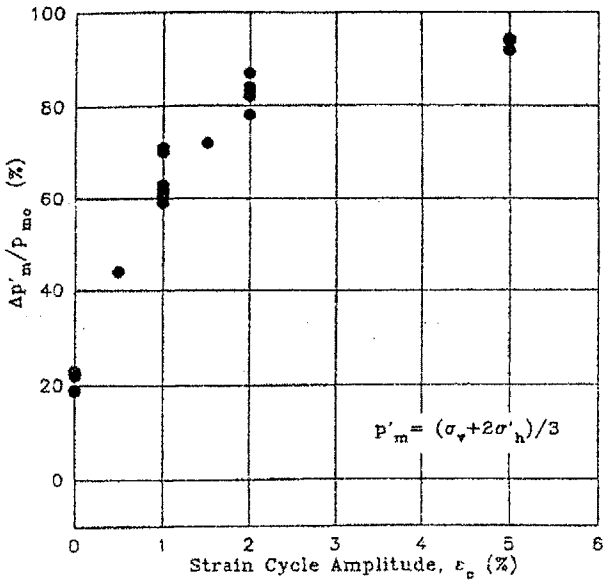

Figure 3.21 Loss of Mean Effective Stress vs. Severity of Disturbance (Santagata, 1994)

It can be concluded from Figure 3.20 (b) that the disturbance also cause the mean effective stress to decrease for OCR = 4 RBBC samples. Comparing Figure 3.20 (a) with Figure 3.20 (b), it can be found that the same level of disturbance causes smaller reduction of mean effective stress for OCR = 4 soil. This means that samples with higher OCR values are less sensitive to disturbance in terms of effective stress change. Actually, if the sample is very heavily over-consolidated, the effective stress may even increase after the "disturbance".

3.4. Move the Sample to Ground Surface

3.4.1. Change of Mechanical Properties

It has been shown in Section 2.2.3 that when the sample is pulled out of the borehole, the pressure acting on the sample is the mud pressure, which decreases

with the decreasing depth (Figure 3.22). A very simple analysis of the change of effective stresses is presented below.

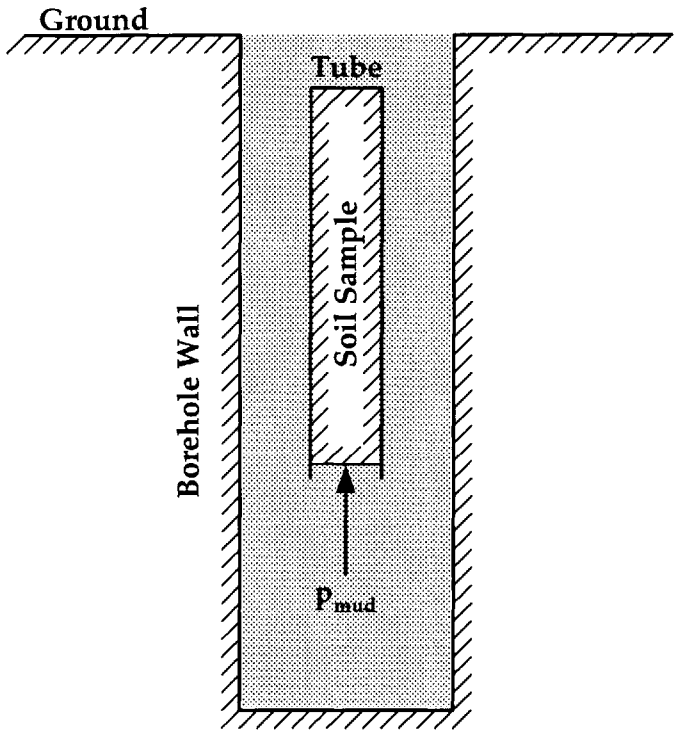

Figure 3.22 Mud Pressure on Soil Sample

The pressure p_{mud} shown in Figure 3.22 is the total pressure acting on the sample. At the surface where the sample is in contact with the mud, the total stress in the sample should be equal to the mud pressure. Therefore:

$$p_{mud} = \sigma = \sigma' + u$$

based on the effective stress principle. As the sample rises in the borehole, p_{mud} will decrease. Since the permeability of the soil is very small, no drainage will usually occur during the pulling up of the sample. Thus the effective stress σ' will remain constant. It follows that the pore pressure decreases with the mud pressure.

However, since the soil sample is actually confined by the tube sampler, its stress state might be very complicated. The results of the above analysis can only be

considered as indicating a trend. To accurately quantify the change of pore pressure and effective stress of the sample, more rigorous analysis is necessary.

In addition, the mud temperature usually varies with depth. When the sample is rising in the borehole, its temperature will be constantly changed by the changing mud temperature. This also causes the effective stress and the pore pressure of the sample to change.

3.4.2. Change of Composition

The composition of the sample is mainly changed by contact with the drilling mud when the sample is retrieved. However, since the mud pressure on the sample is decreasing, the amount of liquid exchange and mud penetration varies with the depth of the sample.

It has been shown in Section 3.4.1 that the pore pressure of the sample is reduced during the pulling up of the sample. Gas exsolution may occur during this pore pressure decrease. The pore pressure at which gas exsolves depends on the temperature, the type of gas and its solubility. For fine grained soils with very small permeability, the exsolved gas is trapped inside the soil (Hight, 2001). Diffusion may take place with time, so that the exsolved gas gathers in larger pores, forming gas bubbles. Coarse grained soils usually have larger permeability. The exsolved gas is drained directly from the soil into the drilling mud.

3.5. Sample Transportation and Storage

3.5.1. Change of Composition Properties

After the samples have been retrieved, they must be transported to the laboratory for testing. This subjects the samples to shaking and bumping. These factors may act on the sample similarly to the drilling machine vibration. However, since these disturbance sources are very difficult to quantify, no systematic studies on transportation induced disturbance appear to have been conducted.

In case that the soil sample is not well sealed, the sample may be in contact with air. As a result, the free water in the sample may evaporate, and the water content of the sample will be decreased. The space that was originally taken by the evaporated water will be taken by air instead. Negative pore pressure may be generated by capillary effects at the interface of water and air. Depending on the pore size of the sample, the effective stress of the sample can be smaller or larger than the original effective stress. Therefore, the void ratio of the sample will be changed. A more detailed description about the negative pore pressure will be given later (Section 3.6.1.1).

A change in chemical composition of the sample may also occur. According to Hvorslev (1949), in soils consisting primarily of quartz and similar relatively inert minerals, the chemical changes which may occur consist mainly of deposition of chemical compounds in the voids and the formation of a bond between the soil grains. In soils containing clay minerals the principal change is a base exchange or

an exchange of cations at the surface or corners of the crystal lattice of the minerals with ions in the pore water. The corresponding changes in physical properties depend on the types of ions which have been exchanged. Organic compounds in the soil may be subject to both oxidation and base exchange. The contact with the sampler may in special cases also cause chemical changes in the soil. The presence of acids or bases in the soil or pore water may produce chemical reaction or electrolytic action. Therefore, the containers and testing equipment should preferably be of electrically inert materials or be made with only one kind of metal to avoid electrolytic action.

During sample storage, the state of the sample may continue to be changed by disturbance sources from borehole drilling, tube sampling, and moving the sample to the ground surface. Although these sources are not acting on the sample any more, the changing of state caused by them lasts for a long time. In Section 2.2, this has been listed as the Time Effect.

The most significant time effect is probably caused by tube sampling. As described earlier, tube sampling may disturb the sample in many ways. Based on the analysis of the tube sampling process, the disturbance is not uniform. Across the cross-section of the sample, disturbance is more serious at the periphery than at the center since the periphery is subject to serious shearing by the internal friction. This non-uniformity causes the state of the sample to continue changing even a long time after the tube penetration. A segment of a sample is shown in Figure 3.23 to illustrate how this non-uniformity of disturbance causes void ratio change and water

redistribution during sample storage. In the in-situ state, the pore pressure and water content of the soil element are uniform; they are denoted u_0 and w_0. After tube penetration the pore pressure at the periphery and at the center become u_p and u_c respectively, and the corresponding water contents become w_p and w_c. The corresponding void ratios are denoted e_p and e_c.

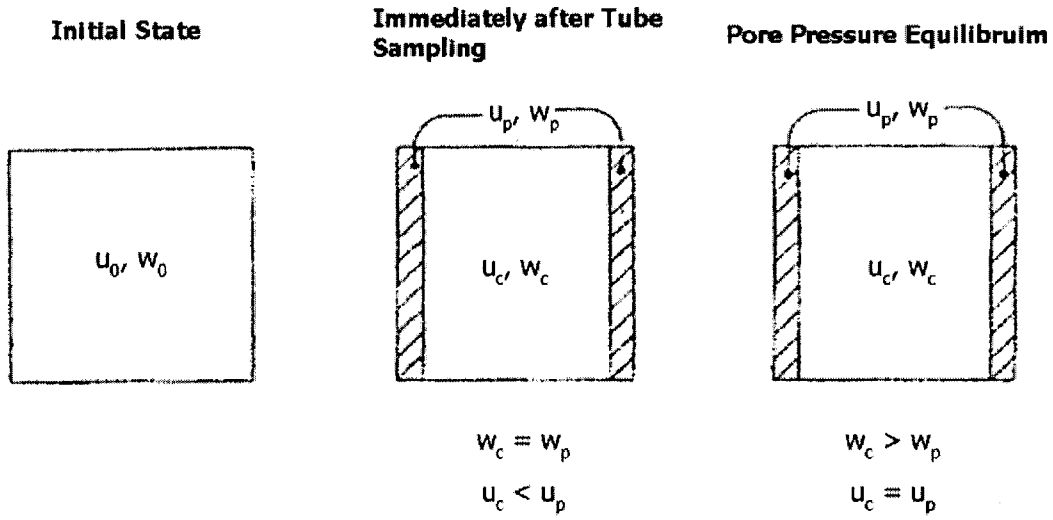

Figure 3.23 Water Migration Due to Tube Disturbance (modified from Hight, 2001)

Since the sampling process is treated as an undrained process, the fabric distortion does not immediately change the void ratio since the volume is constant. Therefore $w_p = w_c$ and $e_p = e_c$ at the end of tube sampling. However, excessive pore pressure will be generated by the excessive shearing of soil at the periphery.

For normally and slightly over-consolidated soil, pore pressure rises as a result of excessive shearing, i.e. u_p increases after tube penetration. Since the center part of the sample is disturbed to a smaller extent, u_p becomes larger than u_c immediately after tube sampling. During the storage of the samples, the non-uniformity of the pore pressure will be equalized. The periphery consolidates

since it has higher pore pressure. Water is squeezed out and the void ratio is decreased. In contrast, the center swells since water migrates in, and the void ratio increases. After equalization of pore pressures, one will find that $w_p < w_c$ and $e_p < e_c$, i.e. the water content and void ratio at the periphery decrease, while those of the center increase for normally and slightly over-consolidated soil.

For heavily over-consolidated soil, shearing causes the pore pressure to decrease because of dilatant behavior. Thus u_p is smaller than the original pore pressure u_0 immediately after tube sampling. u_c, the pore pressure at center, may be larger or smaller than u_0 depending on the behavior of the soil. However, since the disturbance is much smaller at the center, the difference between u_c and u_0 should be small. Therefore, it is reasonable to assume $u_p < u_c$ after tube penetration. This will cause migration of water to the periphery and it can be expected that $w_p > w_c$ and $e_p > e_c$ when pore pressure reaches equilibrium. Consequently, the water content and void ratio at the center decrease, while those at the periphery increase for heavily over-consolidated soils.

The water content distribution across the diameter of the tube has been measured for normally and slightly over-consolidated soil and heavily over-consolidated soil (Vaughan, 1993). The diameter of the measured tube samples was 100mm, and the measured distributions of water content across the diameter are shown in Figure 3.24. As has been discussed, the water content at the center is higher than at the periphery for normally and slightly over-consolidated soils, and the reverse is true for heavily over-consolidated soils.

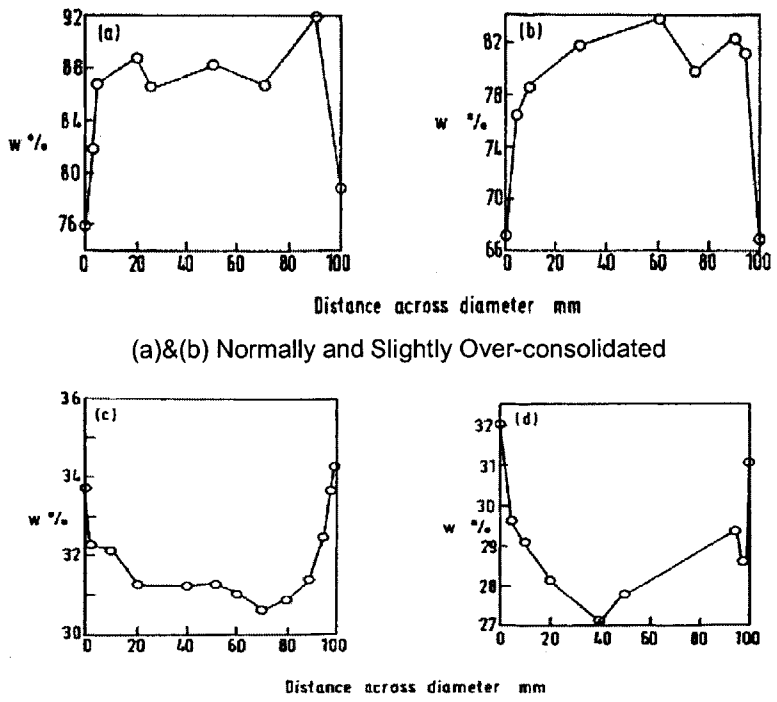

(a)&(b) Normally and Slightly Over-consolidated

(c)&(d) Heavily Over-consolidated

Figure 3.24 Measured Water Content Across the Diameter of Tube (Vaughan, 1993)

3.5.2. Change of Mechanical Properties

During transportation and storage of the samples, the temperature of the samples is easily affected by the temperature of the environment, which in turn is determined by the weather conditions. It is known that the temperature change of the sample will cause the change of pore pressure and effective stress in the sample. However, since the temperature of an area is a random variable, the stress changes caused by the temperature change also involves great uncertainties.

If the sample is not properly sealed and it is in contact with air, negative pore pressure can be generated at the boundary where the sample is in contact with air. The effective stress of the sample can be changed by this negative pore pressure. However, it is likely that the generation of negative pore pressure is only locally at

this stage.

Based on Section 3.5.1, pore pressure equalization occurs during sample storage as the time effect of tube sampling. The areas with higher pore pressure will consolidate, causing the effective stress to increase. The areas with lower pore pressure will swell, corresponding to the decrease of effective stress. For normally or slightly over-consolidated soil, pore water redistribution causes the effective stress in the center to decrease. For heavily over-consolidated soil, pore water redistribution causes the effective stress in the center to increase. Given that the decrease of the mean effective stress during tube penetration is smaller for high OCR soil (Figure 3.19) compared to normally and slightly over-consolidated soil, the final mean effective stress may be higher than the in-situ mean effective stress.

3.6. Sample Preparation

3.6.1. Change of Mechanical Properties

3.6.1.1. Sample Extrusion

The first step of sample preparation is to extrude the sample out of the tube. At this time, the total stress on the sample that is locked in the tube will be suddenly relieved to the atmospheric pressure. Although the real process of how the stress is changed to atmospheric pressure remains unclear, the total stress relief is usually divided into two components: the deviatoric stress relief and the isotropic stress relief.

The deviatoric stress relief during extrusion is different from that caused by borehole drilling, in that it is not started from the in-situ state. The effective stress in the sample has already been changed by borehole drilling, tube sampling, sample transportation and storage, and possibly other factors that are not yet known. Recall that in the simulation of tube sampling on RBBC samples, deviatoric stress relief caused by sample extrusion is also simulated for the centerline strain cycle. From the effective stress paths the RBBC samples followed during the deviatoric stress relief (Point 6→7 in Figure 3.20), it can be seen that the mean effective stress for all OCR = 1 and OCR = 4 samples decreases. Therefore, it may be reasonable to say that the deviatoric stress relief during sample extrusion reduces the mean effective stress for normally and slightly over-consolidated soil. However, the magnitude of reduction is very small compared with the mean effective stress reduction caused by tube penetration.

Upon removal of the isotropic stress component of a soil element, the state of the sample will be determined by the balance of the swelling of the soil skeleton and the negative pore pressure that the soil can sustain. On the one hand, elastic rebound occurs due to the stress relief and the volume of the soil element tends to increase. On the other hand, the compressibility of soil skeleton is generally larger than that of water. The pore volume tends to get larger and the pore water tends to retreat into the soil element. Since the sample is in direct contact with the atmosphere, water menisci will form and negative pore pressure is generated. The negative pore pressure keeps the water menisci from retreating into the soil and prevents the

sample from swelling. The effective stress change during this process can be analyzed below:

Suppose the atmospheric pressure is taken as 0, and the negative pore pressure is $-p_w$, then the total stresses on the sample are:

$$\sigma_h = \sigma_v = 0$$

According to effective stress principle, the effective stresses are:

$$\sigma'_h = \sigma'_v = p_w$$

Therefore, the final effective stresses in the sample are the same as the negative pore pressure that can be sustained.

Clearly, sustainable negative pore pressure varies with different kinds of soils. Soils with smaller pore size can sustain larger negative pore pressure. The relationship between the maximum sustainable negative pore pressure and the pore diameter of soil is shown in Figure 3.25. Consequently, the effective stress changes must be discussed for different soils.

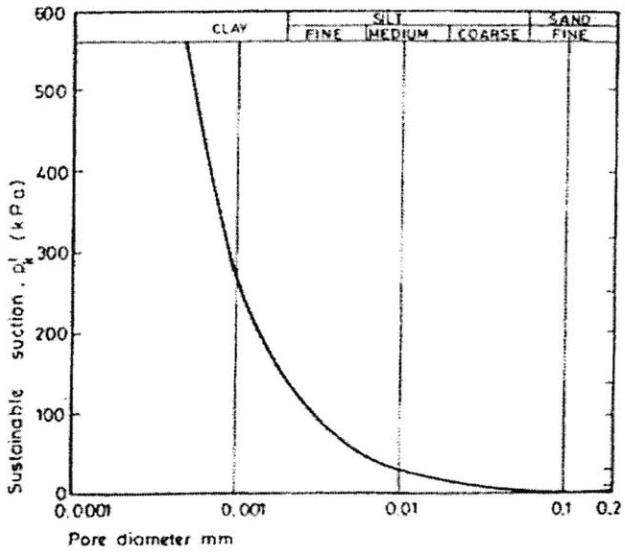

Figure 3.25 Sustainable Soil Suction vs. Pore Diameter (modified from Hight, 2001)

- Fully saturated clays and other fine-grained soils with a large content of sheet mineral particles often have a great tendency to expand. On the other hand, they have very small pore space, allowing large negative pore pressures to be generated. Therefore, the effective stresses in the removed sample can reach considerable magnitude, even approaching the mean effective in-situ stress if the soil has not been subject to structural disturbance.
- For coarse grained soil, the pore sizes are usually large enough so that the sustainable negative pore pressure is very small. Therefore, the water menisci are generally drawn into the soil and air is admitted to the outer pores. Water may only be retained in the smallest pores of the sample, and the effective stress produced by the negative pore pressure only exists locally. As a result, the overall effective stresses in these soils will usually decrease so that the soil grains may actually fall apart.
- The situation is more complicated in stratified soils, where fine grained soils and coarse grained soils are interlayered (Figure 3.26). Upon stress relief, the different soils sustain different negative pore pressures. The negative pore pressure generated is much larger in fine grained soil than in coarse grained soil. Due to this pore pressure imbalance, water migrates from higher pressure in the coarse grained soil to lower pressures in the fine grained soil. As a result, the effective stresses in both the fine grained and the coarse grained soils decrease.

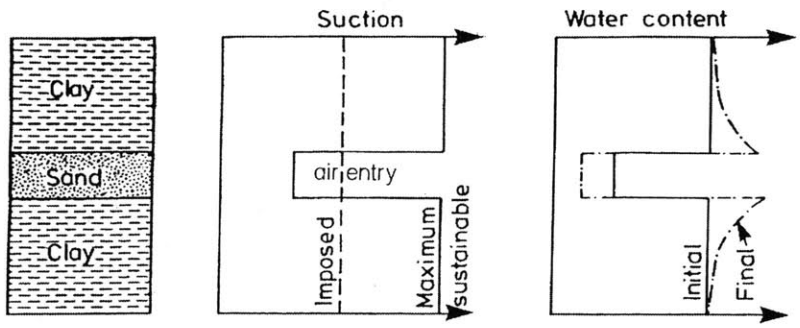

Figure 3.26 Water Migration in Stratified Soil (Hight, 2001)

3.6.1.2. Sample Trimming

Different sample trimming methods are applied in different tests. For triaxial tests, the samples are cut with wire saw (Figure 3.27 (a)). Samples for oedometer tests are prepared by a cutting ring (Figure 3.27 (b)). This cutting ring is forced into the original tube sample much like the penetration of a smaller tube. Compared with the wire saw preparation, the disturbance caused by the cutting ring is much larger.

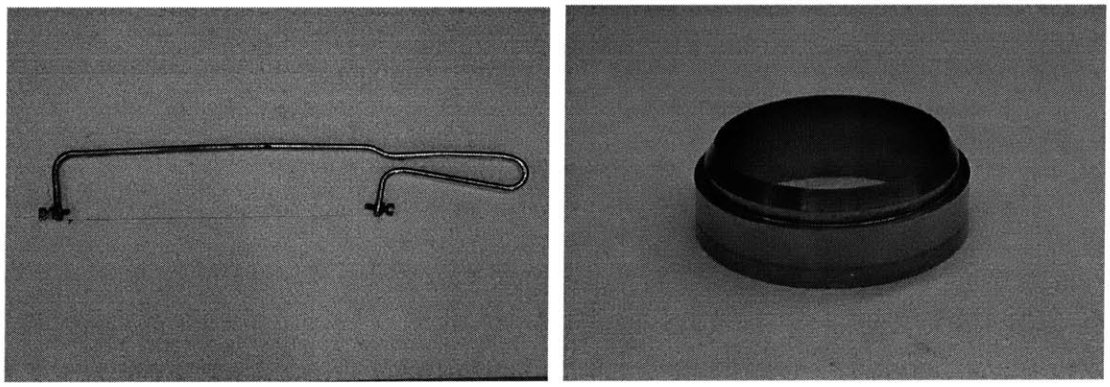

(a) Wire saw (b) Cutting Ring

Figure 3.27 Tools Used for Sample Preparation

If the sample is trimmed by a wire saw the disturbance is usually small and the effective stress change is not much. If it is cut by a ring cutter, then the disturbance is larger. Based on the analogy between a cutting ring and a tube

sampler, it may be reasonable to say that the cutting decreases effective stress for normally consolidated samples, and may slightly decrease or even increase the effective stress for heavily over-consolidated samples.

3.6.2. Change of Composition

It has been shown in Section 3.6.1 that for fine grained soil, the sustainable negative pore pressure is very large, and the effective stress after stress relief can even approach the mean effective in-situ stress. As a result, the swelling of the soil skeleton due to stress relief should be very small. The change of void ratio and water content is small too.

However, the existence of large negative pore pressure in fine grained soil means that the pore pressure decreases due to stress relief. During the pore pressure decrease, gas exsolution again can occur. In extreme cases the absolute pore water pressure may become negative, i.e. tensile stress is generated in the pore water. When this tensile stress exceeds the tensile strength of water, water cavitation may occur. The theoretical value for the tensile strength of water is 500MPa. However, due to the existence of dissolved gas and impurities, the tensile strength is usually decreased. When the tensile stress exceeds the tensile strength, tensile failure may occur in pore water and cavitation takes place.

For coarse grained soil, it has been shown in Section 3.6.1 that air will be admitted and water can be drained. The remainder water will retreat to the smallest pores. Since the sustainable negative pore pressure is very small, the sample is then

free to expand. However, coarse grained soils usually have small tendency to expand due to their low compressibility. Hence the change of void ratio is also small, but the water content is decreased due to water drainage.

For stratified soils, it has been shown in Figure 3.26 that water will migrate from coarse grained soil to fine grained soil. Since pore water is lost in the coarse grained soil, air entry may occur. The void ratio and water content in fine grained soil become larger due to water coming in.

If the sample is trimmed with a wire saw, the soil at the surface of the triaxial sample will be smeared by the wire saw and the clay particles are reoriented. If a cutting ring is used to cut the sample instead, the composition changes of the sample may be similar to the changes caused by tube sampling. According to the description in Section 3.3.1 and Section 3.5.1, these changes may include fabric change during the cutting and the following void ratio change and water migration.

3.7. Summary

This section analyzed the mechanisms of the disturbance sources listed in Section 2.2 in soil sampling. Generally, the descriptions in this section assume that the soil being sampled is soft clay. The analysis of disturbance mechanisms is mainly focused on how the void ratio, water content, fabric and effective stress are changed. It can be seen that after sampling, the state of the sample has been changed in many aspects from its in-situ state. This again shows that sample disturbance is an important yet unavoidable problem.

As has been said in Section 2.4, various simplifications have been introduced in order to understand the disturbance mechanisms. Each disturbance source is discussed separately, and the coupling of disturbance sources has not been considered. Simplifications are also used to characterize the disturbance sources and the soil behavior. For example, the ISA assumes the tip of the sample tube is rounded, and the behavior of soil is equivalent to the behavior of ideal fluid. However, there are still some disturbance sources whose mechanisms are not clearly understood, such as the vibration of the drilling machine, the temperature change, etc. This is either because the disturbance source is difficult to characterize, or because of the difficulty of considering coupled behavior.

A very important result of this section is the effective stress change in a centerline soil element during the sampling process. The effective stress changes in different stage of sampling can be summarized in the following table:

Table 3.1 Effective Stress Change in a Centerline Soil Element

Stage of Sampling	Mean Effective Stress Change	
	Normally and Slightly Over-Consolidated	Heavily Over-Consolidated
Borehole Drilling	Decrease	Increase Slightly
Tube Sampling	Decrease Greatly	Increase Slightly
Transportation & Storage	Decrease	Increase
Sample Extrusion (Deviatoric Stress Relief)	Decrease Slightly	Small Change
Sample Extrusion (Isotropic Stress Relief)	Decrease	Decrease
Sample Preparation	Decrease	-
Resultant Effect	Decrease Greatly	-

From what is shown in the table, one can conclude that after disturbance, the effective stress in normally and slightly over-consolidated soil will be reduced. For heavily over-consolidated soil, no simple conclusions can be made.

In our analysis, each sampling procedure has been analyzed separately, and only the effective stress paths of stress relief and tube sampling are shown (see Figure 3.7, Figure 3.8, and Figure 3.20). In order to show the whole story of effective stress change, the hypothetical effective stress path presented by Ladd (2003) is also shown here (Figure 3.28).

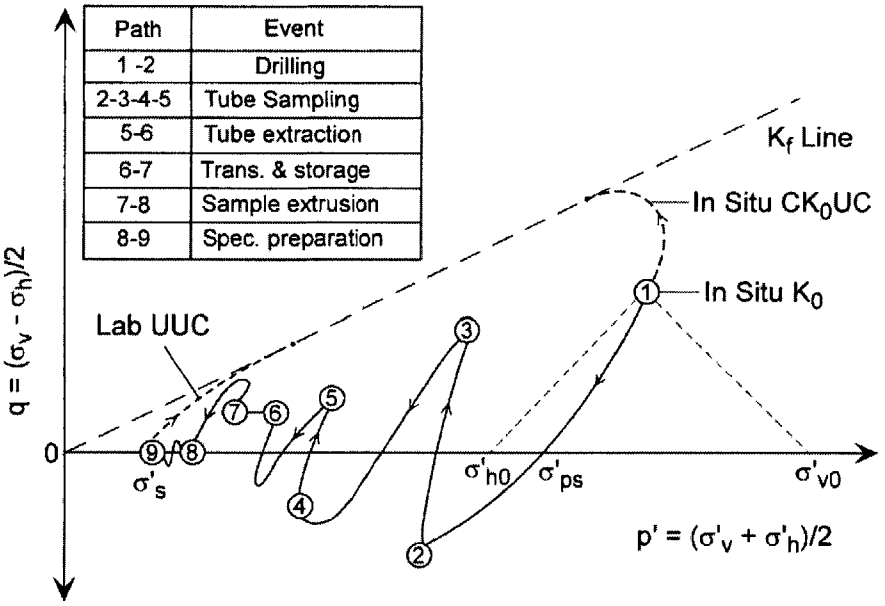

Figure 3.28 Hypothetical Effective Stress Path for a Centerline Soil Element (Normally or Slightly Over-Consolidated) (Ladd et al., 2003)

The numbers on the effective stress path marks different sampling procedures. Comparing Figure 3.28 with Table 3.1, it can be seen that the trends shown in Table 3.1 for normally and slightly over-consolidated samples are correct, i.e. all the sampling procedures decrease the mean effective stress in the sample.

Based on the preliminary understanding of the disturbance mechanisms in soil sampling, it is possible for us to judge which disturbance sources are important and which are not. Then the significant disturbance sources can be used to approximate the real disturbance problem.

Since the effective stress is probably the most important mechanical property in a soil sample, it is chosen as the criterion to judge which disturbance sources are important. For centerline soil elements, the effective stress changes at different stages of sampling have been summarized in Table 3.1. Based on the discussion and simulations presented in Section 3.3.2, the reduction of effective stress in normally and slightly over-consolidated soil by tube sampling accounts for a major portion of the total mean effective stress decrease. Therefore, the disturbance caused by tube sampling can be considered to be a first approximation of the complex disturbance problem in normally and slightly over-consolidated soil.

4. Effects of Disturbance on Soil Behavior

The previous section analyzes the mechanisms of the disturbance ***sources*** listed in Section 2.2. From the understanding of the disturbance mechanisms, one can conclude that tube sampling is an important disturbance source for normally and slightly over-consolidated soils.

Following the structure outlined in Section 2.4, this section will study the ***effects*** of disturbance in soil sampling. Taking the research on Resedimented Boston Blue Clay (RBBC) in MIT as an example (Santagata, 1994), this section shows how these effects are obtained and how they affect the consolidation and shearing behavior of RBBC samples. The whole research is based on the principles of the Ideal Sampling Approach since only the tube sampling disturbance is considered.

4.1. Methodology

The research on RBBC at MIT was conducted by Santagata (Santagata, 1994) based on the principles of Ideal Sampling Approach. According to the ISA principles described in Section 3.3.2, the disturbance of tube sampling process (and the sample extrusion) on centerline soil elements can be simulated by reproducing the centerline strain cycle with triaxial tests. The simulation of tube sampling disturbance on RBBC samples of this research has been described in Section 3.3.2.3.

In Santagata's research, the following steps are then followed to obtain the effects of tube sampling disturbance (Santagata, 1994):

1) A large RBBC soil cake is artificially made (Santagata, 1994). This soil cake is made to be very uniform. Therefore, any triaxial specimens cut from this soil cake are supposed to have the same initial state.
2) Standard triaxial specimens are cut from this soil cake and installed in the standard triaxial cells following exactly the same procedures. When these specimens are installed in the triaxial cells, their states should still be the same, although probably not quite the same as their initial state.
3) These specimens are supposed to be centerline soil elements in a tube sample, and the disturbance caused by tube penetration is simulated by imposing the centerline strain history (Figure 3.16) on them. The details of simulation process have been introduced in Section 3.3.2.3. For different specimens, different peak axial strain $(\varepsilon_{zz})_{max}$ is applied, so that these specimens are subject to different disturbance severities.
4) Consolidation tests or shear tests are then performed on these disturbed samples, again following the same procedure, to obtain their behavior.

Based on the procedures described above, it can be seen that $(\varepsilon_{zz})_{max}$ is controlled to produce different disturbance severity. Everything else is the same for all the specimens, including their initial state, the cutting and installing procedure, the testing procedure, etc. Consequently, the only difference for these specimens is that they have been subject to different severities of tube sampling disturbance. Finally, the difference of their behavior can be solely attributed to the different

severities of disturbance. Comparing the behaviors of these specimens, the trend of behavior change with increasing (or decreasing) disturbance can be obtained.

In the research on RBBC, the one-dimensional consolidation tests and undrained shear tests have been conducted on "disturbed" RBBC specimens. The effects of disturbance on the consolidation behavior and shearing behavior of RBBC specimens are summarized below.

4.2. Effects on Consolidation Behavior

The consolidation behavior of the soil can be obtained by one-dimensional consolidation (or K_0 consolidation introduced in Section 3.1) tests performed with a triaxial cell. The consolidation stress σ'_v is increased step by step, and the height of the sample after consolidation at each stress level is recorded. The results of an one-dimensional consolidation test are usually presented by the compression curve, which plots the change of the sample's void ratio e at each stress level (calculated from the height of the sample) against the corresponding logarithm of compression stress $\log(\sigma'_v)$ (see Figure 4.1 for example curves). If the soil sample is over-consolidated, then the maximum consolidation stress it has been subject to is usually denoted σ'_p, which is often called "pre-consolidation pressure". Before the consolidation stress σ'_v reaches σ'_p, the sample is said to be in "recompression", and the slope of the compression curve is usually small. When σ'_v exceeds σ'_p, the sample is said to be in "compression" and the slope of the compression curve increases dramatically.

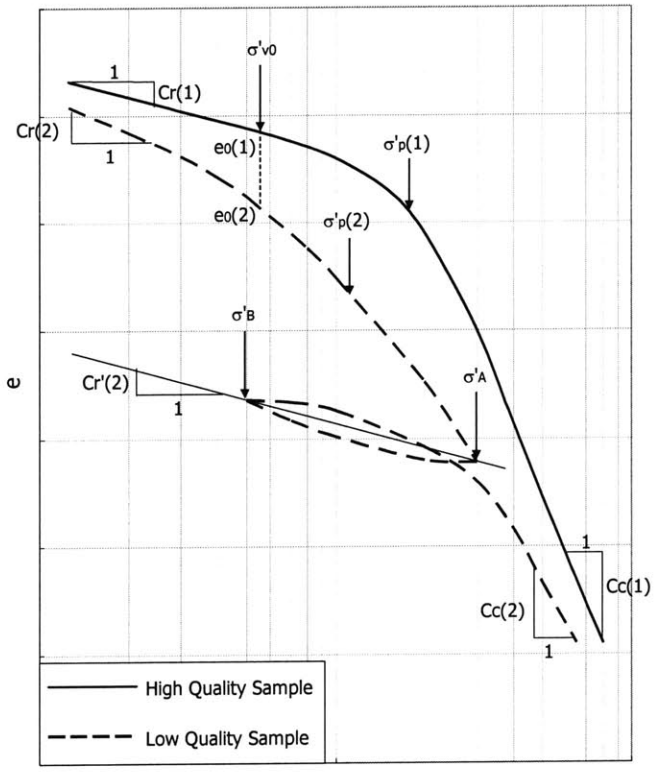

Figure 4.1 Effects of Disturbance on the Shape of Compression Curve

Disturbance usually changes the shape of the compression curve. Therefore, all the consolidation parameters obtained from the one-dimensional compression curve will be affected accordingly. The effects of disturbance on the shape of compression curve obtained from Santagata's research are shown by comparing two hypothetical curves of different sample quality in Figure 4.1. The solid curve represents the behavior of a high quality sample, while the dashed curve a low quality sample. For the consolidation of the low quality sample, unloading is performed when the consolidation stress reaches σ'_A until the stress level decreases to σ'_B. σ'_A then becomes the pre-consolidation pressure for the low quality sample. When the consolidation stress is again increased from σ'_B, the sample is in the

recompression state before σ'_A is reached. The recompression slope of the compression curve in the unload-reload cycle may not be the same as the initial recompression slope.

There are several parameters that are usually obtained by measuring the geometry of the compression curve. They are very important for the engineers since they are vital for settlement prediction. Therefore, the attention should be focused on the effect of disturbance on them. The parameters shown in Figure 4.1 are:

1. The in-situ vertical stress σ'_{v0};
2. When the samples are consolidated to σ'_{v0}, the corresponding void ratio for the high quality sample is $e_0(1)$, for low quality sample is $e_0(2)$.
3. The pre-consolidation pressures for both curves are determined by graphical construction methods (e.g. the Casagrande Method, Schmertman Method, Strain Energy Method, etc.). They are marked in Figure 4.1 with $\sigma'_p(1)$ for the high quality sample, and $\sigma'_p(2)$ for the low quality sample.
4. The compression ratio $Cc = de/d(\log\sigma'_v)$ is the slope of the curve in compression. Again Cc(1) is for high quality sample and Cc(2) is for low quality sample.
5. The recompression ratio $Cr = de/d(\log\sigma'_v)$ is the slope of the curve in recompression, with Cr(1) for high quality sample and Cr(2) for low quality sample. For the low quality sample, the recompression slope determined from the unload-reload cycle is denoted Cr'(2).

The following conclusions are obtained from Santagata's research, which are also shown in Figure 4.1.

- The transition between recompression and the compression becomes more gradual with increasing disturbance, and the location of pre-consolidation pressure becomes obscured. Usually the pre-consolidation pressure measured from low quality sample ($\sigma'_P(2)$) is smaller than that measured from high quality sample ($\sigma'_P(1)$).
- The initial recompression ratio tends to increase with disturbance, i.e. $Cr(2) > Cr(1)$. However, the recompression rate determined from load-unload cycle is less affected, which means that $Cr'(2) \approx Cr(1)$. Therefore, a load-unload cycle should be included in the one-dimensional compression test to get a meaningful Cr value.
- When the consolidation stress is brought back to the in-situ vertical stress, the void ratio is smaller for the low quality sample, i.e. $e_0(2) < e_0(1)$.
- Usually the rate of compression Cc will be reduced by larger disturbance, so $Cc(2) < Cc(1)$.

4.3. Effects on Shear Behavior

Many aspects of the shear behavior of soil are affected by disturbance. In this section, these effects will be presented based on the results of laboratory tests performed on Resedimented Boston Blue Clay at MIT. After being "disturbed" in the triaxial apparatus, these samples are subject to undrained shearing following the

steps outlined in Section 4.1. The following description compares the shear behavior of the specimens subject to different severities of disturbance.

4.3.1. Effect on Undrained Shear Strength

It has already been shown that the disturbance of tube sampling can be simulated by triaxial tests based on the principles of Ideal Sampling Approach, and the severity of disturbance is determined by the magnitude of $(\varepsilon_{zz})_{max}$. Figure 4.2 shows the stress-strain curves of these samples for OCR = 1 and OCR = 4 specimens. ISA±N means that the sample is "disturbed" based on the ISA and the magnitude of $(\varepsilon_{zz})_{max}$ is N%. The larger N is, the higher the disturbance severity. One can see that more disturbed samples have smaller strength.

4.3.2. Effects on Strain at Peak

Figure 4.2 also shows the effect of disturbance on the strain at peak stress. The strain at peak stress increases with increasing disturbance, both for normally and over-consolidated RBBC samples. For intact normally consolidated RBBC sample, the strain at peak stress is about 2%. After the disturbance of ISA±5, the strain at peak stress becomes 12 – 14%, which is a great increase.

This means that after disturbance, the soil becomes less brittle and more ductile.

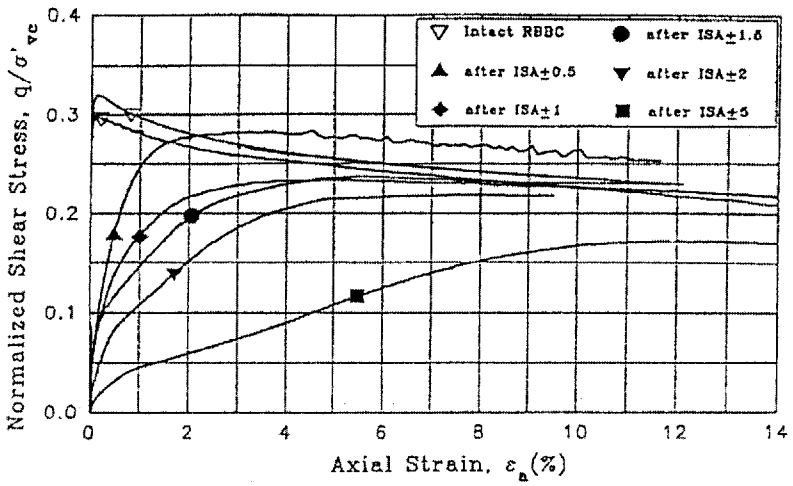

(a) Stress-Strain Curves for OCR =1 RBBC Samples

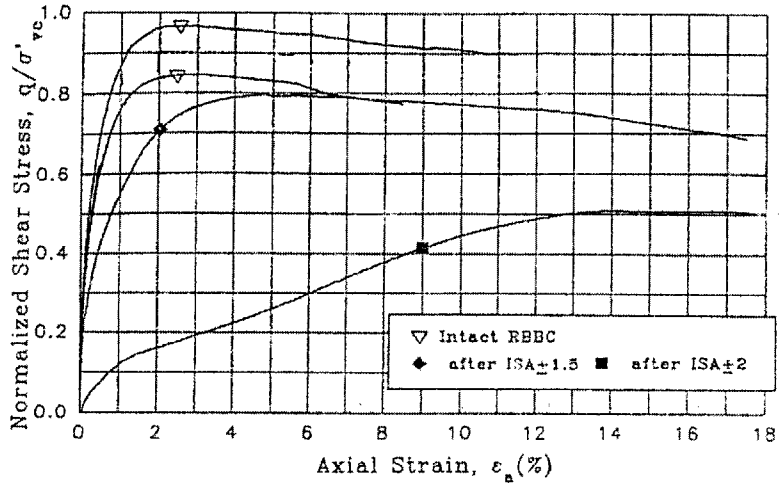

(b) Stress-Strain Curves for OCR = 4 RBBC Samples

Figure 4.2 Stress Strain Curves for Disturbed RBBC Samples (Santagata, 1994)

4.3.3. Effects on Soil Stiffness

Due to the very high non-linearity of soil, the stiffness of soil changes significantly during the shearing process. At very small strain levels, soil may have a linear stress strain relationship and its stiffness has the maximum value. The stiffness decreases with the increase of strain level and becomes 0 at the peak stress. To compare the stiffness of disturbed samples, E_{u50} is taken to be a representative average value. It is defined as the undrained modulus at 50% peak stress.

For normally consolidated samples, the ratio of Eu_{50} of disturbed samples ($(Eu_{50})_{Dist.}$) to that of intact samples ($(Eu_{50})_{Intact}$) is plotted against the peak axial strain $(\varepsilon_{zz})_{max}$ (shown as "Strain Cycle Amplitude ε_c") in Figure 4.3 (a). Note that since the scale for $(Eu_{50})_{Dist.}/(Eu_{50})_{Intact}$ is logarithmic, even very small disturbance has a very severe effect.

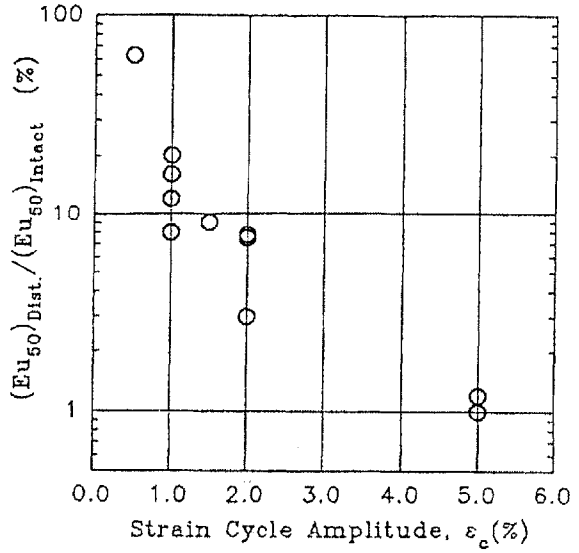

(a) Normally Consolidated RBBC

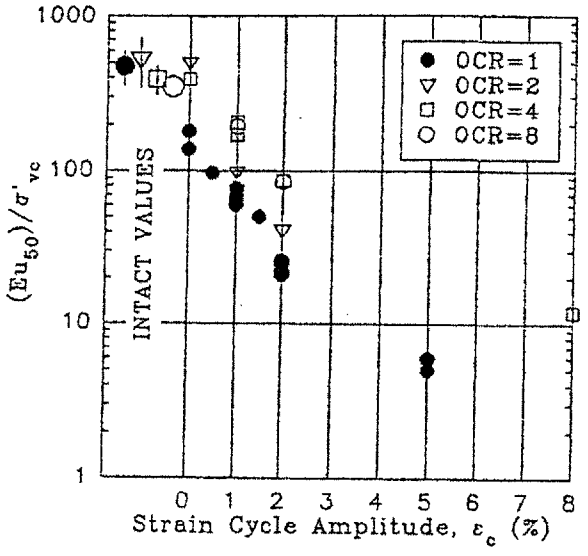

(b) Over-consolidated RBBC

Figure 4.3 Effects of Disturbance on Eu_{50} (Santagata, 1994)

Figure 4.3 (b) shows the change of Eu_{50} vs. disturbance for different OCR values. This time, Eu_{50} is normalized to the vertical effective stress of the "in-situ" stress state, σ'_{vc}. For a certain peak axial strain (again shown as strain cycle amplitude ε_c), the tendency is that the Eu_{50}/σ'_{vc} value for OCR = 1 RBBC is always the smallest, and that for OCR = 2 is the second smallest. The Eu_{50}/σ'_{vc} values for OCR = 4 and OCR = 8 RBBC almost coincide with each other and are the largest. Therefore, it can be concluded that increasing disturbance causes the Eu_{50} to decrease, and the rate of decrease is smaller for higher OCR soils.

Based on these different effects that disturbance exerts on soil samples, it can be concluded that the more disturbed soil becomes softer and more ductile. Strain softening behavior following peak stress gradually disappears with increasing disturbance. It is also worth pointing out that since ISA only covers the disturbance caused by tube sampling and subsequent stress relief, the real effects of disturbance are still larger.

4.4. Evaluation of Disturbance Severity

It has been shown that sampling disturbance has many effects on the behavior of the samples. According to what has been said about the effects of disturbance, the following methods can be used to evaluate the severity of the disturbance.

4.4.1. Visual Examination

Section 3.3.1 shows the possible fabric distortion that sampling disturbance may cause on sample. Therefore, the first step of identifying sampling disturbance and its severity is to examine the extruded sample carefully and see whether there is detectable fabric distortion. Sometimes the distortion is hard to detect when the sample is wet. Slices of the sample can be taken and air dried. Usually the fabric is revealed when the slice is half dried.

4.4.2. Radiography

Radiography has been used in MIT for more than 20 years to evaluate the quality of soil samples. As a non-destructive method, radiography allows one to evaluate the quality of sample without cutting the tube and extruding the sample. In addition, it can also capture features that cannot be detected by simple visual examination.

4.4.3. Initial Effective Stress Measurement

It has been shown that the more severe the disturbance is, the greater the effective stress loss for normally or slightly over-consolidated soil (Figure 3.20 (a)). Hence, the initial effective stress in the sample could be measured and compared with its in-situ effective stress, to judge the severity of disturbance.

4.4.4. Volumetric Strain at In-situ Stress

When the disturbed sample is brought back to its in-situ stress state, the void ratio is usually smaller than that of the in-situ value (Section 4.2). This means that volumetric strain has been generated. Consequently, the magnitude of this volumetric strain is also an indication of the severity of disturbance. In other words, the void ratio for low quality samples brought back to in-situ stress state is smaller than that of high quality samples, larger volumetric strain will indicate a more severe disturbance.

4.4.5. Compression and Shear Behavior

In general, a straight or slightly concave virgin compression curve and a fairly sharp transition between this curve and the initial recompression curve with a good definition of the preconsolidation pressure will usually indicate that the sample has not been subjected to appreciable disturbance.

For the shearing behavior, Hvorslev (1949) suggested that when the stress-strain curve is straight until the stress reaches 30 to 50 percent of the shear strength, it will usually indicate that the sample is not seriously disturbed. While a stress-strain curve which is curved from the start and which falls close to the curve for remolded soil usually indicates serious disturbance.

4.5. Summary

In this section, the effects of disturbance on the behavior of the samples were

studied. To simplify the disturbance problem, only the disturbance caused by tube sampling is considered by using the ISA principles. Examples were shown on how tube sampling disturbance changes the consolidation and shearing behavior of soil. Based on these studies, possible ways of evaluating the disturbance severity are proposed. Although the research presented in this section is simplified compared with the real situation where all the disturbance sources are present, it offers a first approximation and the methodology used may be also applicable to other materials like rock or shale.

In order to study the effects of disturbance, it is necessary to focus on specific disturbance sources which can be controlled to get different disturbance severity. The disturbances caused by the controlled sources are then simulated on samples whose internal states are identical, so that the difference between the disturbed states of these samples can be solely attributed to the difference of disturbance severity. Then laboratory tests with the same procedure can be performed on these samples to get their disturbed behavior. The differences of their disturbed behavior can also be solely attributed to the difference of disturbance severity.

In this section, the behavior of the disturbed specimens is obtained through different soil tests. As an alternative, their behavior can also be predicted by a behavioral model. The next section will show how one can obtain the effective stress paths and predict the disturbed behavior of the specimens based on a simple soil model.

5. Study Disturbance Problem in Soil with a Simple Soil Model

The simulation of tube sampling disturbance on RBBC specimens was described in Section 3.3.2.3. The effective stress path during the simulation of disturbance and the consequent effects on consolidation and shearing behavior were presented in Section 3.3.2.3, 4.2 and 4.3. All these results come from laboratory measurements. Based on the principles of ISA, the mechanism and effects of tube sampling disturbance can also be predicted by a soil model, which will be described here.

This section first introduces a simple behavioral framework of soil which was proposed by Hight (1993). "Imaginary tests" are then conducted whose outcomes are predicted based on this framework. The steps for an "imaginary test" are as following:

1) Imagine there is a sample whose initial state is known.
2) The centerline strain cycle (Figure 3.16) is imposed on this sample to simulate tube sampling disturbance. The effective stress path that the sample follows can be predicted by the behavioral framework. After imposing the centerline strain cycle, the sample is in its disturbed state, which is also known based on the framework.
3) The behavior of the sample in one-dimensional consolidation and shearing test can then be predicted by the framework based on the

disturbed state of the sample and its stress history.

Changing the magnitude of $(\varepsilon_{zz})_{max}$ of the centerline strain cycle in step 2), the effective stress paths and the behavior for samples with different disturbance severity can be obtained.

In this framework, the behavior of soil is governed by several surfaces in the triaxial stress space, namely the bounding surface and the yield surfaces.

5.1. Bounding Surface and Yield Surface

The bounding surface is the boundary of possible stress states of soft soil in undrained condition. The effective stress paths of the soil during undrained shearing cannot reach the area outside of the bounding surface. In this section, the bounding surface is defined in the normalized p′ – q space (Figure 5.1). Both p′ and q are normalized to a reference stress σ'_{ap}, which is the maximum vertical effective stress a point on the bounding surface could have. According to what has been said about the p′ – q stress space, the corresponding axial (or vertical) effective stress σ'_a of a point can be obtained by drawing a line with the slope of –1 from that point, and getting its intersection with the p′ axis (Figure 3.6). Specifically, σ'_{ap} can be obtained by drawing a line with slope –1 that is tangential to BS and taking its intersection with p′ axis (Figure 5.1). After normalization, σ'_{ap} becomes 1.0.

As shown in Figure 5.1, the bounding surface is composed of three parts: a very curved cap, which is convex to the top right direction; and the upper and lower boundary that are relatively close to straight.

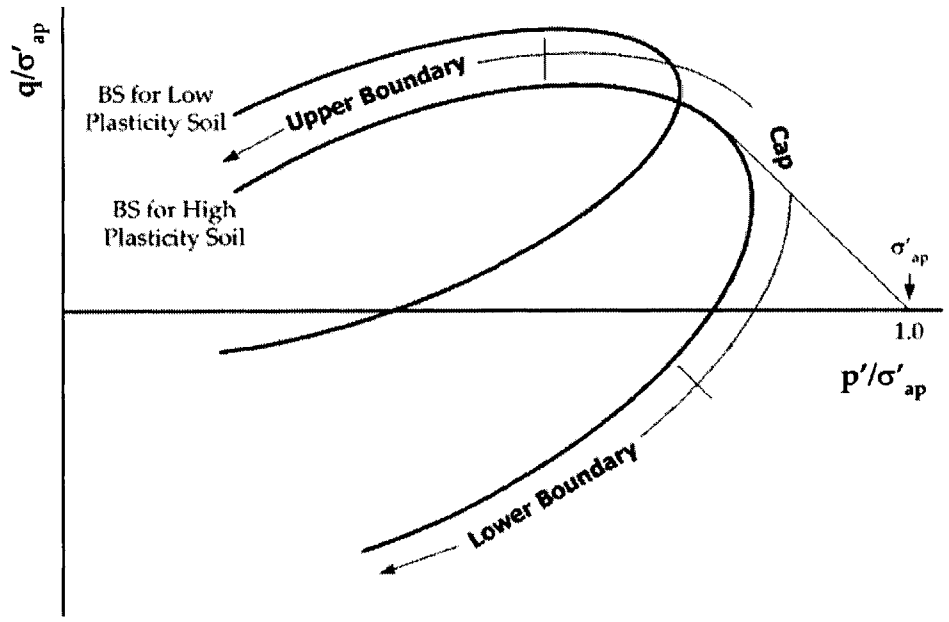

Figure 5.1 Effect of Soil Plasticity on Bounding surface

For reconstituted soils, the bounding surface can be defined using the effective stress paths from undrained triaxial compression and extension tests on K_0 normally consolidated soil. The bounding surface of reconstituted soil, which is called the intrinsic bounding surface, is a lower bound for the intact natural soil. The reason is that many post-depositional processes such as aging increase the strength of natural soil and expand the bounding surface. The process of sampling disturbance acts in the opposite direction, i.e. the structure of the soil is destroyed and the size of the bounding surface is reduced.

The position of the bounding surface is greatly affected by the plasticity of the soil. This is also illustrated in Figure 5.1. Compared with high plasticity soil, the bounding surface of low plasticity soil is higher but much narrower, i.e. the distance between the lower and upper boundary is much smaller. The lower boundary of the bounding surface swings more to the origin of the stress space.

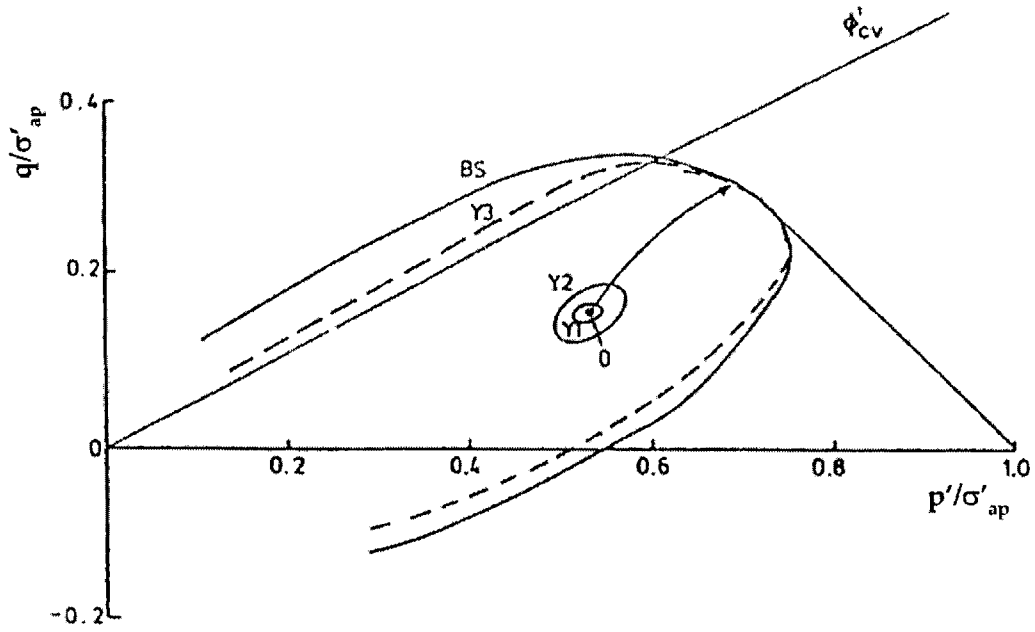

Figure 5.2 Yield Surfaces and Bounding Surface of the Framework (Hight, 1993)

In addition to the bounding surface, yielding surfaces are another important component of the behavioral model. The yield surfaces defined here are not exactly the same as the yield surfaces defined in the mechanics of plasticity. Instead of only one yield surface, three different yield surfaces are defined. They are shown in Figure 5.2 as Y1, Y2 and Y3.

Y1 and Y2 are two kinematic yield surfaces that follow the current stress state of the soil. Y1 marks the boundary to linear elastic behavior, and Y2 is the boundary to non-linear elastic behavior. Stress-strain behavior within Y1 is linear and reversible. Once the effective stress exceeds Y1 but not Y2, the behavior becomes non-linear but still reversible. Due to very high non-linearity and plasticity of soil, the sizes of both Y1 and Y2 are very small.

Y3 is the large scale yield surface (Jardine et al., 1991) that marks large scale fabric distortion. Y3 is located inside the bounding surface and its shape is very

similar to that of the bounding surface. It can be seen from Figure 5.2 that the cap of Y3 is very close to the cap of the bounding surface. The upper and lower boundaries of Y3 are at a certain distance inside the bounding surface but nearly parallel to those of the bounding surface.

The critical state line is also shown in Figure 5.2 (the straight line marked ϕ'_{cv}). After extreme shearing, most soil samples will reach their critical state and their effective stress paths finally end up on this line. ϕ'_{cv} stands for the friction angle of a soil sample in its critical state.

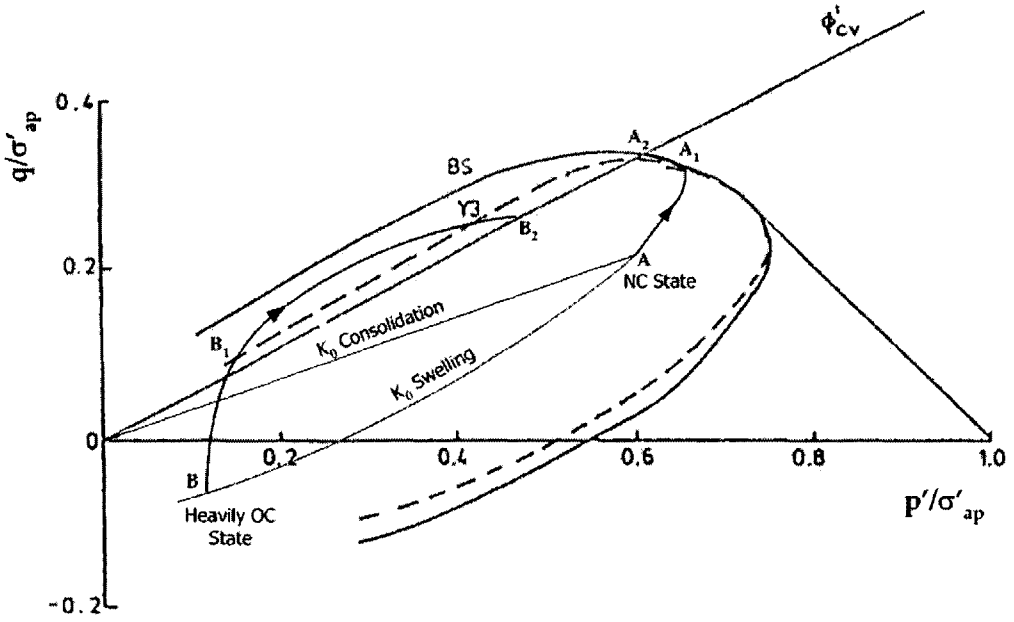

Figure 5.3 Typical Effective Stress Path for NC and Heavily OC Soil in Undrained Shear

Figure 5.3 illustrates the typical effective stress paths of normally consolidated soil and heavily over-consolidated soil with regard to the position of the Y3 surface and the bounding surface. Shearing is performed by increasing the vertical stress. As a result, the deviatoric stress q is increased and the stress paths shown in Figure 5.3 go upward from their starting points.

Normally consolidated soil have only experienced loading, therefore its in-situ stress state is located near the cap of the bounding surface, marked by Point A in Figure 5.3. During undrained shearing, the effective stress path first reaches the bounding surface at A_1. Since it cannot exceed the bounding surface, it goes along it and finally reaches the critical failure envelope at Point A_2. The cap of the Y3 surface and the bounding surface are very close to each other. Thus the point at which the effective stress path crosses the Y3 surface is very close to Point A_1.

For heavily over-consolidated clay, unloading has occured along the K_0 swelling line. The in-situ state has retreated so much that it is located between the upper and lower boundary at Point B. During undrained triaxial compression, the effective stress path first reaches Point B_1 where it crosses Y3 surface. Since it cannot exceed the bounding surface, it then changes its direction and proceeds between Y3 and the bounding surface, until finally reaches the critical state line at B2.

For both normally consolidated soil and heavily over-consolidated soil, the direction of the effective stress changes significantly after reaching Y3 surface.

5.2. Strain Limits for Different Surfaces

The strains that need to be mobilized in order for the effective stress path to reach different surfaces are quite different.

Y1 marks the boundary of linear elastic behavior. For normally consolidated soil, the strain limit for Y1 surface is very small. Hight (1993) proposed that in compression tests, $\varepsilon_{Y1} < 0.001\%$ for uncemented soil and $\varepsilon_{Y1} < 0.01\%$ for cemented soil.

Y2 is the limit for non-linear elastic behavior. According to Jardine et al. (1991), ε_{Y2} tends to increase with soil plasticity but generally is less than 0.04% for clays.

For normally consolidated soil, the strain that needs to be mobilized to reach the bounding surface ε_{bs} is similar to the axial strain at peak deviatoric stress (Hight, 1993), which is denoted ε_{ap}. The measurements of ε_{ap} for some clays with different PI and OCR are presented in Figure 5.4.

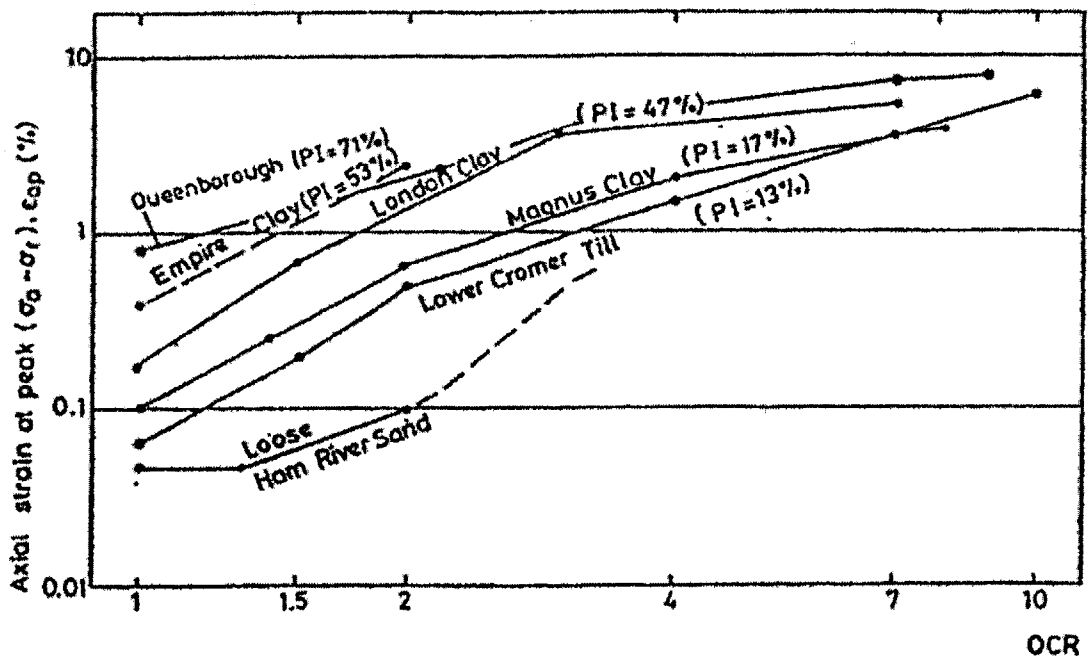

Figure 5.4 Strain at Peak Stress in Triaxial Compression Tests (Hight, 1993)

It is clear that ε_{ap} (thus ε_{bs}) increases with plasticity and OCR of the soils. For most of the soils presented in Figure 5.4, ε_{ap} is less than 1% when the soil is normally and slightly over-consolidated (OCR < 4). Therefore, it is reasonable to take 1% as the strain limit ε_{bs} for normally and slightly over-consolidated soils.

For heavily over-consolidated soil, usually the effective stress path intersects the Y3 surface and then goes between the Y3 surface and the bounding surface

(Figure 5.3). Hight (1993) proposed that for heavily over-consolidated soil, ε_{Y3} is roughly between 0.7% and 1%.

Generally, very large strains must be mobilized for the effective stress path to finally reach the critical state line (Point A_2 and B_2).

5.3. Predict Effective Stress Path during Tube Sampling

With the framework introduced above, the effective stress path that a centerline soil element follows during the tube sampling process can be predicted.

Suppose a soil element is located at the centerline of a tube when the tube sampling process starts. In Section 3.3.2.1, the strain history that this centerline soil element is going to experience has been introduced (Figure 3.16). Basically, it is a compression – extension – compression strain cycle, with the peak value of $(\varepsilon_{zz})_{max}$ in compression and $-(\varepsilon_{zz})_{max}$ in extension. The tube sampling process can be simulated by imposing this strain cycle on the centerline soil element. Based on the framework introduced in Sections 5.1 and 5.2, the response of this soil element when the strain cycle is imposed can be predicted, and the effective stress path it follows can be obtained.

In Section 3.3.2.3, the triaxial simulation of the centerline strain cycle on RBBC samples have been presented. The measured effective stress paths for RBBC samples of OCR =1 and OCR = 4 have been shown in Figure 3.20. The measured effective stress paths can be compared with the predicted ones for verification:

5.3.1. Predicted Effective Stress Path (NC Soil)

Figure 5.5 shows the predicted effective stress path of a centerline soil element that is normally or slightly over consolidated. Different strain levels are marked along the effective stress paths by numbers.

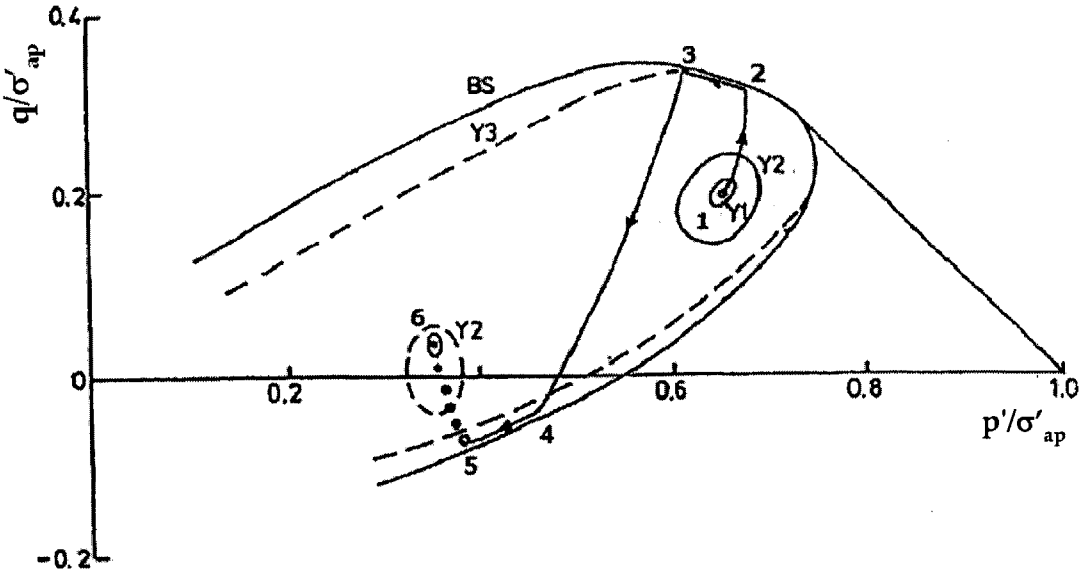

Figure 5.5 Predicted Effective Stress Path for NC and Slightly OC Soil (Hight, 1993)

The in-situ state of the sample is marked as Point 1. Denote the horizontal and vertical effective stress at this in-situ state to be σ'_{v0} and σ'_{h0}. For normally and slightly over-consolidated soil, σ'_{v0} is generally larger than σ'_{h0}.

When the tube starts to penetrate, compressive strain is first imposed on the centerline soil element. To generate this compression, the vertical effective stress σ'_v on the sample must be increased. From Figure 5.4, the strain limit of the bounding surface ε_{bs} for normally and slightly over-consolidated soil is less than 1%. However, from Figure 3.16, the peak axial strain $(\varepsilon_{zz})_{max}$ caused by tube penetration is roughly 1% for the B/t = 40 sampler. Given that the strain value in Figure 3.16 is only a lower

bound for real cases, it is reasonable to assume that in most cases $(\varepsilon_{zz})_{max} > \varepsilon_{bs}$. Therefore, the compression strain caused by tube sampling is large enough to bring the effective stress path to the bounding surface at Point 2. Then the effective stress path can only go along the bounding surface but cannot go outside of it. The effective stress goes along the bounding surface until it reaches Point 3, where the imposed strain reaches $(\varepsilon_{zz})_{max}$.

Following compression, extension strain increments are imposed by the tube sampling process. To generate this extension, the vertical effective stress σ'_v must be decreased. Due to the strong non-linearity of the soil, a major part of the compressive strain $(\varepsilon_{zz})_{max}$ may be plastic strain. When σ'_v is brought back to σ'_{v0}, the plastic strain cannot be recovered and the total strain of the sample is still in compression. However, the extension caused by tube penetration not only brings the total strain of the sample back to zero, but also brings it to $-(\varepsilon_{zz})_{max}$. Therefore, σ'_v must decrease strongly, and it is possible that σ'_h will have to increase substantially. As a result, the deviatoric stress $q = (\sigma'_v - \sigma'_h)/2$ will decrease and even become negative. The mean effective stress $p' = (\sigma'_v + \sigma'_h)/2$ should also decrease since the decrease of σ'_v is greater compared to the increase of σ'_h. The effective stress path thus moves down to within the bounding surface and to the left side.

During this extension, the soil specimen may or may not reach the lower bounding surface. This is determined by whether the magnitude of maximum extension strain $-(\varepsilon_{zz})_{max}$ is large enough to bring the effective stress to the lower boundary of the bounding surface. Suppose the effective stress path reaches the

bounding surface at Point 4 before the imposed extension strain reaches $-(\varepsilon_{zz})_{max}$, then it will still go along the bounding surface until the imposed strain reaches $-(\varepsilon_{zz})_{max}$ at Point 5.

Finally, a compression strain is imposed on the specimen, which means the vertical effective stress is again increased. The effective stress path goes up again and back to the inside of the bounding surface. At the end of this strain cycle, the stress state of the soil element ends at Point 6.

The prediction of this simple framework (Figure 5.5) can be compared with the effective stress path obtained from triaxial tests for normally consolidated RBBC (Figure 3.20 (a)):

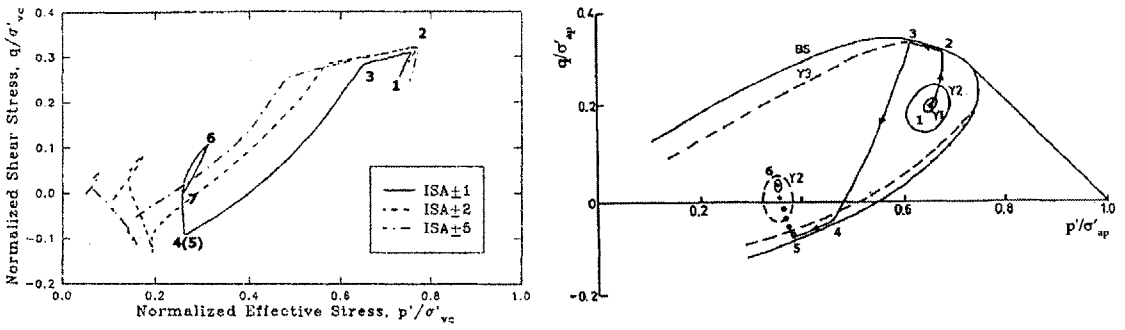

(a) Figure 3.20 (a) (b) Figure 5.5

Figure 5.6 Comparison between Effective Stress Paths in Figure 3.20(a) and Figure 5.5

The effective stress path in the simulation and the predicted effective stress path are quite similar at corresponding strain levels. Two differences can be identified though:

1) In Figure 3.20(a), a segment of the effective stress path that goes along the lower boundary of the bounding surface (Point 4→5 in Figure 5.5) cannot be identified. It is reasonable to say that the effective stress path of

normally consolidated RBBC in the simulation does not reach the bounding surface in extension. Therefore, Point 4 and Point 5 end up being the same point, as shown in Figure 3.20(a).

2) The predictions of the effective stress path do not include the final relief of deviatoric stress, which is shown in Figure 3.20(a) from Point 6 to Point 7.

5.3.1.1. Effects of Soil Plasticity

Suppose there are three centerline soil elements that are all normally consolidated but with different plasticity, non-plastic, low plastic and medium to highly plastic. The behavior framework can be used to predict the effective stress these soil elements follow when identical centerline strain cycles are imposed. Figure 5.7 shows the predicted effective stress paths. The bounding surfaces for these soil elements are shown by dashed lines. Based on the analysis in Section 5.3.1, Points A_N, A_L, and A_M mark the position on the effective stress paths where the compression strain reaches $(\varepsilon_{zz})_{max}$; Points B_N, B_L, and B_M mark the position on the effective stress paths where the extension strain reaches $-(\varepsilon_{zz})_{max}$.

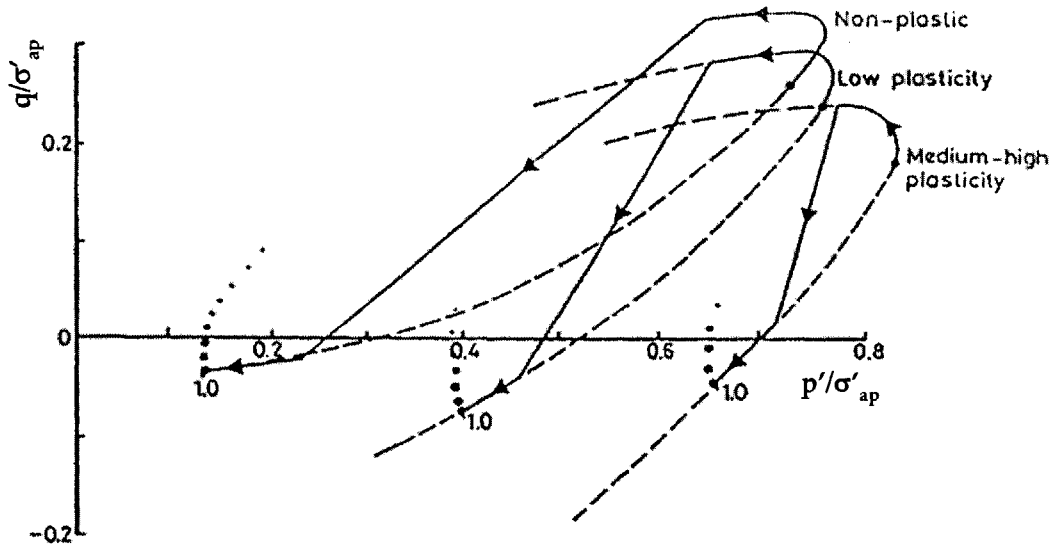

Figure 5.7 Effects of Soil Plasticity on Effective Stress Path (Hight, 1993)

The effects of soil plasticity on the behavior of soil can be explained below:

1. In Figure 5.1, it has been shown that the shape and location of the bounding surface is changed by soil plasticity. The bounding surface for low plasticity soil is higher and the lower boundary swings more to the origin of the stress space. The bounding surfaces shown in Figure 5.7 are constructed based on this conclusion.

2. The strain limit of the bounding surface ε_{bs} for low plasticity soil is much smaller than that of high plasticity soil (Figure 5.4). Since $(\varepsilon_{zz})_{max}$ is the same for the three centerline soil elements, the effective stress path of a soil element with low plasticity is more likely to be brought to the bounding surface (Point 2 in Figure 5.5) and travels longer (from Point 2 to Point 3 in Figure 5.5) on the bounding surface. This explains why the effective stress path for the non-plastic soil element travels the longest before reaching Point A_N (corresponding to Point 3 in Figure 5.5), and that of the medium-high plasticity soil element travels the shortest to reach A_M.

3. Compared with high plasticity soil, low plasticity soil is usually less

compressible. Therefore, to cause the same amount of volumetric strain ε_{vol}, the change of mean effective stress is much larger for low plasticity soil than for high plasticity soil. For a centerline soil element, the vertical strain ε_{zz} is dominant compared with the horizontal strain ε_{rr} as shown in Figure 3.15. Since the volumetric strain can be expressed by:

$$\varepsilon_{vol} = \varepsilon_{zz} + 2\,\varepsilon_{rr}$$

Thus:

$$\varepsilon_{zz} \approx \varepsilon_{vol}$$

As a result, if the vertical strain ε_{zz} is changed by the same amount for both high plasticity soil and low plasticity soil, the change of mean effective stress must be larger for low plasticity soil than for high plasticity soil.

In Figure 5.7, the vertical strain changes from A_N to B_N, from A_L to B_L, and from A_M to B_M are all the same, because in all cases the strain changes from $(\varepsilon_{zz})_{max}$ to $-(\varepsilon_{zz})_{max}$. Therefore, the mean effective stress change is the largest for the non-plastic soil element, and the smallest for the medium-high plasticity soil element. This explains why the slope from A_N to B_N is the smallest, while the slope from A_M to B_M is the largest.

From Figure 5.7, it is evident that for the same disturbance severity, low plasticity soil will have much larger decrease of mean effective stress than high plasticity soil.

5.3.1.2. Effects of Different Disturbance Severity

Other parameters being constant, changing disturbance severity also changes the effective stress path that the centerline soil element follows during tube sampling. This can also be predicted by the behavior framework.

Suppose there are three centerline soil elements which are originally identical. They are subject to the centerline strain cycle to simulate the disturbance of tube sampling. Since the tube sampling process is simulated by the centerline strain cycle, more disturbance means larger $(\varepsilon_{zz})_{max}$. The element disturbed with the least $(\varepsilon_{zz})_{max}$ simulates the behavior of a high quality sample. Increasing $(\varepsilon_{zz})_{max}$, the behavior of a medium quality and a low quality sample can be simulated. In the following discussion, we will call these element low quality element, medium quality element and high quality element for simplicity. Figure 5.8 shows the predicted effective stress paths during the simulation of low, medium, and high quality samples.

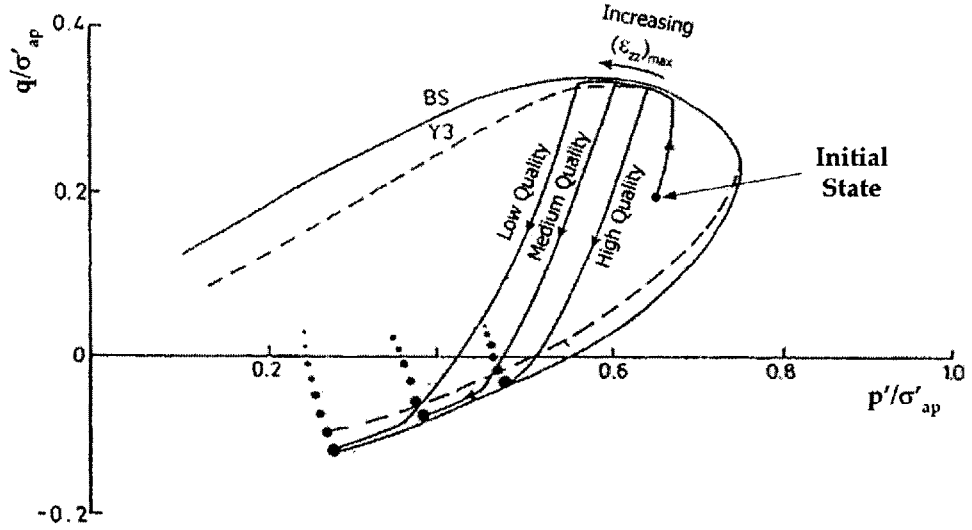

Figure 5.8 Effects of Severity of Disturbance (Hight, 1993)

Since the three elements originally are identical, they have the same bounding surface, yielding surfaces and the in-situ stress state (starting point of their effective stress paths). Increasing $(\varepsilon_{zz})_{max}$ increases the length the effective stress path travels on the bounding surface. As a result, the effective stress path of the low quality element travels the longest along the bounding surface, and is the left most among the three samples, while the effective stress path of the high quality element is the right most.

Since the three specimens are originally identical, they should have the same compressibility. Therefore, the effective stress paths are roughly parallel when the strain is changed from $(\varepsilon_{zz})_{max}$ to $-(\varepsilon_{zz})_{max}$. Since the effective stress path of the low quality sample is the left most, the intersection of it with the lower boundary of the bounding surface is still the left most. The intersection for the high quality sample is still the right most. After imposing the final compression strain, the relative positions of their effective stress paths remain unchanged.

For the soil elements that are originally at identical state, it is clear from Figure 5.8 that more severe disturbance causes larger mean effective stress loss.

5.3.2. Predicted Effective Stress Path (Heavily OC Soil)

The predicted effective stress path for heavily over-consolidated soil is shown in Figure 5.9. When the centerline soil element is heavily over-consolidated, its K_0 value may become larger than one, i.e. $\sigma'_{v0} < \sigma'_{h0}$. Thus the in-situ state shown in Figure 5.9 is below the p'-axis. Again a compression – extension – compression strain

cycle is imposed on this soil element. Its effective stress path is predicted based on the framework.

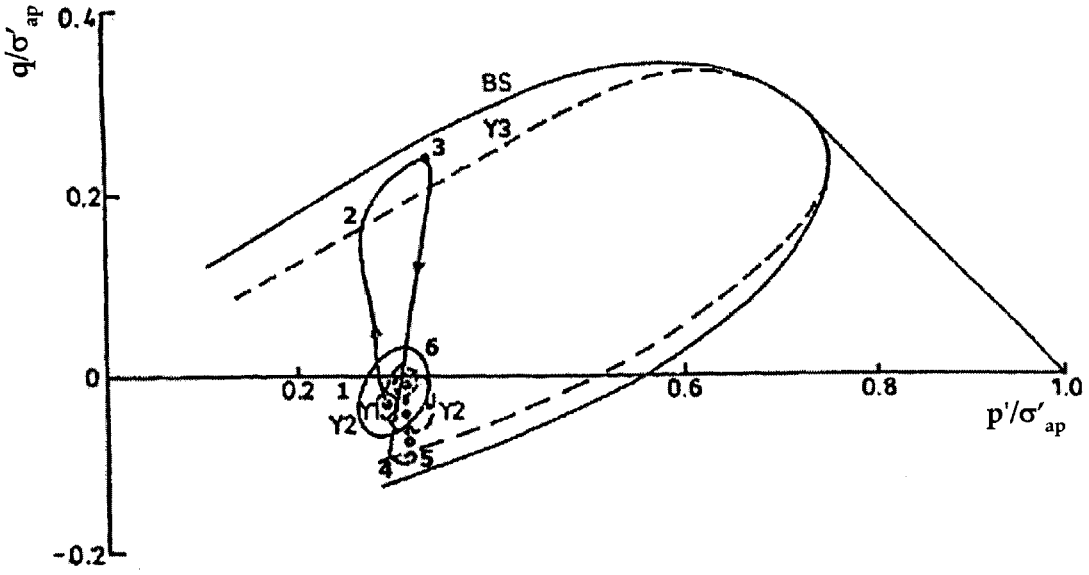

Figure 5.9 Predicted Effective Stress Path for Heavily OC Soil (Hight, 1993)

It has been shown in Figure 5.3 that typically, the effective stress path of heavily over-consolidated clay crosses Y3 and then proceeds between Y3 and the bounding surface. Since ε_{Y3} is usually between 0.7% and 1.0%, it is also surpassed by the maximum compressive strain $(\varepsilon_{zz})_{max}$, which is around 1.0%. Therefore, the compression strain $(\varepsilon_{zz})_{max}$ caused by tube sampling is large enough to bring the effective stress path of heavily over-consolidated soil to the Y3 surface (Point 2 in Figure 5.9). After reaching Point 2, the effective stress path travels between Y3 and the bounding surface until Point 3, where $(\varepsilon_{zz})_{max}$ is reached.

When extension strain is imposed from Point 3, the effective stress path may or may not reach Y3 surface on the lower side. Again it depends on if $-(\varepsilon_{zz})_{max}$ is large enough to bring the effective stress path to the lower side of Y3. If it reaches Y3 at Point 4 before the extension strain reaches $-(\varepsilon_{zz})_{max}$, as shown in Figure 5.9, it will

travel between Y3 and the bounding surface until the extension strain is $-(\varepsilon_{zz})_{max}$ (Point 5). The final compressive strain will bring the effective stress back to Point 6.

It can be seen from Figure 5.9 that the mean effective stress in the soil specimen may increase after tube penetration. This is entirely possible although in the test on OCR = 4 RBBC (Figure 3.20(b)) the mean effective stress decreases. However, both Figure 3.20(b) and Figure 5.9 show that the effective stress change of heavily over-consolidated soil after tube penetration is much smaller than the change for normally and slightly over-consolidated soil.

5.4. Prediction of Disturbance Effects on Mechanical Behavior

The simple framework of soil behavior can explain not only the effective stress path during tube sampling, but also some of the disturbance effects on the mechanical behavior of disturbed sample. This section describes the predictions the simple model can make regarding the effects of tube sampling disturbance on normally consolidated samples. The effects of tube sampling disturbance on the shearing behavior and consolidation behavior of RBBC samples have been studied by simulating the disturbance with triaxial tests (Section 4.3). The major effects for shear behavior are:

- Disturbance decreases the shear strength;
- Disturbance increases the strain at peak stress;
- Disturbance decreases the stiffness of the samples.

The major effects on consolidation behavior are:

- The pre-consolidation pressure measured on the low quality sample is smaller than that measured on the high quality sample;
- The initial recompression ratio tends to increase with disturbance;
- When the consolidation stress is brought back to the in-situ vertical stress, the void ratio is smaller for the low quality sample.
- Usually the rate of compression Cc will be reduced by larger disturbance.

These conclusions will be used in this section to check whether the predictions are correct. However, it should be noted that since the simple behavior model does not describe anything about stress strain relationships, its ability of predicting disturbance effects is limited. Although stress-strain curves are also shown in the following description, they are only provided since they were also in the graphs of the original papers. They actually cannot be predicted from the behavior model.

5.4.1. Shearing Behavior

The shearing behavior for samples subject to different levels of disturbance can be roughly outlined with the framework, as illustrated in Figure 5.10.

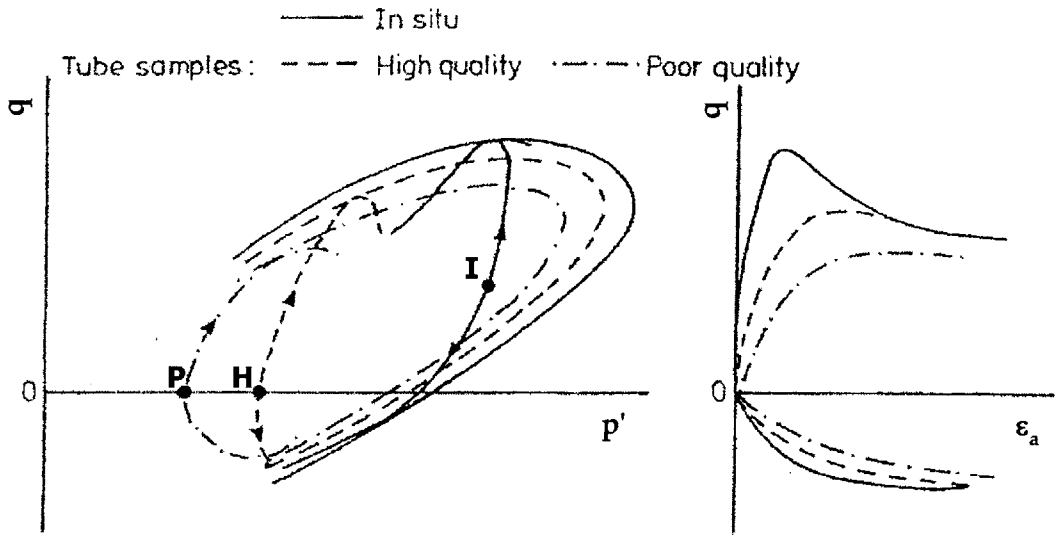

(a) Bounding Surfaces and Effective Stress Paths (b) Stress Strain Curves

Figure 5.10 Shearing Behavior Predicted by the Framework (Hight, 1993)

In Figure 5.10, the bounding surface, effective stress path, and the stress strain curve for the in-situ behavior are shown with solid lines. The dashed lines represent those of a high quality sample, and the dash-dot lines represent those of a poor quality sample.

Since the bounding surface shrinks with disturbance severity, the in-situ bounding surface is the largest, and the bounding surface of the poor quality sample is the smallest, as shown in Figure 5.10 (a).

Point I Figure 5.10 (a) represents the in-situ stress state, while Point H and Point P stand for the initial stress state of the high quality sample and the poor quality sample respectively. The initial stress state of the in-situ state is K_0 consolidated and $K_0 < 1$. Therefore it is located above p'-axis. For the disturbed samples, since the deviatoric stress has been relieved, their initial stress states are located on the p'-axis. Based on what has been said on the effective stress change

during sampling in Section 5.3.1.2, poor quality samples have lower initial mean effective stress than high quality samples. Hence both Point P and Point H are located on the p' axis but Point P is to the left of Point H.

If shearing is performed by increasing the axial stress, then the deviatoric stress q is increased and the stress paths go upward and reach their corresponding bounding surfaces. Since the intact soil element has the largest bounding surface, the point at which its effective stress path reaches the bounding surface is the highest. Similarly, this point is the lowest for the poor quality sample, and intermediate for the high quality sample. Therefore, the framework correctly predicts the decrease of strength with increasing severity of disturbance.

The possible stress-strain curves for the three cases are shown in Figure 5.10 (b). As has been said, they are not predictions of the behavior model.

Shearing can also be performed by reducing the vertical stress. In this case, the deviatoric stress q will be reduced and the effective stress paths are heading downward. Figure 5.10 also shows the effective stress paths and the corresponding stress-strain relationships for such shearing.

5.4.2. Shearing after Consolidation

Before shearing is performed, the samples are sometimes consolidated to their in-situ stress. Suppose both the high quality sample and the poor quality sample are brought back to the K_0 state before shearing, then all three cases share the same initial stress state (Point I in Figure 5.11 (a)). Again, the solid lines show the in-situ

behavior; the dashed lines are for a high quality sample; and the dash-dot lines are for a poor quality sample.

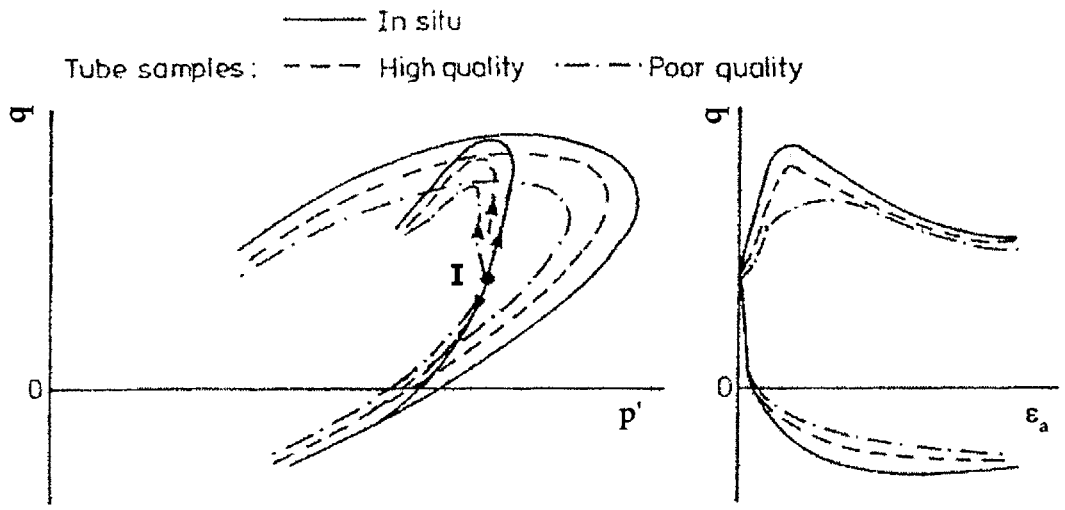

(a) Bounding Surfaces and Effective Stress Paths (b) Stress Strain Curves

Figure 5.11 Shearing Behavior after Consolidation to In-situ Stress (Hight, 1993)

Again we can see that the strengths of these three cases are determined by the size of the bounding surface. The intact soil element still has the highest strength, and the poor quality sample still has the lowest one. However, since the initial stress states of the samples are the same as the intact soil element, the differences between these strengths are reduced. Thus this framework predicts that by bringing the sample's stress state back to its in-situ stress state the detrimental effect of disturbance on strength can be reduced.

Figure 5.11 (b) shows schematically the stress-strain curves that correspond to the effective stresses shown in Figure 5.11 (a).

5.4.3. Compressive Behavior

This simple framework can also explain why high quality samples usually give higher pre-consolidation pressure σ'_p. For one-dimensional compression, σ'_p is the dividing point between recompression and virgin compression (Figure 4.1). It can be seen that when vertical effective stress exceeds σ'_p, the slope of the curve suddenly becomes steep, indicating a decrease of stiffness. Therefore, σ'_p can be treated as the yield stress during one-dimensional compression. The location of σ'_p should roughly be at the intersection of the effective stress path and Y3 surface.

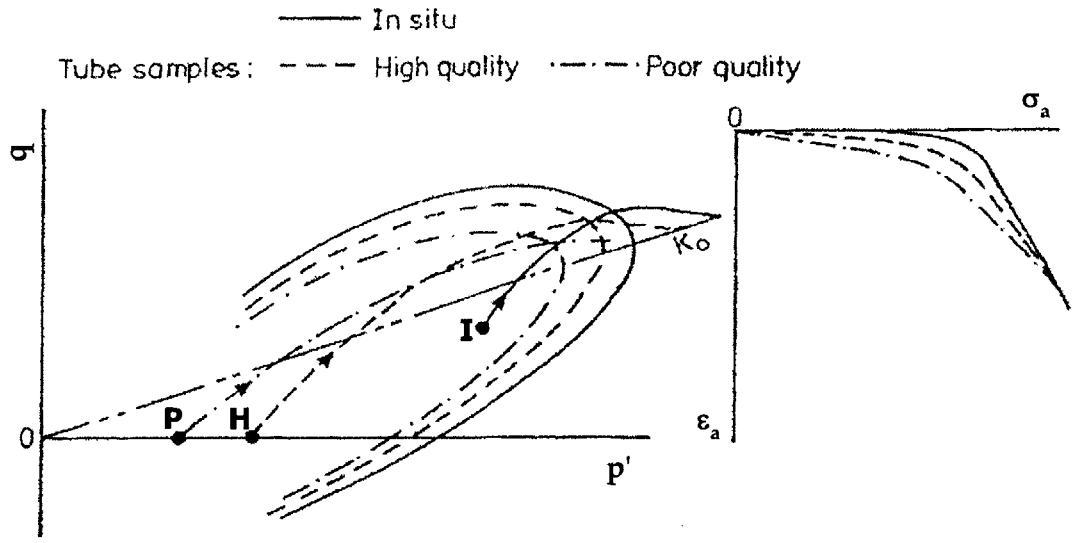

(a) Bounding Surfaces and Effective Stress Paths (b) Compression Curves

Figure 5.12 Prediction of Compression Behavior (Hight, 1993)

Figure 5.12 shows the one-dimensional compressive behavior of the intact soil element and the disturbed samples. Since drainage occurs in consolidation, the effective stress paths cross the boundary surfaces. From Figure 5.12, it can be seen that the place where effective stress paths in one dimensional compression cross the

bounding surface is on the cap of the bounding surface, where Y3 surface and the bounding surface are very close to each other. Therefore, σ'_p can be roughly determined by the intersection of effective stress path with the bounding surface. Since high quality samples have a larger bounding surface, it follows that σ'_p thus determined is higher for high quality samples. As a result, this framework correctly predicts the relative magnitudes of σ'_p for samples with different levels of disturbance.

Possible compression curves are shown in Figure 5.12 (b). Again, they are not predictions of this simple model.

5.5. Summary

This section shows how to study the mechanism and effects of disturbance by means of "imaginary tests" based on a simple soil model. The imaginary tests are performed based on the principles of the ISA, i.e. the only disturbance source is tube sampling.

It can be seen that the framework works very well in predicting the effective stress path a sample follows during the disturbance. It even predicts the effective stress paths of samples with different plasticity. Clearly, the laboratory tests did not show this particular result since they are all performed on the same soil. However, in terms of the disturbance effects, the ability of the framework seems to be limited. This is because the framework does not describe the stress-strain relationship of soil.

6. Sample Disturbance in Rock

Disturbances that may be caused during rock sampling are discussed in this section. The term "rock" is defined as materials that are very strong and brittle so that failure is caused mostly by the development and coalescence of cracks. Rock Mechanics, which studies the crack initiation and propagation, is the technical domain considering these materials.

In some extreme cases, for example very high confining pressure or very high temperature, rock may also show a ductile behavior. However, in conventional laboratory tests on rocks, neither the confining pressure nor the temperature will be high enough to induce this ductile behavior. Therefore, it is reasonable to assume that ductile behavior does not play a role in the sampling process and in the sampling disturbances that we are going to examine in this section.

Sampling in rocks is much different from sampling in soil due to the basic difference of their properties. Some of the important differences are:

- Due to the very high strength of rocks, it is no longer possible to push a sampling tube into this material. Rocks are usually sampled by coring.
- Samples of rock may be taken from thousands of meters depth in the ground, which is much deeper than conventional soil sampling. The in-situ stresses in rock can be very complex because of the great variety of geological features and tectonic effects.
- As said above, the rock matrix is usually strong and brittle. The sample

disturbance of rock usually does not involve yielding and plastic flow of the rock matrix, but involves the propagation and development of cracks. Therefore, crack opening and propagation is the direct and most important disturbance effects.

The development of this section also follows the structure outlined in Section 2.4. However, before the disturbance mechanisms can be analyzed, it is necessary to first introduce the samplers and procedures of rock coring.

6.1. Coring Process

Due to the very high strength of rock, it is impossible to push a sample tube into the rock mass to get samples. Most of the time, samples of rock are taken by coring. The coring devices can be classified as Single Tube Core Barrel and Double Tube Core Barrel (Under very rare circumstances, triple tube core barrels may also be used).

A typical single tube core barrel is shown in Figure 6.1 (a). It has the following components from top to bottom: Core barrel head, Tube body, Drilling bit. Hardened metal teeth are equipped at the end of the drill bit. During drilling, the core barrel is rotated and the metal teeth cut into the rock to isolate a rock core from the rock body. Borehole fluid is fed in through the head of the core barrel, to take out the heat, lubricate the teeth-rock interface and take away the cuttings. It flows inside the tube until it reaches the metal teeth, where the cuttings are taken away. Then the borehole fluid flows to the outside of the tube for circulation.

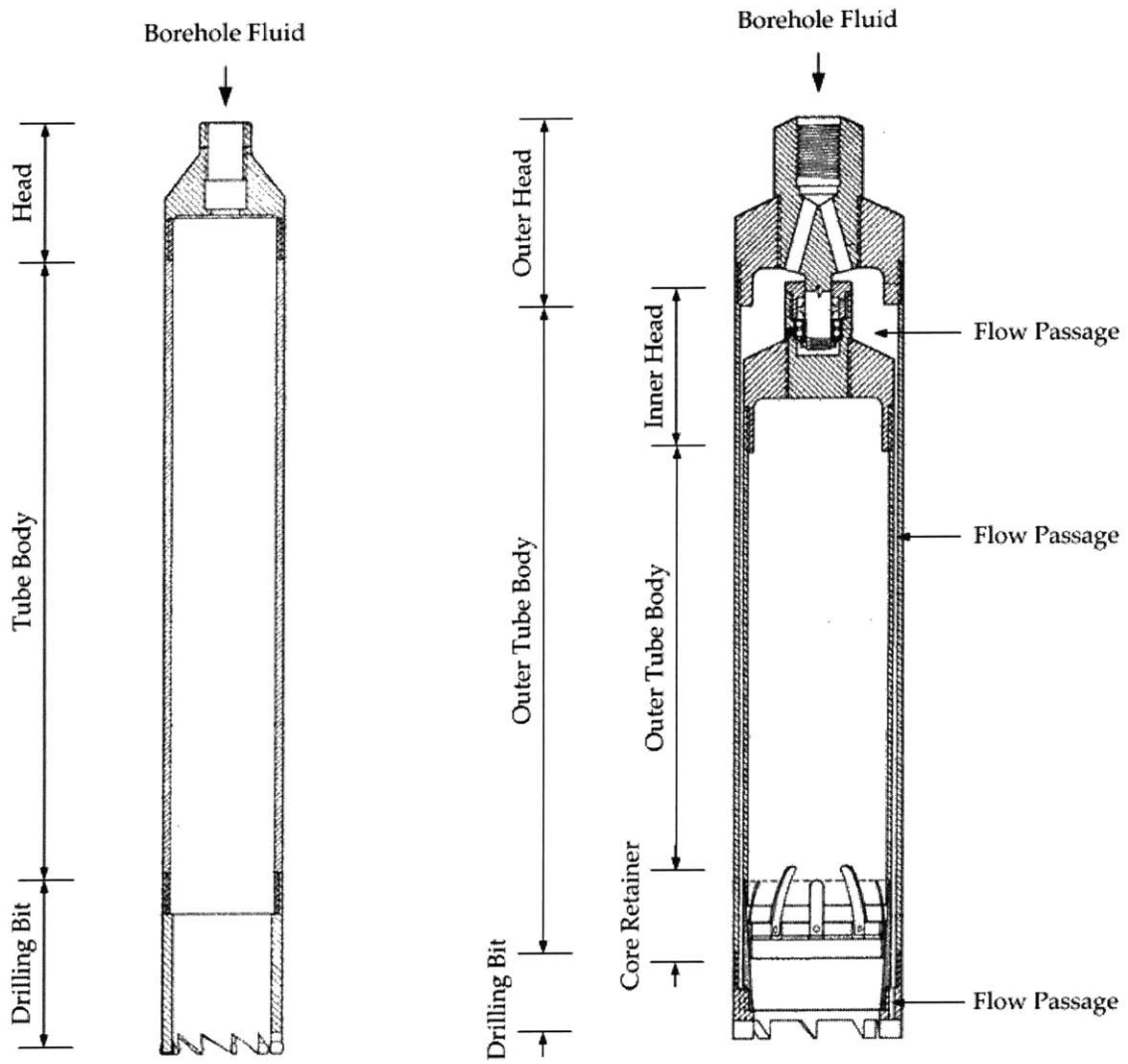

(a) Single Tube Core Barrel (b) Double Tube Core Barrel

Figure 6.1 Single & Double Tube Core Barrel (Hvorslev, 1949)

Single tube core barrels are easily manufactured and operated. The rate of progress is generally higher than for a double tube core barrel of equal outside diameter. Satisfactory cores can be obtained with single tube core barrels in sound and uniform rock body. However, when it is used to core stiff soil, soft or broken rock, the material can be seriously disturbed by the cutting and breaking effect of the metal teeth. In many cases the core may be broken up and partly removed by the circulation of borehole fluid (Hvorslev, 1949). In addition, such materials are often

prone to slaking or swelling in contact with free water, which is a source of serious disturbance for soft rock and stiff soil.

To reduce the disturbance to the core by borehole fluid, and to minimize the breaking and cutting effect on the core, double tube core barrels are often used. The structure of a double tube core barrel is shown in Figure 6.1 (b). The inner tube has a swivel head and it is connected with the outer tube by a ball bearing. Therefore, it does not rotate with the outer tube so that the torsion that the inner tube might apply to the core is very small. The outer tube is also composed of tube head, tube body and drill bit. During drilling, the borehole fluid flows through the space between the inner and the outer tube (flow passage marked in Figure 6.1 (b)), washes the cuttings away at the drilling teeth, and finally flows to the outside of the outer tube for circulation. The contact between the core and the borehole fluid is thus minimized.

In addition to drilling bits with metal teeth, diamond drilling bits are also quite often used in core drilling. The old diamond drilling bits were manufactured by embedding diamond stones in a blank drilling bit (i.e. drilling bit without teeth). Nowadays, polycrystalline diamond coating is widely used in the drilling bit technology. This is an approximately 100nm thick coating of polycrystalline diamond with super-high hardness. The polycrystalline diamond coating has improved both the performance and the longevity of the drilling bits. The principle of metal and diamond drilling bits is the same, i.e. while the coring barrel is rotating, the diamond drilling bit grinds the rock below it and thus isolates the rock core.

Different types of drilling bits may be used for different rocks. According to Hvorslev (1949), a small number of relatively long teeth are preferable for coring of soft and sticky formations which tend to ball up the bit; while a large number of small teeth or cutters provides a greater rate of progress and causes less disturbance of the material when coring in hard formations. Diamond drilling bits are another alternative in hard rocks. It provides a greater rate of progress in hard rock. By grinding the rock instead of breaking, smaller disturbance may be achieved. Therefore, it is possible to use the diamond drilling bit to get cores with smoother surface, larger length and smaller diameter. However, there appears to be no systematic guidance regarding the selection of different drilling teeth.

6.2. Mechanism of Disturbance in Rock Coring

6.2.1. In-situ State of Rock

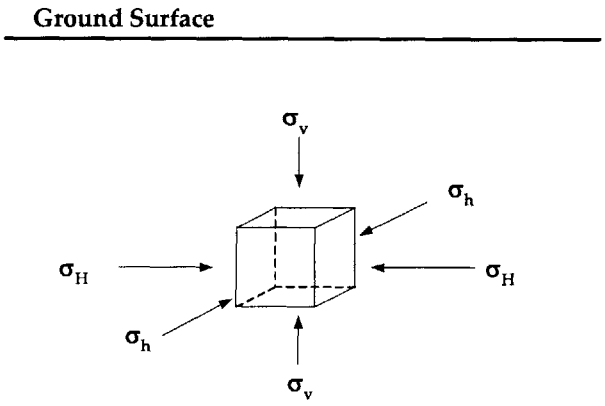

Figure 6.2 In-situ Stress State in Rock

Natural rock in its in-situ state can be subject to very complicated stress fields due to the great variety of geological conditions. A crude but useful approximation is

to assume that the vertical stress σ_v is one principal stress and that the other two principal stresses are horizontal (Figure 6.2). However, the two horizontal principal stresses may or may not be equal to each other. They are therefore denoted σ_h and σ_H. In natural rock formations, the horizontal stresses are frequently much larger than the vertical stress.

6.2.2. Making a Borehole

Suppose there is a rock element at certain depth in the natural rock body, a borehole must be made to reach this rock element. The borehole can be made by coring, or non-core drilling (cone, percussion, etc.).

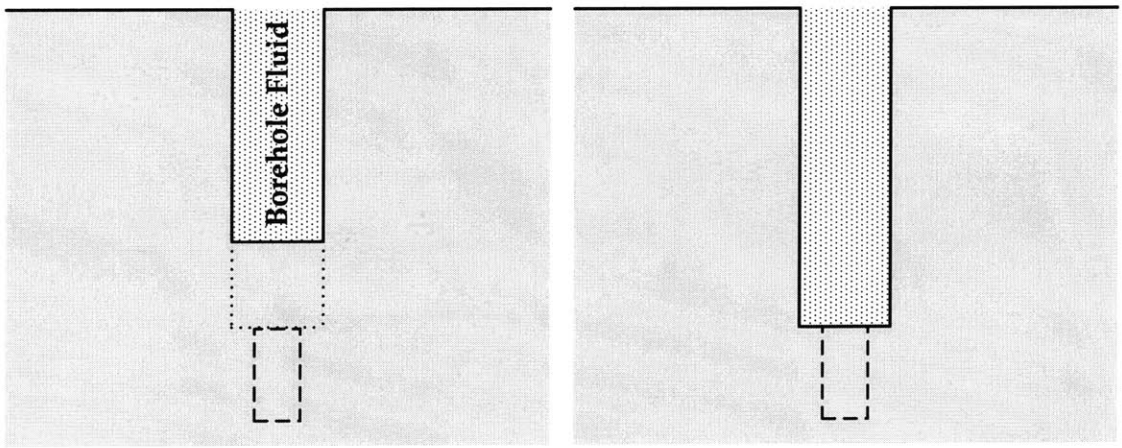

(a) Advancing of Borehole (b) Bottom of Borehole Reaches the Sample

Figure 6.3 Making a Borehole in the Ground

When the borehole is made and the overlying rock is taken away, the stress on the wall and the bottom of the borehole is relieved. Due to this stress relief, the stress field around the borehole will be disturbed and stress concentration will occur. An example of stress concentration on the wall of the borehole is shown in Figure 6.4. The in-situ stress field is supposed to be the one shown in Figure 6.2. If the borehole

is long enough, then the stress state in a cross-section at the middle of the borehole can be considered as plane strain state (Figure 6.4 (a)). For simplicity, the two horizontal principal stresses are supposed to be equal, i.e. $\sigma_h = \sigma_H$. In a cylindrical coordinate system, this means $\sigma_r = \sigma_\theta$ for the in-situ stress state. When the borehole is made, stress concentration occurs at the wall of the borehole (Figure 6.4 (b)). If the behavior of the rock is linear elastic, σ_θ is doubled and σ_r becomes zero. The effect of stress concentration decreases with the radial distance from the borehole and finally converges to the original stress field in the far field.

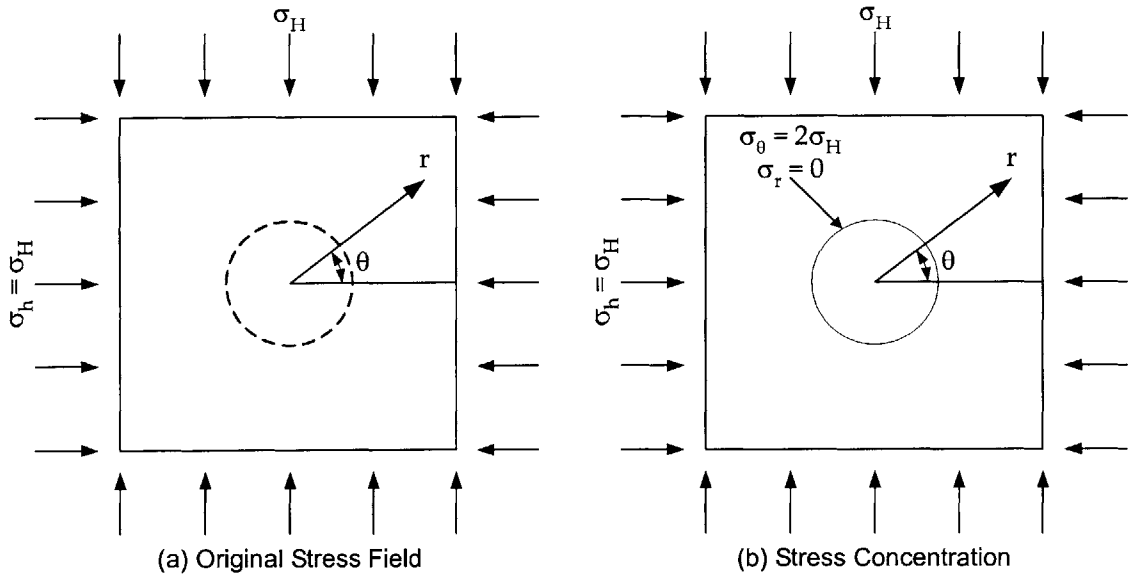

Figure 6.4 An Example for Stress Concentration

The simple example shown in Figure 6.4 assumes that σ_h is the same as σ_H, and the σ_θ caused by stress concentration at the wall of the borehole is still compressive stress. However, when there is a large difference between σ_h and σ_H, σ_θ may become tensile (Obert and Duvall, 1967). Since the tensile strength of rock is usually relatively small, this might cause crack opening in the surrounding rock and further change the in-situ stress field in the rock.

Suppose the rock element ABCD (Figure 6.5) is to be cored, and the borehole has advanced to the top of it, then the stress state in element ABCD will be disturbed by the stress relief on the wall of the borehole. In addition, the element is also disturbed by the stress relief at the bottom of the borehole, as shown in Figure 6.5.

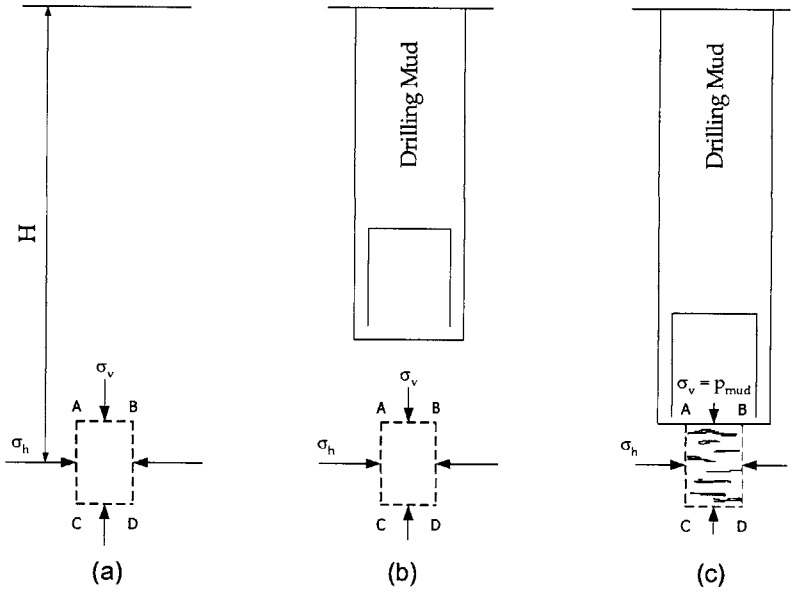

Figure 6.5 Total Stress Relief

Figure 6.5 (a) shows the in-situ stress state of the element. When the borehole is advancing toward this rock element, the total vertical stress, σ_v, is decreased due to the removal of overlying rock (Figure 6.5 (b)). At the time the bottom of the borehole reaches the top of this rock element (Figure 6.5 (c)), σ_v is decreased to the mud pressure p_{mud} at the bottom of the borehole (suppose mud pressure is less than the original overburden pressure). The change of total horizontal stress σ_h is very complicated and difficult to predict. However, due to the stress concentration around the borehole wall, it is likely that σ_h will be increased. Therefore, the magnitude of deviatoric stress ($\sigma_h - \sigma_v$) becomes larger and larger during the stress relief. At some point, horizontal cracks may start to develop in the rock element

ABCD. This may cause core discing if the horizontal cracks are developed across the whole cross-section of the element.

Apart from the stress relief, the element ABCD may also be disturbed by the vibration of drilling or coring, by the load the drilling machine or coring bit exerts on the rock body. The temperature of the sample may be changed due to the heat generated by the drilling or coring process, or simply by the temperature of drilling mud. This temperature change may induce thermal stresses in the surrounding rock and disturb the stress state of the sample. If the rock contains chemically active components, then chemical effects may also come in and disturb the sample.

6.2.3. Coring Process

When the borehole advances to the top of the sample, a core barrel is used to remove the rock beside the sample and collect the sample (Figure 6.6).

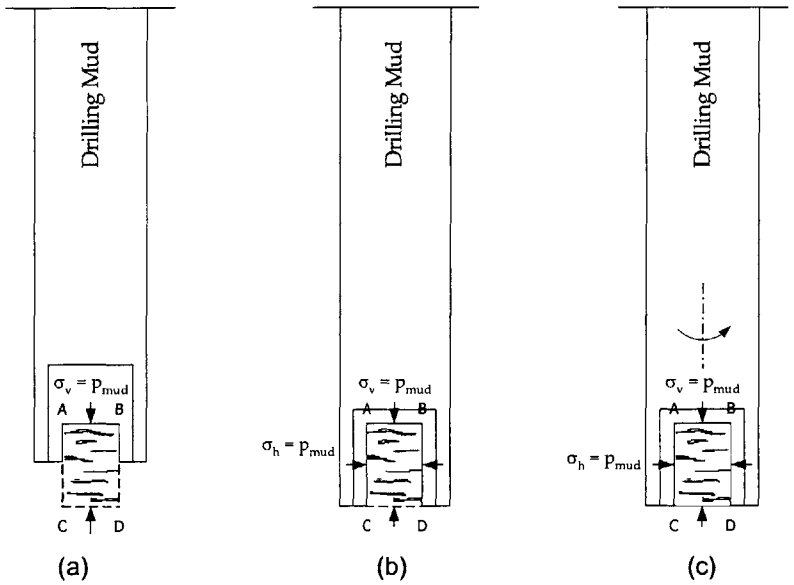

Figure 6.6 Stress Relief on a Rock Element during Coring

As has been described in Section 6.1, the coring bit will break and remove the

rock around the rock core (Figure 6.6 (a)). During this cutting process, vibration and the load exerted by the coring bit may disturb the sample. Temperature change and chemical effects may again come in.

When the rock around the element ABCD is removed, stress relief will cause the stress field around the cutting to change. Since the geometry of the surface on which the stress is relieved is very complicated, numerical analysis seems to be necessary. To study this stress field change, Santarelli (1991) reported the results of a numerical simulation based on a finite element program named PETRO-CESAR (Humbert, 1989). The numerical model used in the simulation is shown in Figure 6.7.

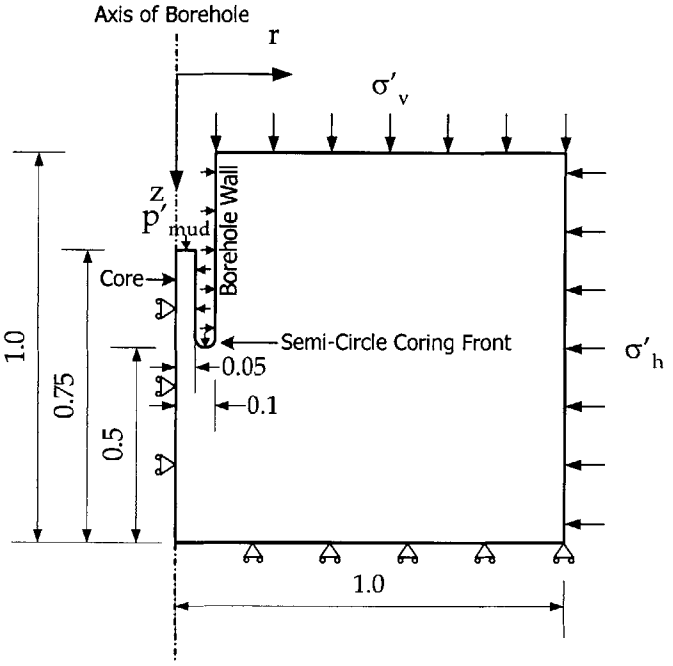

Figure 6.7 Numerical Models for FEM Simulation (Santarelli et al, 1991)

The following simplifications are made in this numerical model:

- The coring bit is supposed to have a semi-circle shape. Hence the coring front it produces also has a semi-circle shape, as indicated in Figure 6.7.
- In this model, great simplifications are made regarding the in-situ stress

state. It is assumed that $\sigma'_v = \sigma'_h = \sigma'_H$. It is also assumed that the mud pressure, p_{mud}, balances the pore pressure in the formation p_{form}, i.e. $p'_{mud} = p_{mud} - p_{form} = 0$, so that hydrodynamic and transient effects can be ignored. Under this stress state, the problem becomes axi-symmetrical with regard to the borehole axis. A cylindrical coordinate system is used so that the z-axis is located in the axis of the borehole, as shown in Figure 6.7.

- The constitutive model for the rock is isotropic and elastic. No yielding and plastic flow is involved.

Although the model has been much simplified, meaningful results can be obtained. A zone of tensile stress and a zone of high compressive stress are identified from the results of the finite element program. They are shown by shaded areas in Figure 6.8. Two points M_t and M_c marks the location of maximum tensile and compressive stress.

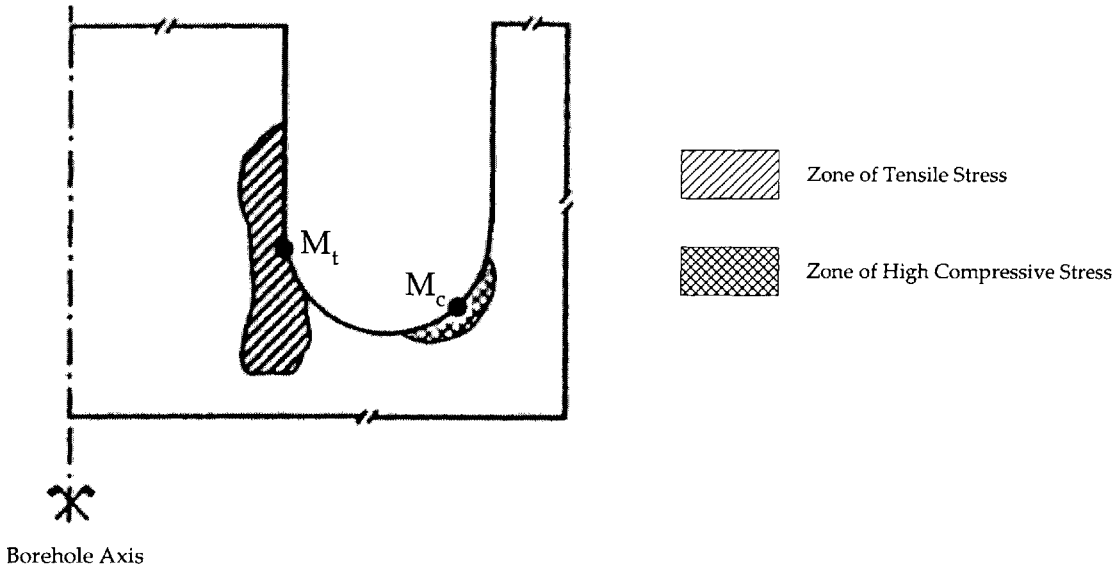

Figure 6.8 Stress Concentration around the Coring Front (Santarelli et al., 1991)

The tensile stress zone is located at the external surface of the core, just beside

the coring bit. According to the analysis shown in Figure 6.4, σ'_θ at the wall of the borehole should be twice the original value due to stress concentration. The high compressive stress zone in Figure 6.8 marks the area where σ'_θ is even larger than this value.

Due to the low tensile strength of rock, the presence of an area with tensile stress may cause serious disturbance to the core. Small tensile stresses can cause tensile cracks on the surface of the core, or cause the existing cracks to propagate. Large tensile stresses may break the whole cross-section of the core. The geometry of the coring front is a very important factor in determining the shape and location of the tensile stress zone, and the magnitude of the tensile stress.

The simulation that was described above is for an isotropic in-situ stress state. More detailed simulations have been conducted by Santarelli et al. (1991) for anisotropic in-situ stress states and different mud pressure. The results of these simulations are presented below.

6.2.3.1. Effects of In-situ Stress Anisotropy

The numerical models used in the simulation of in-situ stress anisotropy are almost the same as the one shown in Figure 6.7. However, it is assumed that in the in-situ stress state, $\sigma'_h = \sigma'_H = K_0 \cdot \sigma'_v$. An anisotropic in-situ stress state means that $K_0 \neq 1$. Suppose the maximum tensile stress in the tensile stress zone is $(\sigma_t)_{max}$, it has been found that the stress concentration factor $(\sigma_t)_{max}/\sigma'_v$ is directly related to the K_0 value in the in-situ stress state. The results of these simulations are plotted in Figure

6.9 to show the variation of $(\sigma_t)_{max}/\sigma'_v$ versus the in-situ K_0 value.

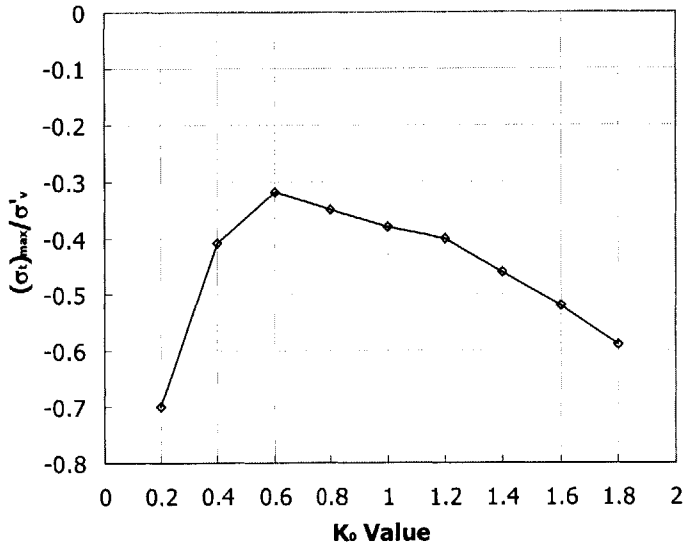

Figure 6.9 Maximum Tensile Stress in the Core vs. Stress Anisotropy (Santarelli et al, 1991)

Figure 6.9 clearly shows that the magnitude of $(\sigma_t)_{max}/\sigma'_v$ is smallest when K_0 is around 0.6, where the magnitude of $(\sigma_t)_{max}$ is slightly greater than 30% of σ'_v. The magnitude of $(\sigma_t)_{max}/\sigma'_v$ increases when K_0 deviates from 0.6, i.e. the magnitude of $(\sigma_t)_{max}$ becomes larger. As has been said, usually K_0 is much larger than 1 in natural rock. According to the trend shown in Figure 6.9, the magnitude of $(\sigma_t)_{max}$ may approach the magnitude of σ'_v or even exceed it.

6.2.3.2. Effects of Mud Pressure

The maximum tensile stress $(\sigma_t)_{max}$ is also dependent on the mud pressure during coring. Again, numerical simulations are performed based on the basic configuration shown in Figure 6.7 to show the effects of different mud pressures. In these simulations, it is assumed that the in-situ stress state is isotropic (i.e. $\sigma'_v = \sigma'_h = \sigma'_H$), but the mud pressure is varied. The stress concentration factors $(\sigma_t)_{max}/\sigma'_v$

obtained from the simulations vary with the mud pressure. The values of $(\sigma_t)_{max}/\sigma'_v$ are plotted against corresponding p'_{mud}/σ'_v in Figure 6.10.

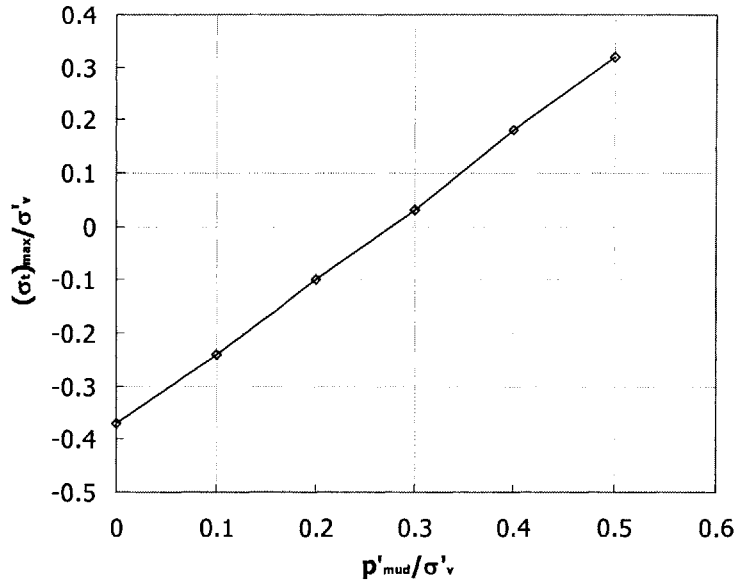

Figure 6.10 Maximum Tensile Stress in the Core vs. Mud Over-pressure
(Santarelli et al, 1991)

Figure 6.10 shows quite clearly that increasing mud pressure will decrease the magnitude of $(\sigma_t)_{max}$. When $p'_{mud}/\sigma'_v \approx 0.28$, the magnitude of $(\sigma_t)_{max}$ becomes 0, which means no tensile stress is generated by stress concentration and the zone of tensile stress disappears. Further increase of the mud pressure ensures that only compressive stress is acting on the core during coring process.

If the anisotropy of the in-situ stress field and the mud pressure are both fixed, the value of $(\sigma_t)_{max}/\sigma'_v$ is also fixed based on the simulation discussed. In this case, the magnitude of $(\sigma_t)_{max}$ depends solely on the magnitude of σ'_v. Since σ'_v usually increases with depth, $(\sigma_t)_{max}$ also increases with depth.

When the element is isolated from the rock body and enters the core barrel (Figure 6.6 (b)), a torque is applied on the sample to break its end and detach it from

the underlying rock body (Figure 6.6 (c)). Since the torque is used to break the rock, its magnitude might be very large. Therefore, the torque itself can be a source of disturbance.

6.2.4. Moving the Sample to the Ground Surface

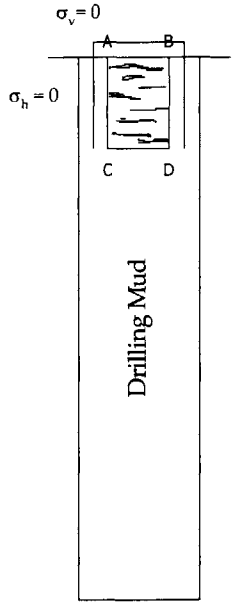

Figure 6.11 Moving the Sample to the Ground

When the element is detached successfully, it is then subject to an isotropic stress state, in which $\sigma_v = \sigma_h = p_{mud}$ (Figure 6.6 (c)). The core must be moved to the ground surface by pulling it up in the borehole (Figure 6.11). During this operation, the total stress on the core is always equal to the mud pressure p_{mud}, which decreases with the elevation of the core. Suppose the pore fluid pressure in the rock core is u when it was at its original depth H. This u may be very large if H is very large. The effective stress in the element can be expressed as:

$$\sigma'_v = \sigma'_h = p_{mud} - u$$

Usually the rock core is pulled up very quickly and hence p_{mud} decreases very quickly. However, the pore pressure u that was locked in the rock core may not be able to decrease as quickly if the rock element has low permeability. It thus follows that for rock cores taken from large depth and with small permeability, the effective stress keeps on decreasing during the pulling up. At some point the effective stress may become tensile and causing crack development or failure in the core.

Gas exsolution may also disturb the sample. Pore fluids in rock often contain dissolved gas which starts to exsolve when the fluid pressure is decreased to some point. The rapid decrease of pore pressure during pulling up may allow gas to exsolve very quickly. The exsolved gas can form gas bubbles, the volume of which continues to increase with further decrease of pore fluid pressure. If the matrix of rock is not strong enough, structural damage can be caused by the expansion of these gas bubbles.

6.2.5. Sample Transportation and Storage

After the core is retrieved from the borehole, disturbance can still occur during transportation and storage.

During the transportation of the rock cores, they may be subject to random bumping and shaking. The temperature of the core may be changed, which in turn is determined by weather conditions. Both these disturbance sources can change the stress state in the core.

If the cores are not properly sealed, they will be in contact with air and

disturbance may be introduced. The pore water in the core can evaporate and negative pore pressure may develop. Chemical reactions may occur between the rock core and the air. Different kinds of rocks may require different handling processes and storage environments to minimize disturbance. Some recommendations for core handling process are presented by the API (Skopec, 1991).

6.2.6. Sample Preparation

As has been described in Section 2.2.5, sample preparation is different for different tests. In order to obtain specimens with suitable geometry, the rock cores can be cut by a lathe or by a laboratory core drill. Different sample preparation methods will introduce different disturbances.

6.2.7. Identification of Important Disturbance Source

Based on the descriptions in the previous sections, a certain understanding has been gained about the disturbance mechanisms in rock sampling. Therefore it is possible now to identify the relative importance of the disturbance sources.

It is well known that rocks have relatively small tensile strength, and they are vulnerable to crack opening when subject to tensile stresses. Therefore, the disturbance sources that can generate tensile stress in the rock core can be considered as important ones. The descriptions of Section 6.2.2, 6.2.3 and 6.2.4 clearly show that stress relief is capable of causing tensile stress in the core. Consequently, stress relief can be identified as an important disturbance source.

6.3. Effects of Disturbance on Rock Behavior

This section will describe a testing program that was performed on the Lac du Bonnet granite (Martin et al., 1994; Eberhardt et al., 1999) to show the effects of disturbance on the mechanical behavior of rock. This testing program was performed on the samples of Lac du Bonnet granite by the Underground Research Laboratory (URL), which is owned by Atomic Energy of Canada Limited. This test program is based on the assumption that stress relief is the major disturbance source. Before introducing how this assumption is applied in this testing program, it is necessary to first introduce the site conditions.

6.3.1. Site Descriptions

According to Martin et al. (1994), the URL site where the granite cores are taken is situated in southeastern Manitoba. It is located within the Lac du Bonnet granite batholith, which is considered to be representative of many granitic intrusions of the Precambrian Canadian Shield. The batholith, dated as late Kenoran age, lies in the Winnepeg River plutonic complex of the English River gneiss belt of the western Superior Province. The batholith is a relatively undifferentiated massive prophyritic granit-granodiorite. The massive, medium to coarse grained prophyritic granite is relatively uniform in texture and composition through the entire batholith, although locally it displays subhorizontal gneissic banding. The URL shaft intersects two major thrust faults that dip about 15° – 30° southeast. They are shown as the Fracture Zone 2 and Fracture Zone 3 in Figure 6.12, and their splays are referred to

as Fracture Zone 2.5 and 1.9.

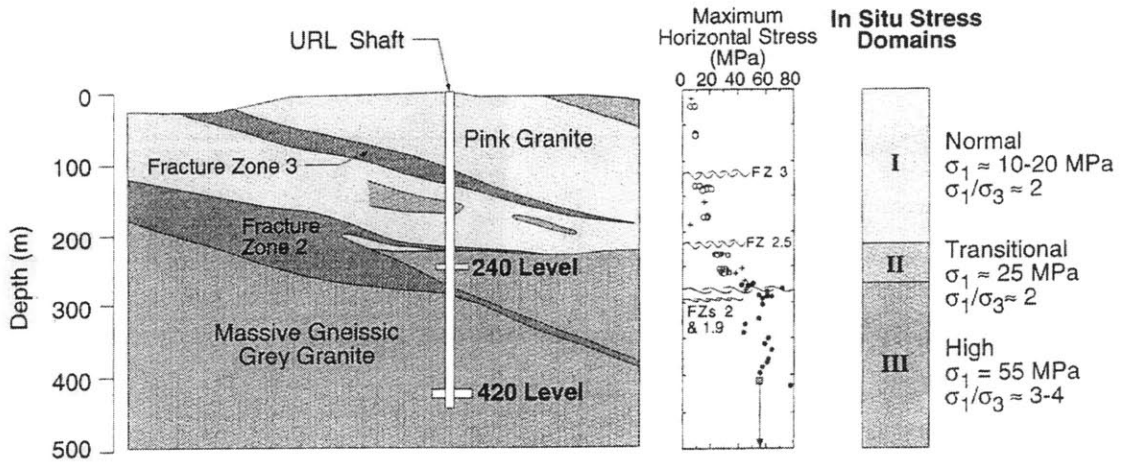

Figure 6.12 Site Overview and Stress Domains (Martin et al, 1994)

According to the in-situ stress level, three stress domains have been defined. The separation of the stress domains and their in-situ stress levels are also shown in Figure 6.12. In all three stress domains, the major principal stress is horizontal, i.e. $\sigma_1 = \sigma_H$ and $\sigma_3 = \sigma_v$.

Stress Domain I extends from the surface to Fracture Zone 2.5 at the depth of 200m. The maximum horizontal stress in this stress domain is within the range of 10 ~ 20MPa and increases with depth. The in-situ stress state is anisotropic, with $K_0 = \sigma_H/\sigma_v \approx 2$. In Stress Domain II, which is located from depth 200m to about 300m, the maximum horizontal stress is around 25MPa, and also increases with depth. The anisotropy of this stress domain also has $K_0 = \sigma_H/\sigma_v \approx 2$. Stress Domain III occupies depth 300m through depth 500m, where the maximum horizontal stress is around 55MPa and does not vary very much with depth. The anisotropy of the in-situ stress state is stronger, with $K_0 = 3 \sim 4$. Based on these data, the horizontal and vertical stress levels of these three stress domains are listed below (σ_v is calculated from σ_H

and K_0):

Table 6.1 In-situ Stress Level of the Stress Domains

Stress Domain	K_0	Maximum Horizontal Stress σ_H (MPa)	Vertical Stress Level σ_V (MPa)
I	2	10~20	5~10
II	2	25	12~13
III	3~4	55	14~18

6.3.2. Methodology of the Testing Program

The testing program is based on the assumption that stress relief is the major disturbance source. Generally, in a rock formation, the in-situ stress level increases with depth. Therefore, a rock core taken from deeper location will have larger stress relief. According to the analysis of Section 6.2.2, 6.2.3, and 6.2.4, larger stress relief means:

- The deviatoric stress ($\sigma_h - \sigma_v$) will be larger when the borehole reaches the top of the sample (Figure 6.5);
- The maximum tensile stress $(\sigma_t)_{max}$ will be larger during coring of the rock sample (Figure 6.8);
- The reduction of mud pressure when the core is moved to the ground surface will be larger (Figure 6.11).

If the rock formation is very uniform, e.g. the grain size, crack density, mineral composition are all very uniform and do not change with depth, then it is reasonable to say that the ability of two rock cores taken from different depths to withstand disturbance is the same. Finally, one could reach the conclusion that deeper rock cores will have larger disturbance provided that:

- In-situ stress level increases with depth;
- The rock formation is uniform.

For the URL site described in 6.3.1, it is evident from Table 6.1 that the in-situ stress level increases with depth. However, for such a natural rock formation, the condition of uniformity is a big question. In this testing program, at least two parameters of the samples were checked to ensure uniformity.

The first parameter is the in-situ P-wave velocity. Since P-wave velocity is very sensitive to crack density, it can be used as a good indicator of in-situ crack density distribution with depth. Figure 6.13 shows the measured in-situ P-wave velocity variation with depth.

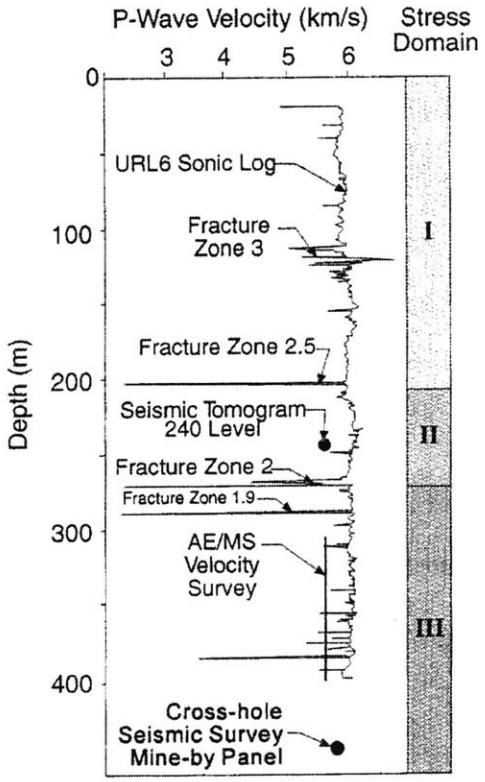

Figure 6.13 In-situ P-wave Velocity Measurements (Martin et al, 1994)

The results shown in Figure 6.13 are actually a compilation of the results of several

in-situ velocity borehole surveys carried out at the URL site. It can be seen from the graph that different geophysical techniques are used, including Sonic Velocity Log, Seismic Tomogram, and Cross-hole Seismic Survey. All geophysical techniques give almost constant P-wave velocity with depth except in the fracture zones. Therefore, it is reasonable to conclude that the in-situ crack density is relatively uniform along the depth.

The other parameter used to check uniformity is the grain size and mineral component of rock cores. It has been found that the rock cores taken from the Lac du Bonnet site mainly have two grain sizes. Most of the cores have an average grain size of 3mm, while the rest have an average grain size of 1mm (Eberhardt et al., 1999). Although their mineralogy is similar, it has been noticed that cores with smaller grain size are less vulnerable to disturbance. Therefore, only cores with 3mm grain size are tested in this testing program.

With these measures, it is then reasonable to say that the cores taken from deeper locations will be subject to larger disturbance due to stress relief effects. In this testing program, the rock cores are grouped by the stress domains shown earlier. Cores of Stress Domain I have the smallest in-situ stress level and the smallest disturbance. Cores from Stress Domain III have the largest in-situ stress level and disturbance severity. Cores from different stress domains are tested, and the difference of their behaviors can then be correlated with the disturbance severities.

The testing results presented in this thesis are collected from two different research reports: Martin et al (1994) and Eberhardt et al (1999). Eberhardt's research

is performed on samples from depths of 130m, 240m and 420m to represent the three stress domains. In Martin's research, the cores are only grouped by stress domains, and the specific depths of them are unavailable. Besides, there are other differences between these two research reports, which are listed below:

Table 6.2 Differences between the Two Researchs

	Martin et al. (1994)	Eberhardt et al. (1999)
Borehole Diameter	75mm	-
Sample Diameter	45mm	61mm
Length/Diameter	2.5	2.25
Loading Rate	0.75MPa/s	0.25MPa/s

The effects of disturbance on the properties of the rock cores from different stress domains are compared to see how these properties are changed by increasing disturbance.

6.3.3. Effects of Disturbance

6.3.3.1. Visual Evidence of Sample Disturbance

The visual evidence of sample disturbance includes cracking and core discing. When the disturbance effects are slight, they cause the formation of smaller cracks in the sample. These smaller cracks are called microcracks hereafter. Microcracks are distributed throughout the sample.

When the disturbance effects are very severe, core discing may occur. Core discing has been observed in core samples ranging in diameter from 18mm to 1.25m in the samples from Lac du Bonnet granite. According to Martin (1994), these discs were observed immediately upon core retrieval and are believed to have formed

during the sampling process. During the drilling of the 1.25m diameter core, the discing occurred continuously as the core barrel advanced several millimeters. The thickness of the discs varies from a few millimeters (grain size) to several centimeters depending on in-situ stress magnitudes. Core discing has been observed only in Stress Domain III and near fracture zones. This indicates the higher level of disturbance in Stress Domain III. An example of core discing is shown in Figure 6.14.

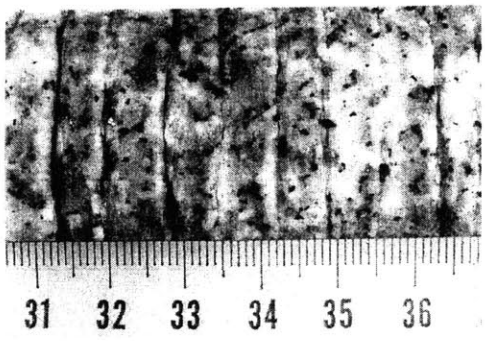

Figure 6.14 An Example of Core Discing (Martin et al, 1994)

6.3.3.2. Density of Microcracks in Samples

Thin sections have been obtained from the samples retrieved from different depths. SEM analysis is performed on these thin sections to measure the density of observed microcracks. The results of these measurements are shown in Table 6.3.

Table 6.3 Density of Microcracks in Samples (Eberhardt et al, 1999)

Sample No.	Depth (m)	Minimum Count (cracks/mm^2)	Maximum Count (cracks/mm^2)	Average Count (cracks/mm^2)
1	130	0.005	0.01	0.0075
2	240	0.01	0.05	0.03
3	420	10	20	15

Table 6.3 shows that the sample from 420m depth has developed much more microcracks than samples from 130m and 240m depths. Based on the measurements

of in-situ P-wave velocity (Figure 6.13), it can be shown that the in-situ crack density is almost constant with depth. Therefore, the variation of crack density with depth shown in Table 6.3 must be caused by sample disturbance. This confirms that the disturbance severity increases with depth.

6.3.3.3. P-wave Velocity

Based on the field measurement of P-wave velocity shown in Figure 6.13, the in-situ P-wave velocity can be roughly taken as 5900m/s for the depths. Eberhardt et al. (1999) also reported the in-situ S-wave velocity, which is roughly 3440m/s.

The P-wave and S-wave velocities on samples taken from 130m, 240m and 420m depths have also been measured with the AE transducers across the samples. The measured results are shown in Table 6.4, together with the average microcrack densities at these depths (from Table 6.3).

Table 6.4 Measured P-wave & S-wave Velocities on Samples from Different Depths (Eberhardt et al, 1999)

Depth (m)	Average Crack Density (cracks/mm^2)	P-wave Velocity V_P (m/s)	S-wave Velocity V_S (m/s)	V_P/V_S
In-situ	-	5900	3440	1.72
130	0.0075	4885 (±190)	3030 (±115)	1.61
240	0.03	4445 (±295)	2905 (±85)	1.53
420	15	3220 (±100)	2160 (±55)	1.49

Comparing the P-wave velocity measured in the laboratory and in-situ, it can be seen that the P-wave velocity measured on the samples is consistently lower than the in-situ P-wave velocity and decreases with depth. Since the velocity of P-wave is smaller in the air than in the rock matrix, the decrease of P-wave velocity then indicates more opening of microcracks. Therefore, the decrease P-wave velocity is

consistent with the increase of microcracks with depth.

A similar statement is also applicable to the decrease of S-wave velocity with depth. It seems the S-wave velocity is not as sensitive to disturbance as P-wave velocity. Although it also decreases with increasing depth, the rate of decrease for the S-wave velocity is smaller. The ratio of P-wave velocity V_P to S-wave velocity V_S decreases with increasing depth.

Figure 6.15 plots the P-wave and S-wave velocities vs. the logarithm of the average crack density. It can be seen that the relationships are close to linear.

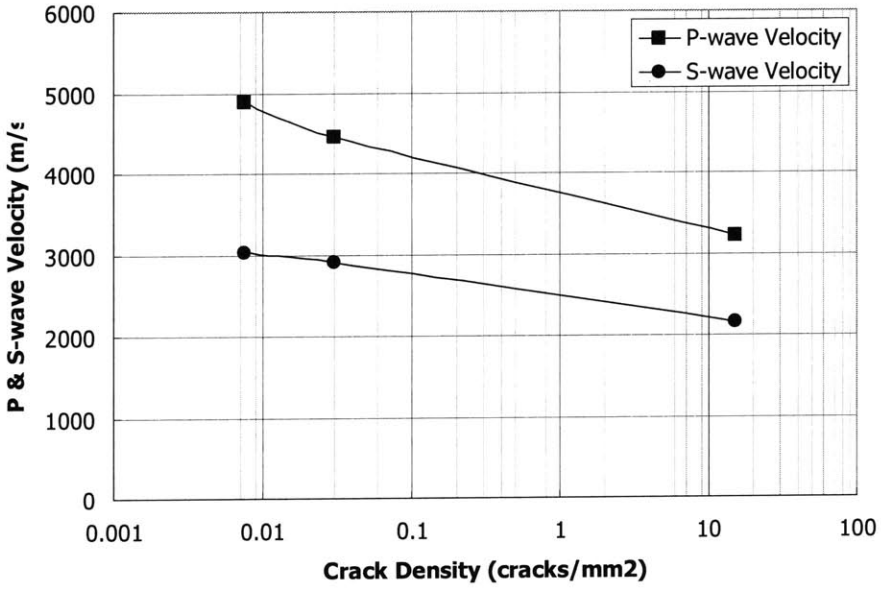

Figure 6.15 Correlation of P-wave and S-wave Velocity with Crack Density

6.3.3.4. Threshold Stresses in Uniaxial Compression

The behavior of a typical rock sample in the uniaxial compression test is illustrated in Figure 6.16. On the left of Figure 6.16, the axial stress – axial strain behavior is plotted; the axial stress – volumetric strain behavior is plotted on the

right. It can be seen that the behavior of the rock sample can be divided into several stages that are separated by so called "threshold stresses". These stages, together with the threshold stresses, are briefly discussed below.

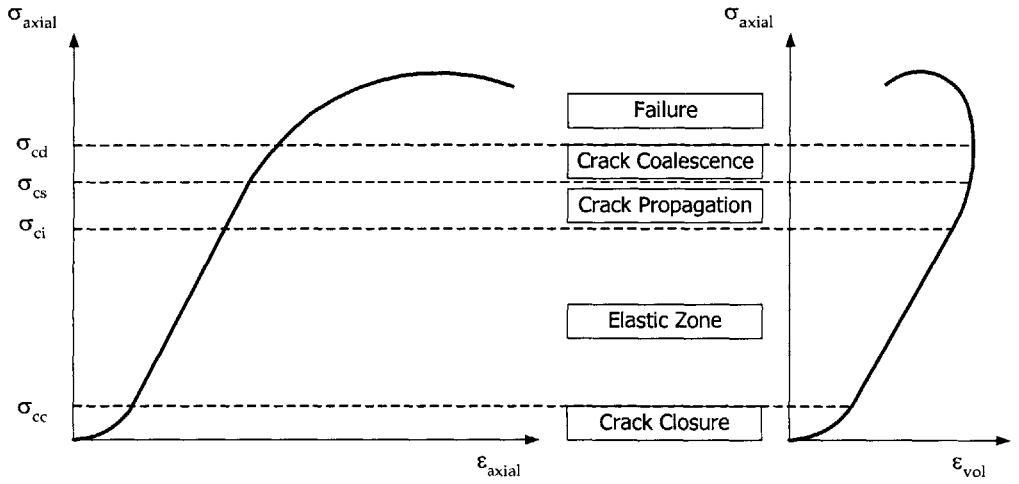

Figure 6.16 Typical Rock Sample Behavior in a Uniaxial Compression Test

- Crack Closure. The curvature of the curves at the beginning is caused by the closure of the existing cracks in the sample. Strictly speaking, this curvature can also be caused by the seating problem of the testing apparatus. However, Figure 6.16 presents a conceptual model rather than a real test curve. Thus it is assumed that the curves show the real behavior of the sample and no testing problem is considered. The limit axial stress for this stage is called crack closure stress σ_{cc}.
- Elastic Zone. The axial stress σ_{axial} is now larger than σ_{cc}, so that all the open cracks have been closed. Increasing the magnitude of σ_{axial} may cause the two sides of some of the cracks to slide against each other. However, the displacement caused by sliding can be recovered upon unloading. The overall behavior of the sample is linear elastic. The limit

for this stage is called crack initiation stress σ_{ci}.

- Crack Propagation. When σ_{axial} is larger than σ_{ci}, maximum friction is mobilized on some cracks. Sliding occurs along these cracks and they start to propagate one after another. With the increase of σ_{axial}, more and more cracks are mobilized and start to propagate. The crack propagation in this stage is stable, and the axial stress – axial strain behavior is still close to linear. However, the axial stress – volumetric strain behavior starts to show some non-linearity, which means that dilation component is introduced although the total volume change is still contraction. The limit stress of this stage is called crack coalescence stress σ_{cs}.
- Crack Coalescence. Due to further increase of σ_{axial}, the cracks grow longer and longer. They may intersect each other in this stage, and seriously decrease the stiffness of the sample. Therefore, the axial stress – axial strain behavior deviates from linearity. In terms of the volumetric strain, the dilation component keeps on increasing so that the rate of volume contraction gradually decreases and finally contraction stops. The limit stress of this stage is called crack damage stress σ_{cd}.
- Failure. When axial stress σ_{axial} exceeds σ_{cd}, the crack propagation is no longer stable. The elastic energy that has been stored in the sample is sufficient for the cracks to continue propagating even without increasing the axial stress. The cracks will keep on propagating until the sample fails and falls apart.

Based on these descriptions, it is clear that the threshold stresses mark the different stages of crack propagation. Since disturbances on rock samples cause crack opening and propagation, they must influence the value of these threshold stresses. These threshold stresses have been measured for rock samples of 130m, 240m and 420m. The results are shown in Table 6.5 and plotted in Figure 6.17.

Table 6.5 Measurements of Threshold Stresses (Eberhardt et al, 1999)

Depth (m)	σ_{cc} (MPa)	σ_{ci} (MPa)	σ_{cs} (MPa)	σ_{cd} (MPa)
130	47.3	81.5	132.8	156.0
240	55.6	79.6	127.6	147.4
420	74.8	76.4	85.5	100.4

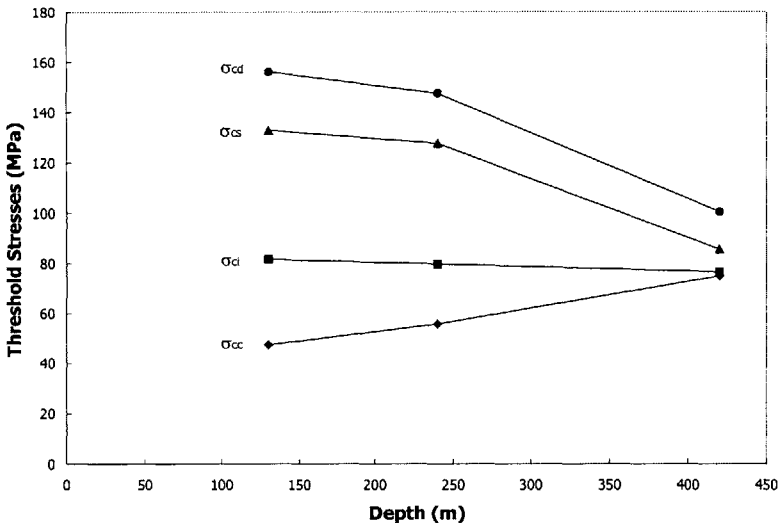

Figure 6.17 Stress Threshold Values (Data from Eberhardt et al, 1999)

Increasing the severity of disturbance (i.e. increasing sample depth) has different effects on different threshold stresses. The crack initiation stress σ_{ci} seems to be the least affected. It has very small decrease with increasing disturbance.

Below σ_{ci}, the crack closure stress σ_{cc} increases with increasing disturbance. A possible explanation is that, since increasing disturbance causes more microcracks to open, larger stresses are necessary to close all of the microcracks. Above σ_{ci}, the crack

coalescence stress σ_{cs} and crack damage stress σ_{cd} all decrease with increasing disturbance. This is readily explained by the opening of microcracks. The more microcracks there are, the larger the possibility that they cross and interfere with each other, and the rock is more likely to fall apart.

By definition, we should have:

$$\sigma_{cc} < \sigma_{ci} < \sigma_{cs} < \sigma_{cd}$$

Since σ_{ci} almost remains constant, the effect of increasing disturbance is that the other three threshold stresses converge to the value of σ_{ci}. The following conclusion can be obtained based on the definition of these stress thresholds:

- From Figure 6.16, the linear behavior of rock sample is between σ_{cc} and σ_{cs}. Increasing disturbance then reduces the range of this linear behavior, and the sample will have stronger non-linearity.
- Still based on Figure 6.16, when σ_{axial} exceeds σ_{cd}, the crack propagation will be unstable and the sample will fail. σ_{cd} can thus be treated as the indication of the sample's strength. Increasing disturbance means the strength of the sample is decreased.

6.3.3.5. Axial Stiffness in Compression Tests

The axial stiffness of the rock samples can be calculated based on the axial stress – axial strain curve obtained from the compression tests, either performed unconfined or with confining pressure.

The axial stiffness of samples taken from 130m, 240m and 420m depths in the

unconfined compression tests are plotted against the axial stress level in Figure 6.18. It can be seen that stiffness decreases with depth no matter how high the axial stress level is. Therefore, one can conclude that increasing disturbance will decrease the axial stiffness of the sample.

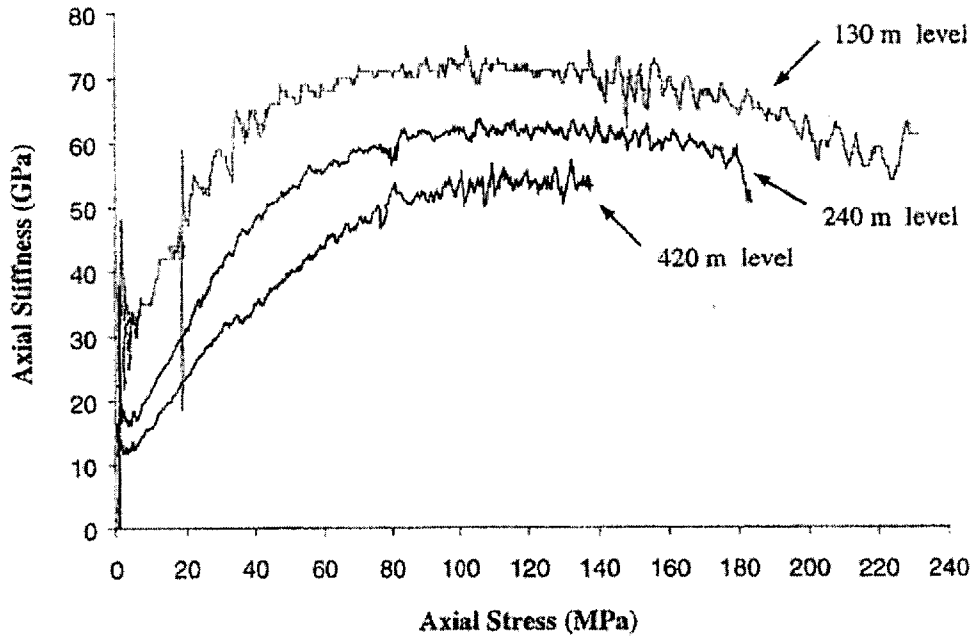

Figure 6.18 Axial Stiffness vs. Axial Stress Curve (Eberhardt et al, 1999)

The decrease of stiffness with depth is also consistent with the increase of microcrack density. The stiffness of the rock samples in compression tests is determined by two components: one is the stiffness of the rock matrix; the other is the behavior of the cracks. When there are few cracks in the rock sample, the rock matrix is continuous. Hence the measured stiffness is close to the stiffness of the rock matrix, which usually is very large. With increasing number of cracks, the rock matrix becomes less continuous and crack sliding and propagation is more likely to occur, which increases the deformation and decreases the stiffness of the rock

sample. Since samples taken from larger depth are more severely disturbed and have more microcracks, their stiffness must be lower.

The curves shown in Figure 6.18 show the stiffness of the samples from crack closure to failure. If we only focus on the behavior in the elastic zone (refer to Figure 6.16), their behavior can be described by two elastic parameters: the Young's Modulus E, which is defined as the slope of the axial stress – axial strain curve within the elastic zone; and the Poisson's Ratio ν which is defined as the ratio between horizontal and vertical strain. Both E and ν can be measured during the compression tests. In the unconfined compression tests, the measured E and ν for samples of 130m, 240m and 420m depths are listed in Table 6.6.

Table 6.6 Measured E and ν from Lab Tests (Eberhardt et al, 1999)

Depth (m)	Young's Modulus E (GPa)	Poisson's Ratio ν
130	66.5	0.31
240	63.8	0.33
420	51.9	0.38

It can be seen that the value of Young's Modulus decreases with the depth of the samples, which conforms to the trend shown in Figure 6.18. Based on the previous analysis, the decrease of Young's Modulus is also caused by the increase of crack density with depth. Figure 6.19 shows the correlation of the Young's Modulus with the crack density in a semi-logarithmic plot. The relationship is also very close to linear.

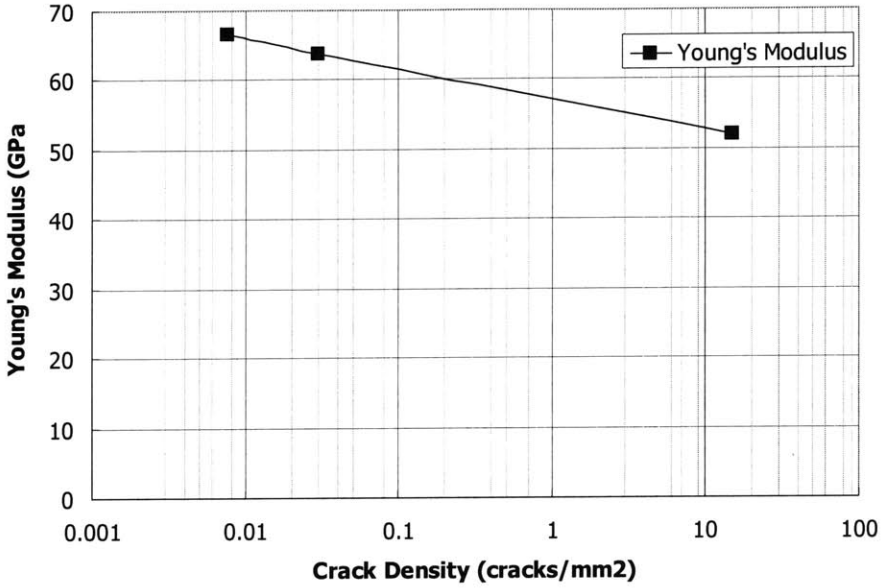

Figure 6.19 Correlation of Young's Modulus with Crack Density

In compression tests that are conducted with confining pressures, it has been found that the measured Young's Modulus E may also change with the confining pressure. Figure 6.20 shows the variation of E with the confining pressure for a sample from Stress Domain I and a sample from Stress Domain III at 420m depth.

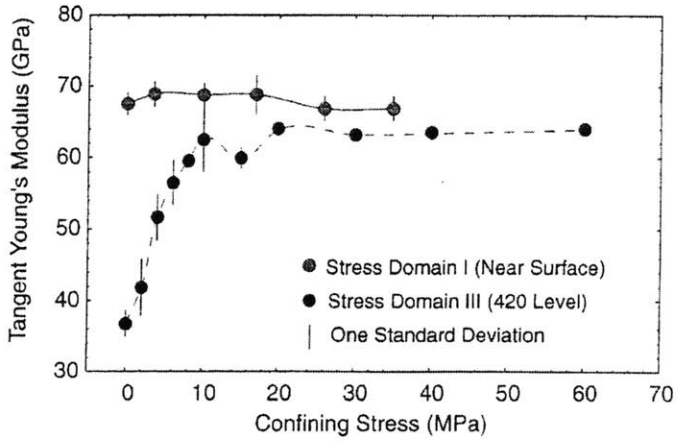

Figure 6.20 Young's Modulus vs. Confining Stress (Martin et al, 1994)

Several observations can be made from Figure 6.20:

1. The Young's Modulus E of the sample from Stress Domain III (denoted E_{III}

in the following discussion) is smaller than the Young's Modulus of the sample from Stress Domain I (denoted E_I in the following discussion). Again, this can be explained by the larger density of microcracks in the sample taken from Stress Domain III.

2. E_I only changes slightly with the confining pressure, i.e. it is largely pressure independent. On the contrary, E_{III} is strongly pressure dependent. This is so because increasing the confining pressure closes microcracks, and makes crack sliding and propagation less likely to occur. The sample from Stress Domain III has a large number of cracks due to strong disturbance, thus increasing confining pressure has very significant effects on the recovery of the Young's Modulus. On the other hand, the sample from Stress Domain I has fewer cracks since the disturbance level is low. As a result, its Young's Modulus does not change much with the confining pressure.

3. E_{III} remains lower than E_I even if the confining stress reaches 55MPa, where the maximum in-situ horizontal stress of 420m depth is fully restored. It seems that the loss of stiffness caused by microcracking can not be fully recovered by applying the in-situ confining stress.

By comparing Figure 6.20 with Table 6.5, a very interesting inconsistency can be found. Based on the previous analysis, when the Young's Modulus becomes constant for the sample at 420m level, the closure of the cracks should have been completed by the confining pressure. Since the modulus becomes constant at about 20MPa, the crack closure stress for the sample of 420m level must be smaller than

20MPa according to Figure 6.20. However, Table 6.5 clearly shows that the crack closure stress for the sample at 420m depth is 74.8MPa, which is much greater than 20MPa. The following explanations may be possible for this inconsistency:

- The results presented in Figure 6.20 and Table 6.5 are from two different research projects. The sample size, loading rate and some other parameters are different for the two projects (Table 6.2). Therefore, the threshold stress they measured cannot be identical.
- The results in Table 6.5 are measured from uniaxial compression tests, and the crack closure stress is the axial stress. The results in Figure 6.20 are measured from triaxial tests, and the crack closure stress is the radial stress. Due to the anisotropy of the material, the crack closure stress in the axial and radial directions may be different.

However, a clear and conclusive explanation is still not available before more detailed investigation.

6.3.3.6. Permeability

Katsube (1981) conducted a series of permeability tests on Lac du Bonnet samples taken from boreholes that are 14km away from the URL site. The samples are taken from depth up to 1000m. These tests are conducted on samples with 45mm in diameter and 20~30mm in length. Tests were conducted on samples under unconfined and confined conditions. For confined conditions, the confining pressure is set to be 22.6 (kPa/m)×D, in which D is the depth of the sample. The results of

Katsube are shown in Figure 6.21, where ΔK is the difference between the confined and unconfined permeability.

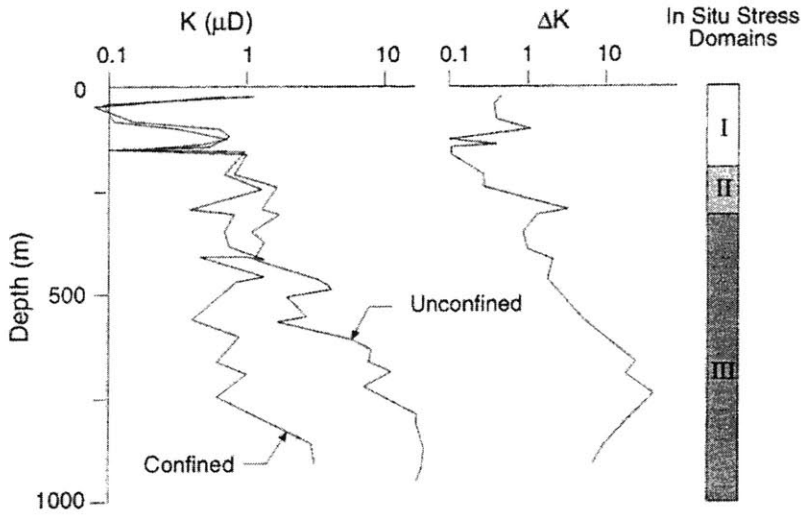

Figure 6.21 Permeability Change vs. Depth ($1\mu D = 9.87\times10^{-19}m^2$) (Martin et al, 1994)

It is clear from Figure 6.21 that the permeability increases with depth, no matter confined or unconfined. However, the in-situ permeability for Lac du Bonnet granite is essentially constant with depth, except in the vicinity of fracture zones (Davison, 1984). Therefore, it can be concluded that increasing sample disturbance increases permeability.

The variation of measured permeability from samples is directly related to the opening of microcracks. Apparently, as more cracks are opened, the permeability of the sample increases. Therefore, the measured permeability of the unconfined samples increases greatly with depth. Applying confining pressure forces some of the cracks to close and thus decreases the permeability of the samples. The permeability measured on confined samples only changes slightly with depth and is closer to the in-situ case.

6.3.3.7. Strength

In order to study the effects of disturbance on compressive strength of rock, samples are taken from Stress Domain I, Stress Domain II at 240m level, and Stress domain III at 420m level. Triaxial tests are conducted on these samples, and the strength envelope for samples of each stress domain is worked out separately. The results of trixial tests are analyzed using the Hoek-Brown failure criterion (Hoek 1983), which is expressed by:

$$\sigma_1 = \sigma_3 + \sqrt{m\sigma_3\sigma_c + s\sigma_c^2}$$

where σ_1 is the axial stress at failure;

σ_3 is the confining stress;

σ_c is the uniaxial compressive strength of intact rock;

m and s are empirical constants.

The Hoek-Brown parameters for samples from different stress domains are summarized in Table 6.7. The failure envelopes are shown in Figure 6.22. It must be noted that Martin et al. (1994) only reports the results of the strength curve and the parameters. The original data points are not available from their paper.

Table 6.7 Strength Parameters of Samples (Martin et al, 1994)

Stress Domain	m	s	σ_c (MPa)
I	47.3	81.5	213.2
II	55.6	79.6	193.5
III	74.8	76.4	149.6

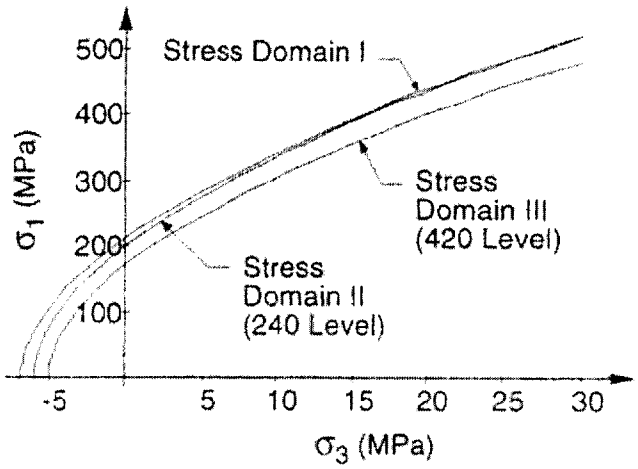

Figure 6.22 Hoek-Brown Failure Envelope for Samples from Different Stress Domains (Martin et al, 1994)

These envelopes are close to each other, indicating that the strength of rock is not sensitive to disturbance. It seems that the strength envelopes for the three stress domains are roughly parallel. Therefore, they should have similar friction angles. However, the location where the envelope intersects the σ_1 axis is lower for Stress Domain III than for Stress Domain II, which is still lower than for Stress Domain I. It appears that the disturbance reduced the "cohesion" component of the strength, but the frictional component is not affected.

The tensile strengths of samples from Stress Domain II and Stress Domain III were also measured in direct tension test. It has been found that the mean direct tensile strength is 3.5±0.3MPa for Stress Domain II and 1.5±0.7MPa for Stress Domain III, i.e. the direct tensile strength for Stress Domain III is only 42% of that of Stress domain II. Clearly, the tensile strength is seriously reduced by disturbance.

6.4. Summary

In this section, the disturbance mechanisms of the sources listed in Section 2.2 are applied to rock sampling. Stress relief is found to be a very significant disturbance source. It is then concluded that in a uniform rock formation, the cores taken from larger depth will be subject to larger disturbance.

A testing program performed on the Lac du Bonnet granite is then described, which illustrates the conclusions described above. Through the results of this testing program, it has been found that crack opening and propagation due to stress relief is the most significant disturbance effect in rock sampling. Most of the other effects, for example the decrease of P-wave velocity, the decrease of stiffness, the increase of permeability etc., seem to be caused by the opening and propagation of cracks and are thus secondary.

With the understanding of the disturbance mechanism and effects, it is possible to come up with ways to evaluate the disturbance severity. For example, since P-wave velocity is a good indication of the crack density, it can also be used as a good index for disturbance severity. In addition, since stress relief is an important disturbance source in rock sampling, any devices that decrease the stress relief will decrease the disturbance effects. Therefore, the study of the mechanisms and effects of rock sample disturbance provides a direction of how to minimize the disturbance effects.

It should, however, be kept in mind that some of the other disturbance effects such as temperature changes and chemical changes may also play a role and need to

be further investigated. Also, disturbance effects may be greatly different for different rock types and different geological conditions in general.

7. Preliminary Study of Sample Disturbance in Shale

Since the sampling of shale also follows the steps outlined in Section 2.2, the disturbance sources listed there will again be used as a template to consider the sample disturbance problem in shale.

In the previous sections, the sample disturbance problem in soil and rock has been described in detail following the structure developed in Section 2.4. The first and most fundamental step of this structure is to understand the disturbance mechanism and identify important disturbance sources. As a transitional material between soil and rock, shale has similarities with both soil and rock. Therefore, predictions can be made on shale sample disturbance based on the disturbance in soil and rock whenever the similarities allow us to do so. On the other hand, the behavior of shale has its own distinctive features. The methods that are used to describe and analyze soil and rock disturbance may have to be modified so that they are applicable to shale.

This section will first present some shale characteristics and behavior as the basis for further discussion. The sources and mechanisms of disturbance will then be analyzed using the list in Section 2.2 as a template. The methods that were used to investigate the mechanisms and effects of soil and rock sample disturbance are then summarized. Suggestions on how to modify these methods to investigate shale sample disturbance are proposed.

7.1. Characteristics of Shale

According to Aristorenas (1992), shale is a term used by geologists and engineers to refer to a vast group of clastic sedimentary rocks composed of fine-grained particles of silt and clay size, indurated by consolidation stresses much larger than the present overburden and by diagenetic bonding of particles. Natural shale often has a bedded structure due to its depositional character. Some of the most important characteristics of shale are described in more detail below.

7.1.1. Clay Content and Plasticity

Shale usually has high clay mineral content. As a sedimentary rock, the minerals of shale are derived from other sedimentary rocks or from igneous and metamorphic rocks through erosion and weathering processes (Aristorenas, 1992). Although many types of minerals may be present in shale, clay minerals usually predominate. The clay minerals that often exist in shale include: Kaolinite, Illite, Smectite, Chlorite, etc. The clay mineral content of some shales are listed in Table 7.1. It can be seen that most of the shales listed have high clay mineral content (>30%).

The Atterberg Limits of shale can be measured after deaggregation of shale. The plasticity charts for the shales listed in Table 7.1 are plotted in Figure 7.1. The areas of data points for most of the shales are above A-Line and fall to the right of 50% liquid limit. Therefore, these shales have medium to high plasticity.

Table 7.1 Clay Fraction of Some Shales (Hsu et al., 1993)

Formation	Clay (%)	Reference
Bearpaw (Canada)	30-65	Ringheim (1964); Eigenbrod (1972)
Bearpaw (USA)	61	Townsend & Gilbert (1974)
Claggett	50	Townsend & Gilbert (1974)
Colorado	45	Townsend & Gilbert (1974)
Eagle Ford	38-88	TETC (1990)
Edmonton (clayey)	30-50	Sinclair & Brooker (1967)
Edmonton (bentonite)	30-55	Thomson (1970)
Pepper	28-56	Stroman & Feese (1984)
Pierre	34-85	Scully (1973)
Taylor	28-90	TETC (1990)

*: **Percentage of smectite and mixed layer illite and smectite of clay fraction.**

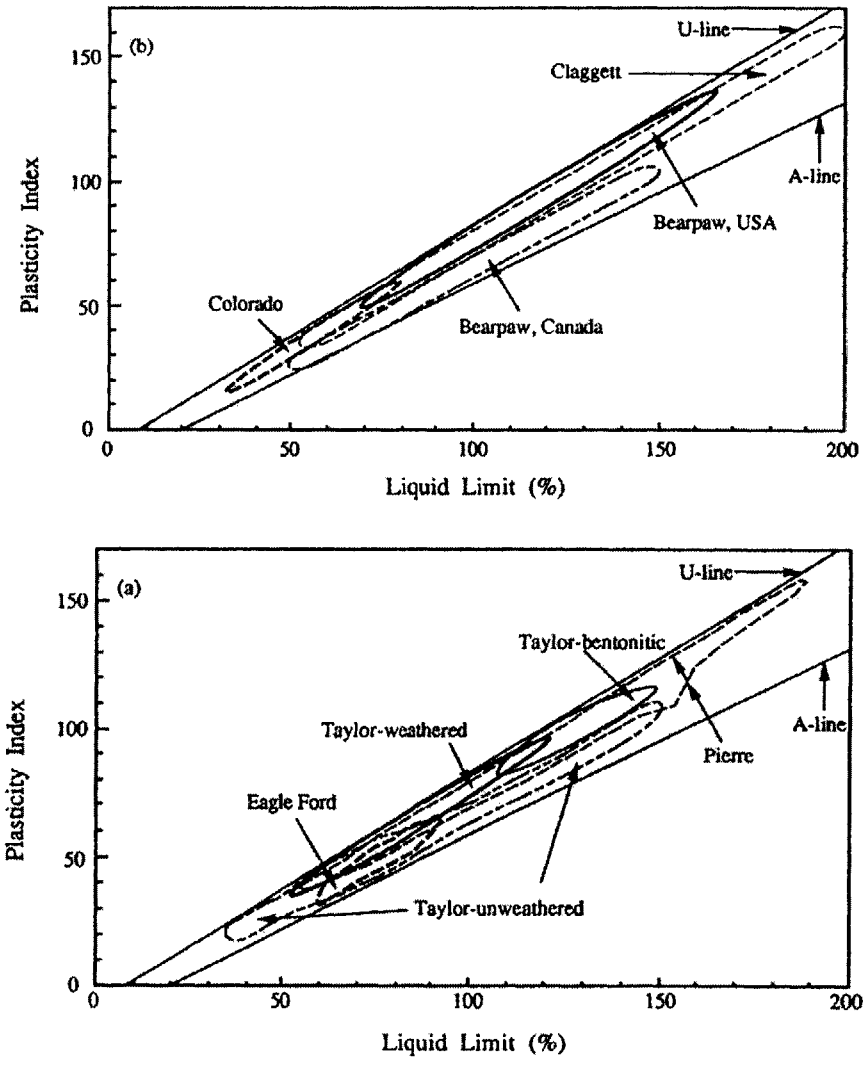

Figure 7.1 Plasticity Chart for Some Shales (Hsu et al., 1993)

However, it should be noted that Atterberg limits are only of limited value for materials like shale, because the measured value of Atterberg limits are greatly affected by sample preparation methods (Aristorenas, 1992). For example, the energy used in deaggregation determines the particle size and thus the specific surface area. Therefore, the less energy used in the deaggregation, the larger the particle size and the smaller the plasticity measured.

7.1.2. Heavily Over-Consolidation

The shale formations encountered in engineering practice are usually exposed on the ground surface. A very important characteristic of these shale formations is the very high degree of over-consolidation. This is determined by the geological history of the shale formations (Figure 7.2).

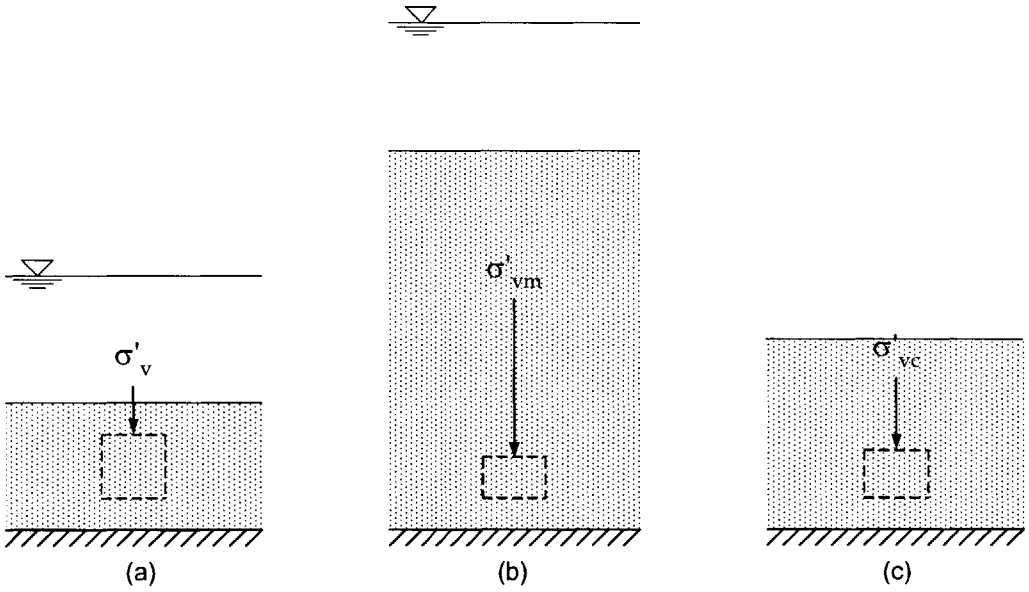

Figure 7.2 Sketch of the Geological History of Shale

During deposition, the thickness of the deposit keeps on increasing. For the element shown in Figure 7.2 (a) by the dashed square, the vertical effectives stress σ'_v

will be larger and larger. Therefore the element will be subject to one-dimensional consolidation, and its void ratio and water content will be decreased. Eventually, unloading may occur due to erosion, and the vertical stress on the element will also be reduced. The element then becomes over-consolidated, and the over-consolidation ratio is:

$$OCR = \sigma'_{vm}/\sigma'_{vc}$$

For shale formations, the OCR value can be very high.

One the other hand, the element at maximum overburden (Figure 7.2 (b)) is also highly compressed. However, by definition its OCR equals 1. Whether it can be called shale at this stage is a very interesting philosophical question.

7.1.3. Very Small Pore Size

It has been shown that shale is usually composed of silt or clay sized particles. These particles are very closely packed, and diagenetic bonding or cementation may further reduce the interparticle spaces. Therefore, the pores in shale are usually extremely small. To illustrate this, the pore size distribution of a North Sea shale sample is shown in Figure 7.3.

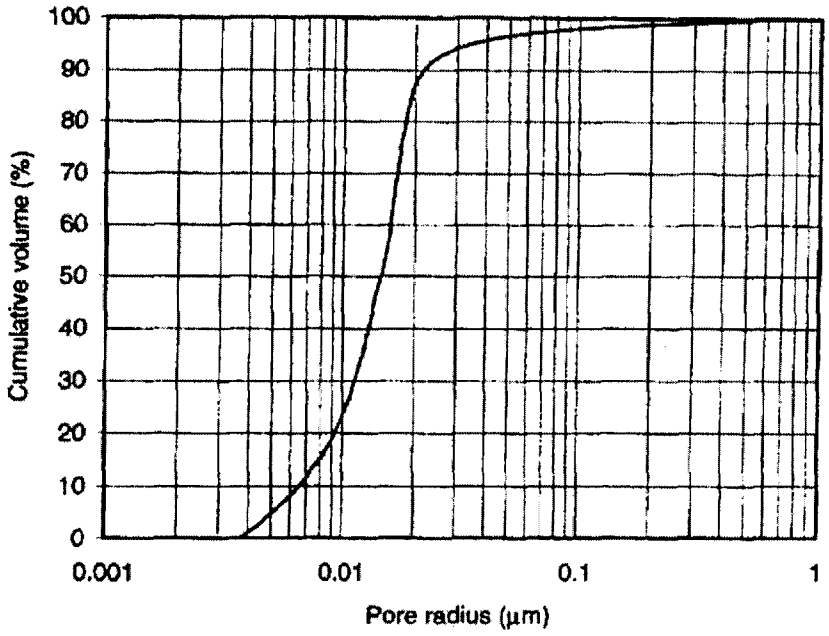

Figure 7.3 Pore Size Distribution of a North Sea Shale Sample (Horsrud et al., 1998)

Based on the description of Horsrud et al. (1998), the pore size distribution is measured by mercury injection (up to 200MPa pressure). To measure this distribution, small samples (about 3g) are first dried at 60°C and the cumulative injected volume of mercury is recorded versus injection pressure. The test is run until no more mercury can be injected. The pore radius r can be related to the injection pressure P by:

$$P = 2\gamma\cos\theta/r$$

in which: γ is the interfacial tension between the wetting and non-wetting phase;

θ is the contact angle between the solid surface and the wetting surface.

The percentage of cumulative volume is then plotted against pore radius for the shale sample.

From Figure 7.3, it can be seen that 90% of the pore volume is occupied by pores with radii less than 0.02μm. Such a small pore size implies that capillary

effects may significantly change the effective stress of the sample. When a shale sample loses water due to evaporation, air entry will occur and the rest of the water in the sample will be drawn to smaller pores since smaller pores can generate larger negative pore pressure. The result is that the negative pore pressure in the pore water increases and the effective stress in the sample will be increased accordingly (refer to Section 3.6.1.1). If the shale sample absorbs water, then the reverse will occur.

In fact, this has been proven by the saturation and desaturation experiments performed on the Opalinus Shale cores from Mont Terri Rock Laboratory (TN 2003-46). When the shale core is put in a humid environment and it can absorb moisture from air, expansion of the shale core was measured in different directions. When the shale core is then put in a dry environment, it loses its water by evaporation and contracts in different directions.

7.1.4. Particle Bonding

It has been shown that due to continuing deposition, the pressure on an element keeps increasing and can reach a very high value. The temperature of the element will also increase with its burying depth. With the increase of pressure and temperature, many physico-chemical processes will occur between component minerals so that bonds between them may be formed. These processes are called diagenesis.

It has been found that under high pressure and temperature, re-crystallization

of the minerals may occur so that true adhesion can develop between particles. Also, cementing agents contained in the groundwater can precipitate in the intercrystalline interstices, and further strengthen this interpartical bonding. Although the processes of re-crystallization and precipitation are extremely slow, their effects are remarkable given the scale of the geological time of deposition. Consequently, the strength of shale is increased by the diagenetic bonds.

However, it should be noted that the strength of shale, although much higher than that of soft soil, is generally lower than for typical rocks, for instance, granite. More importantly, the diagenetic bonds of shale can be easily broken by various physico-chemical processes that occur when shale is in contact with free water.

7.1.5. Characteristics of Opalinus Shale

After the general introduction of some characteristics of shale, it is necessary to briefly comment on the Opalinus Shale, which is the objective of the work for NAGRA.

Opalinus Shale is of marine origin, and is usually of dark-grey color (Bellwald, 1990). Although the shales listed in Table 7.1 mostly have medium to high plasticity, Opalinus shale is a low plasticity shale. The index properties of Opalinus shale are shown in Table 7.2:

Table 7.2 Index Properties of Opalinus Shale (TN 2000-02)

Liquid Limit w_L (%)	38±5
Plastic Limit w_P (%)	23±2
Plasticity Index I_P (%)	15±3

The dominant clay minerals of Opalinus shale are illite and kaolinite, as listed in

Table 7.3:

Table 7.3 Mineral Content of Opalinus Shale (Bellwald, 1990)

Non-Clay Minerals	Quartz (%)	6-25
	Carbonate (%)	6-25
	Siderite (%)	0-6
Clay Minerals	Smectite (%)	-
	Illite (%)	28-32
	Illite&Smectite (%)	10-18
	Kaolinite (%)	21-28
	Chlorite (%)	7-14

7.2. Shale Behavior

Based on the description of the mineral components and geological history of shales, it is not surprising that shale has long been considered to be a transitional material between soil and rock. According to Bjerrum (1967), over-consolidated clays are clays with weak or no bonds having a current consolidation stress less than its maximum past pressure; clay shales are over-consolidated clays with well developed diagenetic bonds; and shales are over-consolidated clay shales with strongly developed diagenetic bonds. These definitions clearly show that when the diagenetic bond is weak, shale is more similar to over-consolidated clay; when the diagenetic bond is strong, shale is more similar to rock.

It is then evident that the behavior of shale can be best introduced by comparing it with the behavior of soil and rock. Therefore, this section will first present how shale behavior is similar to that of soil and rock. The distinctive aspects of shale behavior will be introduced afterwards.

7.2.1. Similarities with Soil Behavior

Due to the inherent similarity of shale and over-consolidated clay, their behaviors are also similar in certain aspects. Based on the research of Bellwald (1990) and Aristorenas (1992), the similarities may reside in the following aspects:

7.2.1.1. Applicability of Hyperbolic Model

The hyperbolic curve is often used to approximate the shear behavior of clay before it reaches failure. The mathematical expression of a hyperbolic curve is:

$$\frac{2q}{\sigma_c'} = \frac{\gamma}{m + n\gamma}$$

in which: q is the shear stress;

σ'_c is the consolidation stress;

γ is the shear strain;

m and n are constants that are used to fit the test curve.

This equation can also be written as:

$$\frac{\gamma\sigma_c'}{2q} = m + n\gamma$$

Therefore, the plot of $\gamma\sigma'_c/2q$ vs. γ should be a straight line with the slope n and the intercept m if the behavior of clay can be described by the hyperbolic model.

Shear tests on Opalinus shale samples have been performed by Bellwald (1990). In Bellwald's tests, the Opalinus shale samples were first isotropically consolidated at σ'_c = 5.0MPa, and then sheared in pure shear compression. A typical stress-strain curve obtained from the tests is shown in Figure 7.4:

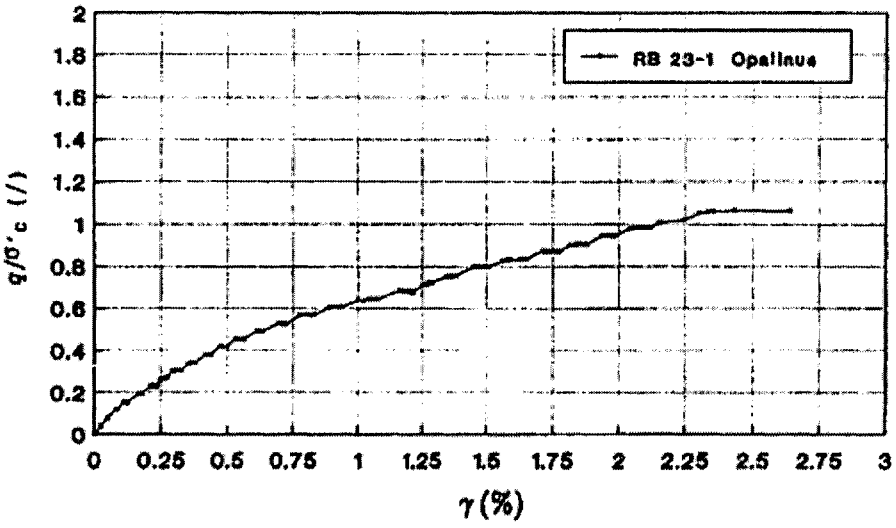

Figure 7.4 Stress Strain Curve of Opalinus Shale Samples in Shearing (Bellwald, 1990)

Based on the curve shown in Figure 7.4, the plot of $\gamma\sigma'_c/2q$ vs. γ can also be obtained, which is shown in Figure 7.5. It can be seen that the plot of $\gamma\sigma'_c/2q$ vs. γ is very close to a line, i.e. the shear stress-strain relationship of Opalinus shale can be well approximated by the hyperbolic model. This may be one similarity between the behavior of over-consolidated clay and the behavior of shale. The constants m and n are shown in Figure 7.5, with m = 0.38 and n = 0.42.

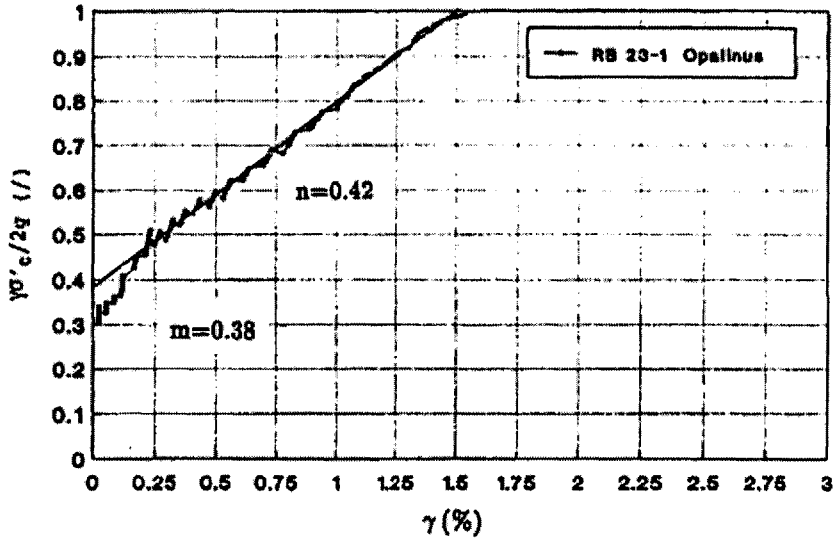

Figure 7.5 Plot of $\gamma\sigma'_c/2q$ vs. γ for Opalinus Shale Sample (Bellwald, 1990)

7.2.1.2. Applicability of SHANSEP

The research of Bellwald (1990) shows that the SHANSEP (Stress History And Normalized Soil Engineering Properties, Ladd et al., 1977) Equation is also applicable to the shear strength of shale. The SHANSEP Equation is used in over-consolidated clay to correlate the undrained shear strength with the stress history of clay (i.e. OCR). It can be expressed as:

$$\frac{s_u}{\sigma_c'} = S(OCR)^m$$

in which: s_u is the undrained shear strength;

σ'_c is the consolidation stress;

OCR is the over-consolidation ratio;

S and m are constants to be determined by the test data.

Bellwald (1990) found that this equation can also be applied to the undrained shear strength of shale. Since one basic assumption of this equation is that the behavior can be normalized by the consolidation stress σ'_c, this indicates that shale may also have normalized behavior. However, this conclusion still needs to be confirmed by more experimental data.

7.2.1.3. Negative Pore Pressure during Shear

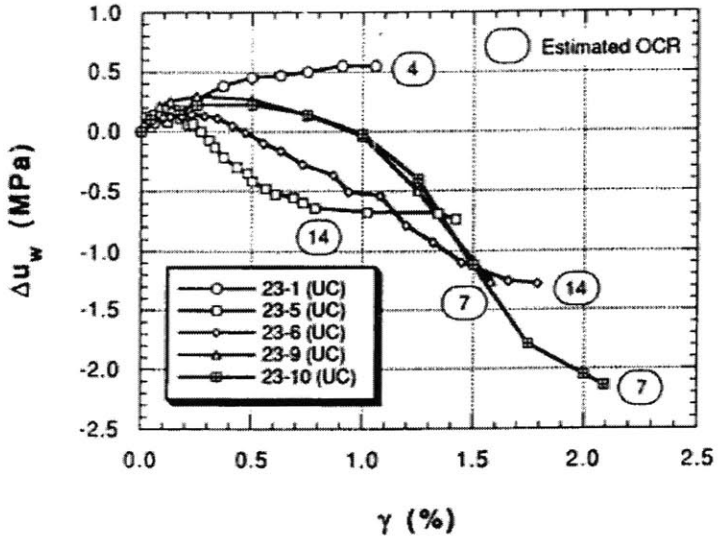

Figure 7.6 Pore Pressure Change during Shearing for Shale Samples (Aristorenas, 1992)

It is well known that during undrained shearing of over-consolidated clay, the volume of the clay sample tends to increase and negative pore pressure will be generated. Undrained shearing tests have been performed on samples of Opalinus shale and Lias α shale, and the changes of pore pressure Δu_w are plotted against shear strain γ in Figure 7.6 (23-1, 23-5 and 23-6 are Opalinus shale samples, 23-9 and 23-10 are Lias α samples). It can be seen that negative pore pressures are generated for most of the samples during shearing.

7.2.1.4. Linear e vs. log(σ'_v) Relationship in Recompression

According to the descriptions of Section 4.2, in one-dimensional consolidation, the e vs. log(σ'_v) curve of soil is composed of two parts: the recompression part when σ'_v is smaller than the pre-consolidation pressure σ'_p, and the compression part

when σ'_v is larger than σ'_p. The two parts are very close to straight lines with a curved transition connecting them.

K_0 consolidation tests have also been performed on shale samples, and the e vs. log(σ'_v) curves for two samples are shown in Figure 7.7 (26B-4 and ERZ4 are both Opalinus shale samples). Since shale has been subject to very large overburden pressures, the shale samples at the stress level shown in Figure 7.7 (σ'_v < 2MPa) are still in recompression. Clearly, the two e vs. log(σ'_v) curves shown in Figure 7.7 are very close to straight lines, and this is similar to the one-dimensional consolidation of soil in recompression.

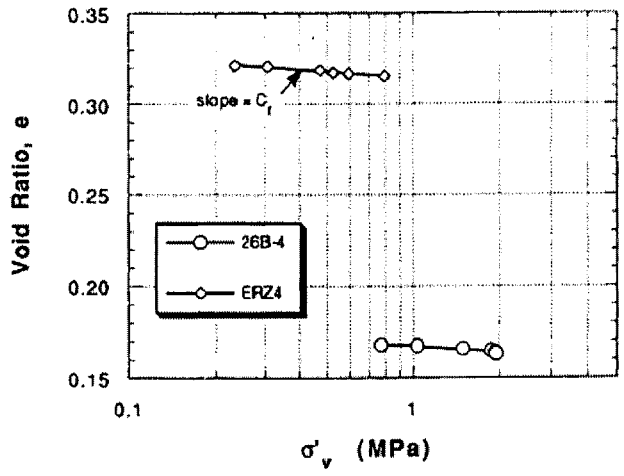

Figure 7.7 e vs. log(σ'_v) Curve for Shale Samples in K_0 Consolidation (Aristorenas, 1992)

7.2.2. Similarities with Rock Behavior

Due to the strong diagenetic bonding of shale, it also shares similarities with rock. In the material realm of rock, crack opening and propagation becomes the major mechanism of deformation and failure. In Section 6.3.3.4, the major features of the stress-strain relationship of rock in uniaxial compression tests are presented

based on the analysis of crack opening, propagation, and coalescence. It has been found that the behavior of shale samples in uniaxial compression tests is quite similar to rock behavior presented in Section 6.3.3.4. This can be shown through the test results on Opalinus shale samples.

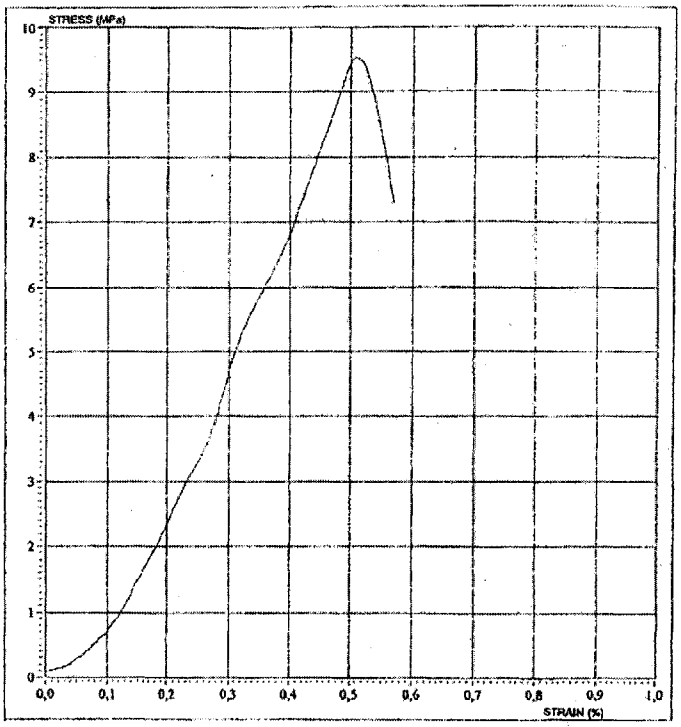

Figure 7.8 Typical Stress-Strain Curve of Opalinus Shale in Uniaxial Compression (TN 98-57)

Figure 7.8 shows a typical stress-strain curve of the uniaxial compression tests performed on Opalinus shale samples. It can be seen that the stress-strain curve is very similar to the typical behavior of rocks in uniaxial compression tests (Figure 6.16). The stages of crack closure, elastic range and the final brittle failure can be clearly identified. Therefore, it is reasonable to say that the mechanism of deformation and failure in the uniaxial compression tests of shale may involve the opening and propagation of cracks. This needs to be further investigated, however.

It is worth noting that the shear behavior of shale in triaxial tests (Figure 7.5)

and in uniaxial compression tests (Figure 7.8) are quite different. It seems that in the triaxial tests, the shear behavior of shale is similar to that of over-consolidated clay, and the stress-strain curves can be approximated by the hyperbolic model (before the peak is reached). In uniaxial compression, however, the stress-strain curve of shale is more similar to typical rock behavior, which is shown in Figure 6.16. More detailed investigations are necessary before the origination of this difference can be revealed.

7.2.3. Distinctive Aspects of Shale Behavior

Besides the similarities with soil and rock behavior, shale also has its distinctive aspects.

7.2.3.1. Bedded Structure

Most shale formations have a bedded structure (Figure 7.9 (a)), the bedding planes are formed by the discontinuity in the deposition process, and they usually form weak connections between two layers.

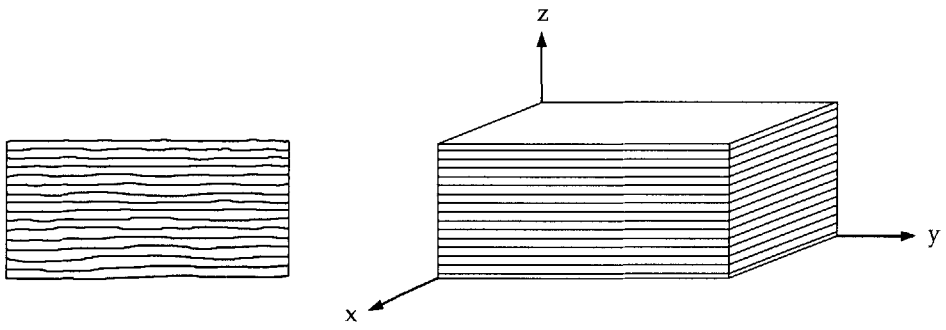

(a) Bedding Planes (b) Definition of Directions

Figure 7.9 Bedding Planes of Shale

Due to this bedded structure, shale is usually strongly anisotropic. Very often the properties in the x, y directions are similar, but quite different from the properties in z direction. Therefore, the mechanical behavior of shale is better approximated by a transverse isotropic model.

This anisotropy is evident from testing results on Opalinus shale samples. Table 7.4 compiles some measurements made on Opalinus shale samples in uniaxial compression tests, including the modulus at 50% peak stress E_{50}, the Poisson's Ratio and the Uniaxial Compression Strength. It can be seen that all these parameters are different in the directions parallel and perpendicular to the bedding planes.

Table 7.4 E_{50}, ν and UCS of Opalinus Shale in Different Directions (TR 2000-02)

E_{50} (GPa)		ν		UCS (MPa)	
E_{50x} & E_{50y}	E_{50z}	ν_{zx} & ν_{zy}	ν_{xy}	UCS_x & UCS_y	UCS_z
8.5±3.7	3.6±1.0	0.24±0.08	0.33±0.05	10.5±6.5	25.6±2.5

The bedded structure also causes anisotropy in crack opening and propagation. Since the bedding plane represents weak planes and discontinuities in shale, crack generation and propagation may be facilitated along these bedding planes.

7.2.3.2. Physico-Chemical Effects

Usually, the particles of shale are heavily compacted and bonded, and shale in its natural, undisturbed state has relatively high strength. However, when shale has access to free water, various physico-chemical effects will occur and the diagenetic bonds in shale can be easily broken by these effects. If these effects are very strong and the diagenetic bonds are completely broken, disintegration occurs and shale will

decay into smaller pieces and particles. The mechanical properties of shale can thus be greatly changed. Such a disintegration phenomenon is called slaking.

According to Moriwaki (1974), four modes of slaking are possible. They are:

- Swelling: described as an increase in bulk volume without visible cracking or significant loss of material;
- Body slaking: which appears to originate from internal processes and which rapidly traverses large portions of mass with no apparent deterioration between cracks;
- Surface slaking: characterized by loss of mass due to "sloughing" of tiny flakes of grains from the entire surface with no apparent cracks in the underlying material;
- Dispersion: characterized by loss of mass resulting from the separation of clay-sized grains which go into spontaneous suspension, rather than settling.

Slaking of shale can be caused by several different mechanisms. It can be caused by the addition of water to clay minerals. When shale has access to free water, the double layer will develop further on the surface of clay particles. Since the particles in shale are originally very closely packed, there is not enough space for the double layer to expand. Repulsion between particles occurs due to the expansion of double layer. This repulsion can be so large that the diagenetic bonds between particles will be broken and the particles will be pushed apart.

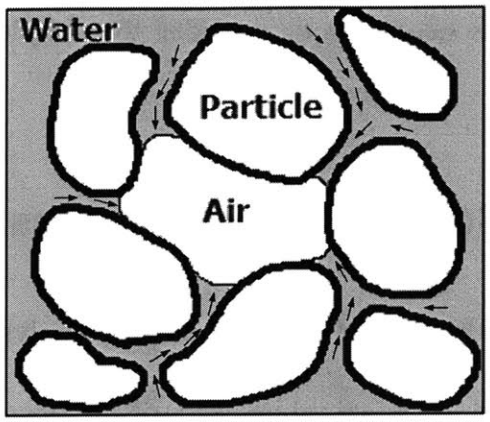

Figure 7.10 Compression of Trapped Air in Shale

The slaking of shale can also be caused by the compression of trapped air (Figure 7.10). When shale is not fully saturated and it is immersed in water, the air in shale will be trapped. Since the pore sizes of shale are very small, very strong capillary force will be generated to pull the water toward the trapped air (shown by arrows in Figure 7.10). The trapped air in shale will then be compressed by this water infiltration, until finally the air pressure and the capillary pressure balance. As a result, the air pressure will be greatly increased and the shale matrix around the air pocket will be subject to tension, which may cause the disintegration of the shale sample.

It must be noted that the definition of "slaking" and "swelling" and their underlying mechanisms are still controversial. According to ISRM (1983), slaking "of swell susceptible rocks can occur if they are subject to swelling-drying cycles or intensive air-drying". Swelling is defined as "the time dependent volume increase involving physico-chemical reaction with water". According to these definitions, swelling is not a type of slaking as described by Moriwaki (1974).

As has been said, slaking disintegrates shale and changes its mechanical

behavior. Therefore, it is necessary to consider the coupled chemical-mechanical effects in shale.

7.3. Disturbance Sources and Mechanisms in Shale

Based on the behavior of shale and the analysis of the disturbance mechanisms of soil and rock sampling, the disturbance mechanisms of shale sampling can be roughly predicted. The disturbance sources presented in Section 2.2 will be used as a template.

7.3.1. Borehole Drilling

During the drilling of the borehole in shale, the following disturbance mechanisms may be important:

The in-situ stress in shale formation will be relieved by borehole drilling. Due to this stress relief, crack opening can be initiated (refer to Figure 6.5). As has been said, the opening and propagation of cracks in shale will be affected by its bedded structure.

The temperature of shale can be changed by the heat generated in drilling and the temperature difference between shale and borehole fluid. In addition, if compressed air is used as the borehole fluid, the evaporation of pore water also contributes to the temperature change. Since shale is a relatively hard material, the friction between the drilling machine and shale may generate a significant amount of heat. The change of temperature in shale can cause different thermal strains in shale

matrix and the pore liquid due to their different reactions to temperature change. As a result, excessive pore pressure will be generated in shale.

If compressed air is used as the borehole fluid, then the pore water evaporates at the surface (i.e. the wall and bottom) of the borehole. Based on the description in Section 7.1.3, very large negative pore pressure will be generated. Therefore, the effective stress of shale will increase and shale at the surface of the borehole is then subject to contraction. However, for shale very close to the surface but not exposed to the air, no negative pore pressure is generated and no contraction occurs. This strain incompatibility can cause stress changes within shale. In addition, since negative pore pressure is generated at the borehole surface, a hydraulic gradient will exist and water will migrate to the surface of the borehole.

If drilling mud is used as the borehole fluid, then various physico-chemical effects introduced in Section 7.2.3.2 are likely to occur. The water in the drilling mud may cause swelling and slaking of shale, and the mechanical properties of shale are changed. With the change of mechanical behavior, the stress and strain field around the borehole will also be changed.

7.3.2. Coring Process

Since natural shale has relatively high strength, it is usually sampled by coring. Some information on coring barrels and coring procedures has been provided in Section 6.1. The possible disturbance mechanisms during coring are listed below.

Stress concentration may occur due to the stress relief in coring. Based on the results of the FEM analysis presented in Section 6.2.3, a zone of tensile stress may also be generated in the coring process of shale (refer to Figure 6.8). However, due to the bedded structure of shale, the consequences of this tensile stress zone on the shale core will be much larger than in rock.

During coring, temperature changes, capillary pressure, and physico-chemical effects also occur. The details have been presented in Section 7.3.1. When the shale sample has completely entered the core barrel, a torque will be applied to detach it from the native shale formation, which will also disturb the sample.

7.3.3. Move Shale Core to Ground Surface

While shale core is pulled up in the borehole, the mud pressure on it decreases with decreasing depth. The pore pressure that was originally in shale also decreases with the mud pressure. In this case, gas exsolution may occur due to the decrease of pore pressure. In addition, the pore pressure in shale may not decrease as quickly as the mud pressure due to its very low permeability, and tensile stresses can be generated in the shale sample by the rapid decrease of mud pressure.

7.3.4. Transportation and Storage

During the transportation and storage of shale, the temperature of the shale sample can be changed with the environment temperature. The mechanism of

temperature change was presented in Section 7.3.1.

If the sample is not properly sealed, it may be exposed to air, and water evaporation will occur, producing negative pore pressures. The effective stress in the shale sample is then changed and contraction of the sample can occur (see Section 7.1.3). Water will migrate to the surface of the sample due to the hydraulic gradient.

In addition, oxidation may also occur when a shale sample is in contact with air. For example, if the shale being sampled contains pyrite, then pyrite can be oxidized to ferrous sulphate $FeSO_4$, which in turn oxidizes to goethite (at relatively high pH) (Brookins, 1988). Both oxidation processes need water to proceed, and they generate free sulphuric acid. Any calcium carbonate in shale will then be altered by the sulphuric acid to sulphate (gypsum) in the presence of water:

$$H_2SO_4 + CaCO_3 + H_2O \rightarrow CaSO_4 \bullet 2H_2O + CO_2$$

The formation of gypsum causes an increase of 23% in volume (Blatt, 1982). If shale is exposed in air for a long time, then gypsum will continue to grow, causing deformation in the surrounding shale matrix.

7.3.5. Sample Preparation

Sample preparation of shale is also different for different kind of test apparati. Since sample preparation is generally performed in air, the mechanisms introduced in Section 7.3.4 are still applicable. However, a step which is extremely important for shale is the resaturation.

Due to water evaporation, cracking and other effects of sampling, the shale

samples that are originally fully saturated in-situ are usually more or less desaturated. Therefore, they need to be resaturated before testing. The resaturation process must be performed very carefully so that the addition of water to clay minerals will not cause slaking of shale, and no air is trapped in the sample.

7.4. Summary

This section basically outlines the study of shale sampling disturbance following the structure presented in Section 2.4. It has been shown that to understand the mechanism and to identify the important disturbance sources, the behavior of the material being sampled must first be understood. Therefore, this section first presented several important points of shale behavior. Based on this and the information collected for soil and rock sample disturbance, the sampling process in shale is outlined and the mechanisms of some disturbance sources are evaluated for shale.

However, the understanding of disturbance mechanism in shale presented in the section is still very crude. More rigorous investigations are necessary to gain refined understanding, which will be presented in next section.

8. Suggestions and Conclusions

The disturbance mechanisms shown in Section 7.3 are based on the behavior of shale introduced in Section 7.2, the general listing of disturbance sources in Section 2.2, and our knowledge on the disturbance mechanisms of soil and rock sampling. Therefore, the mechanisms presented in Section 7.3 are all qualitative predictions. In order to obtain a deeper understanding of the disturbance mechanisms and effects in shale, rigorous analyses are necessary.

8.1. Improve the Understanding of Disturbance Mechanisms and Effects in Shale

Based on the information collected from soil and rock sample disturbance, better understanding of the disturbance mechanisms and effects can be obtained either by theoretical modeling, physical modeling, or a combination of both. Theoretical modeling includes analytical methods and numerical methods. Typical examples are the Strain Path Method in soil (analytical) and the Finite Element Method (numerical). Physical modeling involves the use of artificial material and the simulation of disturbance. Likewise, the disturbance mechanisms and effects in shale can also be analyzed by these methods.

8.1.1. Theoretical Modeling

Before the theoretical modeling methods can be applied, a behavior model of

shale must first be provided. A good theoretical model for shale should be able to cover the major aspects of its behavior. With the characteristics and behavior of shale described in Section 7.1 and 7.2, the following aspects may need to be taken into consideration:

- Anisotropy: Natural shale has inherent material anisotropy, i.e. the bedded structure. Due to this inherent anisotropy, the mechanical properties of shale are also anisotropic.
- Crack opening and propagation: It has been shown in Section 6.3 that crack opening and propagation is the direct and most important effect of disturbance in rock. Other effects, for example the decrease of P-wave and S-wave velocity, the decrease of stiffness, the increase of permeability etc. can all be explained by increasing microcrack density. Therefore, the theoretical model should be able to characterize the development of microcracks and how the different parameters of the behaviors are affected.
- Physico-chemical Effects: The importance of physico-chemical effects in shale behavior has been described in Section 7.2.3.2. In order to analyze the slaking process and its influence on the mechanical behavior of shale, shale is usually modeled as a semi-permeable membrane which isolates the pore liquid in shale from the external liquid. Osmotic pressures can be generated due to the different ion concentrations on the two sides of this membrane, and water exchange is then driven by this osmotic pressure.

For better handling of the problem, this osmotic pressure is often converted into a hydraulic gradient. On the other hand, this semi-permeable membrane of shale is not perfect, i.e. it also allows ions to cross and ion exchange may occur between shale and the external liquid. However, the mechanisms related to the physico-chemical effects are still controversial.

- Thermal Effects: When the temperature of shale changes, different phases of shale will have different thermal strains. The incompatible thermal strains cause thermal stresses to be generated. For the liquid phases in shale, this thermal stress is essentially the excess pore pressure. When there is a temperature gradient in shale, the excess pore pressure generated will also have a gradient, which again causes water migration. It has been found that since shale has very small permeability, water migration in shale is chiefly driven by chemical gradients and thermal gradients.
- Poromechanics: Shale is a multi-phase system, and a theoretical model should be able to describe the behavior of each phase and their interaction. This requires that poromechanics must be included in the model.
- Dynamic Response: Since shale is subject to dynamic disturbance, e.g. the vibration of the drilling machine and the core drilling bit, the dynamic response of shale should be covered by the model.

However, a theoretical model that incorporates all of these factors will

certainly become very complicated. In addition, the number of material parameters will be extremely large. For example, 31 parameters were used by Chen et al. (2001) to calculate the well bore stability by considering the coupled chemical – thermal – poroelastic effects (not all the parameters are material parameters).

Since our objective is to evaluate the disturbance severity, a simplified behavioral model should be sufficient. Based on the descriptions of shale behavior, a transverse isotropic linear elastic model is probably a good first approximation for the mechanical behavior of shale. On the other hand, numerical methods are usually more versatile than analytical methods in complicated problems. Therefore, we recommend the analysis be performed using numerical methods based on the transverse isotropic linear elastic model. However, generally the direction of the borehole axis is not normal to the bedding planes and the problem is no longer an axi-symmetric problem. Figure 8.1 illustrates this point.

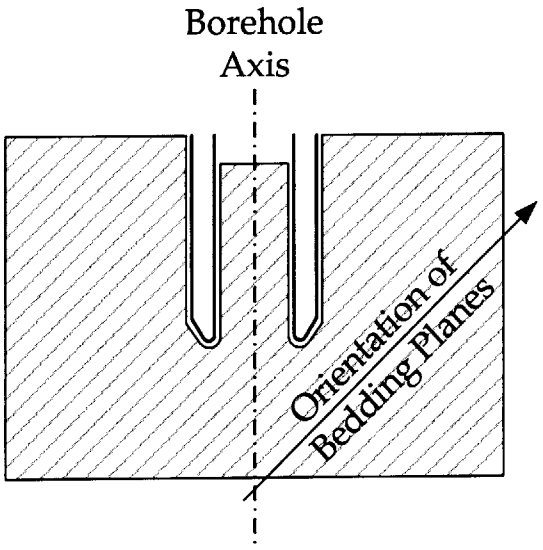

Figure 8.1 Orientation of Bedding Planes and Borehole Axis in Shale Coring

The advantage of the theoretical modeling is that, as long as the behavioral

model is suitable for shale, the stress and strain fields of the whole range considered can be determined, and they can be traced for the entire coring process. However, the accuracy of the stress and strain fields is restricted by the ability of the behavior model. For example, the transverse isotropic linear elastic model can never consider crack opening and the consequent stress redistribution.

8.1.2. Physical Modeling

Another way to gain understanding of the disturbance mechanism in shale is to use an artificial material as a physical model of natural shale, similar to what has been done in soil with Resedimented Boston Blue Clay (see Section 3.3.2.3). As a matter of fact, artificial materials were used in the modeling of rock and shale sample disturbance. For example, Holt et al. (2000) made use of artificial sandstones to study the disturbance effects caused by stress relief. Regarding shale, Nüesch (1991) actually has produced artificial Opalinus Clay Shale and tested it extensively.

If artificial shale is to be used, an important problem is the representativeness of the artificial shale. In general, the representativeness means that the artificial material and the natural material must be similar in the following aspects (Holt et al, 2000):

- The mechanical behavior must be similar.
- The petrophysical properties must be similar (porosity, elastic wave velocities, permeability etc.).
- The visual appearance should be similar.

- The microstructure should be similar.

Once the problem of representativeness is solved, artificial shale can be made at the in-situ stress level at which the real sampling is performed. The "in-situ" state and behavior of the artificial shale can be measured at this stage. Then the coring process can be simulated on the artificial material in the laboratory. The state change of the artificial material can be measured by proper instruments. Comparing the initial state of the artificial shale and the state of the core, the mechanism of disturbance can be obtained. Comparing their behavior with the "in-situ" behavior, the disturbance effects can be obtained.

Clearly, physical modeling can simulate the entire process of shale sampling. The state of the sample can be measured all through the sampling process, and the disturbance effects are also readily obtained. However, all the information obtained is restricted by the measuring capabilities. For example, strain measurements may be only possible on the surface of the artificial material. More importantly, the representativeness of the artificial material determines how well the physical model simulates the real situation. If the artificial material is only similar with the natural material in mechanical properties, then it can definitely not be used to model the coupled chemical – mechanical behavior of the natural material.

8.1.3. Discussion

Through the description of Section 8.1.1 and Section 8.1.2, it can be seen that both modeling methods can be used to gain better understanding of disturbance

mechanisms and effects. Each modeling method has it advantages and disadvantages. In order to make best use of both of them, it is probably wise to combine both of them.

It is worth noting that coupled chemical – thermal – poromechanical problem is not easily solved by either of the modeling methods. For theoretical modeling, coupling leads to an overly complex model and too many material parameters need to be determined. For physical modeling, the simulation of this coupled process requires many similarities between the artificial material and the natural material, including the mechanical properties, chemical properties, thermal properties, petrophysical properties, etc. This is probably too difficult to achieve.

However, once the mechanisms and effects of disturbance in shale can be understood, measures can be developed to minimize the disturbance effects.

8.2. Conclusions

Sample disturbance has long been a research topic for the profession. However, it remains one of the most difficult problems posing major challenges.

Through an extensive literature review, this thesis first examined to what extent the disturbance problem is understood by examining sample disturbance step by step in well researched geomaterials, such as soft soil and rock. Specifically, this review looked at sample disturbance sources starting with borehole drilling, over sample retrieval to preparation for laboratory tests. Although all these sources do have an effect, some are much more important than others and one can, as a first

approximation, concentrate on them. It was found that both theoretical modeling and numerical modeling can be used to understand disturbance mechanisms and effects.

The sample disturbance problem in soil was reviewed first. Through the analysis of disturbance mechanisms, it seems that the most important disturbance source in soil is tube sampling. Stress relief may be another important disturbance source. Both theoretical modeling and physical modeling are applied to understand sample disturbance in soil. For example, in order to understand the mechanism of tube sampling disturbance, the Strain Path Method, a theoretical method, is used to determine the strain field caused by tube penetration. Based on the strain pattern obtained from the Strain Path Method, Resedimented Boston Blue Clay can then be used, for instance, as a physical model of natural soft clay to simulate the disturbance effects.

An alternative way of studying disturbance mechanisms and effects is through a simple theoretical behavioral model which can predict the principles of the disturbance mechanisms and effects. The results are meaningful but limited.

The sample disturbance problem in rock was then reviewed. The most important disturbance source in rock seems to be the stress relief caused by borehole drilling and coring. The literature again shows that the theoretical and physical investigations are used to understand the mechanisms and effects of disturbance. For instance, Finite Element modeling can provide reasonable approximation of the coring process. The physical investigation discussed in this thesis concentrated

mainly on the URL research in which rock cores from different depths showed significantly different sample disturbance effects.

Finally, sample disturbance in shale was investigated mainly by looking at similarities and differences with soil and rock sampling. Due to the limited understanding of shale behavior and sampling disturbance, only qualitative predictions were made on the disturbance mechanisms in shale. Based on the discussion, however, stress relief and various chemical effects are likely to be the most important disturbance sources. According to what has been described on soil and rock sample disturbance, a combination of both theoretical and physical modeling should be applied to analyze the disturbance mechanisms and effects in shale. However, due to the importance of the coupled chemical – thermal – poromechanical effects in shale behavior, there are still fundamental difficulties in the application of these modeling methods. Therefore, understanding this coupled behavior should be the focus of further research.

REFERENCES

1) Aristorenas G.V. (1992). Time-dependent behavior of tunnels excavated in shale. Ph.D. Thesis. Massachusetts Institute of Technology
2) Baldi G., Hueckel T., Pellegrini R. (1988). Thermal volume changes of the mineral – water system in low-porosity clay soils. Can. Geotech. J.. Vol. 25, 807 – 825
3) Baligh M.M. (1985). Strain Path Method. *J. Geotech. Engng. Div., ASCE*, Vol 111, GT 9, 1108-1136
4) Baligh M.M., Azzouz A.S., Chin C.T. (1987). Disturbance Due to "Ideal" Tube Sampling. *Journal of Geotechnical Engineering*. 113(7), 739 – 757
5) Bellwald P. (1990). A contribution to the design of tunnels in argillaceous rock. Ph.D. Thesis. Massachusetts Institute of Technology.
6) Bjerrum L. (1967). Progressive Failure in Slope of Over-consolidated Plastic Clay and Clay Shales. *JSMFD*, ASCE. 93(SM5), 3 – 49
7) Bock H. (2000). TN 2000-28: RA Experiment: Review of Rock Mechanical In-situ and Laboratory Tests.
8) Bock H. (2001). TR 2000-02: RA Experiment Rock Mechanics Analyses and Synthesis: Data Report on Rock Mechanics.
9) Bock H. (2001a). TR 2001-03: RA Experiment Rock Mechanics Analyses and Synthesis: Conceptual Model of the Opalinus Clay.
10) Botts M.E. (1986). The effects of slaking on the engineering behavior of clay shales. Ph.D. Thesis. University of Colorado
11) Botts M.E. (1998). Effects of slaking on the strength of clay shales: A critical state approach. *The Geotechnics of Hard Soils – Soft Rocks*, 447 – 458
12) Brattli B., Broch E. (1995). Statbility problems in water tunnels caused by expandable minerals. Swelling pressure measurements and mineralogical analysis. *Engineering Geology*. Vol. 39, 151 – 169
13) Brookins D.G. (1988). Eh- and pH Diagrams for Geochemistry. Springer, Berlin, 176pp
14) Brouillette R.P., Olson R.E., Lai J.R. (1993). Stress-strain characteristics of Eagle Ford shale. *Geotechnical Engineering of Hard Soils – Soft Rocks*, 397 – 404
15) Bryant L., Mauldon M., Mitchell J.K. (2003). Impact of Pyrite on Properties and Behavior of Soil and Rock. Proc. of Soil and Rock Americal (2003).
16) Burland J.B. (1990). On the compressibility and shear strength of natural clays. *Geotechnique*: 40(3), 329 – 378
17) Burland J.B., rampello S., Georgiannou V.N., Calabresi G. (1996). A laboratory study of the strength of four stiff clays. *Geotechnique*: 46(3), 491 – 514
18) Burland J.B. (2000). Recent studies of the strength of stiff clays. *The Geotechnics of Hard Soils – Soft Rocks*. 1659 – 1663
19) Chandler R.J., Gutierrez C.I. (1986). The filter paper method of suction measurement. *Geotechnique*, 36(2), 265 – 268
20) Chandler R.J., Harwood A.H., Skinner P.J. (1992). Sample disturbance in London clay. *Geotechnique*, 42(4), 577 – 585
21) Chen G., Chenevert M.E., Sharma M.M., Yu M. (2001). Poroelastic chemical and thermal effects on wellbore stability in shales. *Rock Mechanics in the National Interest*, Elsworth, Tinucci&Heasley

(eds). 11 – 18

22) Clayton C.R.I., Hight D. W., Hopper R. J. (1992), Progressive Destructuring of Bothkennar Clay: Implications for Sampling and Reconsolidation Procedures. *Geotechnique*, 42, 2: 219-239

23) Clayton C.R.I., Serratrice J.F. (1997). The mechanical properties and behavior of hard soils and soft rocks. *Geotechnical Engineering of Hard Soils – Soft Rocks*, 1839 – 1877

24) Clayton C.R.I., Siddique A., Hopper R.J. (1998). Effects of sampler design on tube sampling disturbance – numerical and analytical investigations. *Geotechnique*, 48(6), 847 – 867

25) Davison C.C. (1984). Monitoring hydrogeological conditions at the site of Canada's Underground Research Laboratory. *Groundwater Monitoring Review*, 3(4): 95 – 102

26) Eberhardt E., Stead D., Stimpson B. (1999). Effects of Sample Disturbance on the Stress Induced Microfracturing Characteristics of Brittle Rock. *Can. Geotech. J.*, 36: 239 – 250

27) Eigenbrod K.D. (1972). Progressive failure in overconsolidated clays and mudstones. Ph.D. Dissertation. The Univ. of Alberta.

28) Ewy R.T., Daniels E.J., Stankovich R.J. (2001). *Rock Mechanics in the National Interest*, Elsworth, Tinucci&Heasley (eds), 77 – 84

29) Ghassemi A., Diek A. (2001). Effects of ion transfer on stress and pore pressure distributions around a borehole in shale. *Rock Mechanics in the National Interest*, Elsworth, Tinucci&Heasley (eds). 85 – 91

30) Gens A. (1982). Stress-Strain and Strength Characteristics of a Low Plasticity Clay. PhD thesis. University of London.

31) Gens A., Hight D.W. (1979). The laboratory measurement of design parameters for a glacial till. *Proc 7th European Conf. S.M.&F.E.*, Brighton, Vol. 2, 57 – 66

32) Ghafoori M., Carter J.P., Airey D.W. (1993). Anisotropic behavior of Ashfield shale in the direct shear test. *Geotechnical Engineering of Hard Soils – Soft Rocks*, 509 – 515

33) Guerriero G., Urciuoli G. (1997). Some considerations on the ultimate conditions of hard clays in triaxial tests. *Geotechnical Engineering of Hard Soils – Soft Rocks*, 1909 – 1911

34) Hight D.W., Jardine R.J. (1993). Small-strain stiffness and strength characteristics of hard London tertiary clays. *Proceedings of Geotechnical Engineering of Hard Soils – Soft Rocks*, 1993. 533 - 552

35) Hight D.W. (1993a). A review of sampling effects in clays and sands. *Offshore Site Investigation and Foundation Behavior*. Vol. 28, 115 – 146

36) Hight D. W. (1998), Soil Characterization: the Importance of Structure and Anisotropy. 38th Rankine Lecture.

37) Hight D. W. (2001), Sampling Effects in Soft Clay: An Update on Ladd and Lambe (1963). Soil behavior and soft ground construction: Proceeding of the symposium October 5-6, 2001, Cambridge, MA.

38) Hoek E. (1983). Strength of jointed rock masses. *Geotechnique*, 33: 187 – 223

39) Holcomb D. J. (1993). General Theory of the Kaiser Effect. *Int. J. Rock Mech. Min. Sci. & Geomech. Abstr.*, 30: 929 – 935

40) Holt R.M., Brignoli M., Kenter C.J. (2000). Core quality: quantification of coring-induced rock alteration. *International Journal of Rock Mechanics and Mining Sciences*. Vol. 37, 889 – 907

41) Horsrud P., Sonstebo E.F., Boe R. (1998). Mechanical and petrophysical properties of North Sea shales. *Int. J. Rock. Min. Sci.* 35(8), 1009 - 1020

42) Hsu S.C., Nelson P.P. (1993). Characterization of cretaceous clay shales in North America. *Geotechnical Engineering of Hard Soils – Soft Rocks*, 139 – 146

43) Huang S.L., Speck R.C., Wang Z. (1995). The temperature effect on swelling of shales under cyclic wetting and drying. *Int. J. Rock Mech. Min. Sci. & Geomech. Abstr.*, Vol. 32(3), 227 – 236

44) Hvorslev M. J. (1949). Subsurface Exploration and Sampling of Soils for Civil Engineering Purposes. Waterways Experiment Station. Vicksburg, Mississippi.

45) Indraratna, B. (1993). Engineering properties of a clay shale with particular reference to construction problems. *Geotechnical Engineering of Hard Soils – Soft Rocks*, 561 – 568

46) Johnston D.H. (1987). Physical properties of shale at temperature and pressure. Geophysics. Vol. 52(10), 1391 – 1401

47) Katsube T.J. (1981). Pore structure and pore parameters that control the radionuclide transport in crystalline rocks. *Proceedings of the International Symposium on Powder and Bulk Solids Handling and Processing*. Rosemont, III. 394 – 409

48) Katsube T.J., Mudford B.S., Best M.E. (1991). Petrophysical characteristics of shales from the Scotian shelf. Geophysics. Vol 56(10). 1681 – 1689

49) Kavvadas M.J. (2000). Modelling the soil behaviour – Selection of soil parameters. *The Geotechnics of Hard Soils – Soft Rocks*, 1441 – 1481

50) Kawasaki S., Nishi K., Fujiwara Y. (1993). Mechanical properties of deep soft rock ground in the suburbs of Tokyo. *Geotechnical Engineering of Hard Soils – Soft Rocks*, 593 – 600

51) Ladd C.C., Lambe T.W. (1963). The Strength of Undisturbed Clay Determined from Undrained Tests. *Symp. On Laboratory Shear Testing of Soils*, ASTM, STP361, 342-371

52) Ladd C.C. et al. (1977). Stress Deformation and Strength Characteristics. SOA Report. Proc. of 9th ICSMFE, Tokyo

53) Ladd C.C., Degroot D.J. (2003). Recommended Practice for Soft Ground Site Characterization: Arthur Casagrande Lecture. *Proc. of the 12th Panamerica Conference on Soil Mechanics and Geotechnical Engineering*. Cambridge, USA, 2003

54) Lambe T.W., Whitman R.V. (1969). Soil Mechanics. John Willey & Sons.

55) Leroueil S. (2000). Contribution to the round table: peculiar aspects of structured soils. *The Geotechnics of Hard Soils – Soft Rocks*, Evngelista & Picarelli (eds), 2000 Balkema, Rotterdam. 1669 - 1678

56) Leroueil S. (2000). Peculiar aspects of structured soils. *The Geotechnics of Hard Soils – Soft Rocks*, 1669 – 1678

57) Lunne, T., Strandvik, S. (1997). Sample Disturbance Effects in Soft Low Plastic Norwegian Clay. *Recent Development in Soil and Pavement Mechanics*. 1997 Balkema, Rotterdam. 81 – 102

58) Lunne T., Berre T., Strandvi S., Andersen K. H., Tjelta T. I. (2001). Deep Water Sample disturbance Due to Stress Relief. *Proc. Of OTRC 2001 International Conf. on Geotechnical and Geophysical Properties of Deep Water Sediments*, 64-102

59) Maio C.D. (1996). The influence of pore fluid composition on the residual shear strength of some natural clayey soils. *Proc. 7th Int. Sym. Landslides*. Trondheim. 1189 – 1194

60) Martin C. D., Stimpson B. (1994). The Effect of Sample Disturbance on Laboratory Properties of Lac Du Bonnet Granite. *Can. Geotech. J.*, 31, 692 – 702

61) McManis K., Arman A. (1986). Sampling and testing in stiff crustal clay. *Geotechnical Aspects of Stiff and Hard Clays*, Geotechnical Special Publication No. 2, ASCE

62) Nawrocki P.A., Dusseault M.B. (1998). Extracting constitutive behavior laws from triaxial test programs in shale. *The Geotechnics of Hard Soils – Soft Rocks*. 725 – 736

63) Nüesch R. (1991). Das Mechanische Verhalten von Opalinuston. Diss. ETH Zürich Nr. 9349

64) Obert L., Duvall W.I. (1967). Rock Mechanics and the Design of Structures in Rock, John Wiley & Sons, 650 pages
65) Olalla C., Martin M.E., Saez J. (1999). TN 98-57: ED-B Experiment: Geotechnical Laboratory Tests on Opalinus clay Rock Samples
66) Olivares L., Urciuoli G., Picarelli L. (1997). Mechanisms of rupture of reconstituted and natural fissured clay shales in undrained triaxial tests. *Proc. Int. Symp. on Deformation and Progressive Failure in Geomechanics*, Nagoya. 229 – 234
67) Picarelli L. (1993). Structure and properties of clay shales involved in earthflows. Proc. 2nd Int. Symp. *The Geotechnics of Hard soils – Soft Rocks*. 2009 – 2019
68) Picarelli L., Olivares L. (1998). Ingredients for modeling the mechanical behavior of intensely fissured clay shales. *The Geotechnics of Hard Soils – Soft Rocks*. 771 – 780
69) Picarelli L., Olivares L., Maio C.D., Urciuoli G. (2000). Properties and behavior of tectonized clay shales in Italy. *The Geotechnics of Hard Soils – Soft Rocks*. 1211 – 1241
70) Remvik F., Skalle P. (1993). Shale-fluid interaction under simulated downhole conditions, and its effect on borehole stability. *Int. J. Rock. Mech. Min. Sci. & Geomech. Abstr.*. Vol. 30(7). 1115 – 1118
71) Ringheim A.S. (1964). Experiences with the Bearpaw Shale at the South Saskatchewan River Dam. 8th Intern. Congress on Large Dams, Edinburgh, Great Britain, 4 – 8 May 1: 529 – 549
72) Santagata, M.C. (1990). Simulation of Sampling Disturbance in Soft Clays Using Triaxial Element Tests. M.S. Thesis. Massachusetts Institute of Technology.
73) Santarelli F.J., Dusseault M.B. (1991). Core quality control in petroleum engineering. *Rock Mechanics as a Multidisciplinary Science*. Roegiers (ed.), 111 – 120
74) Schmitt L., Forsans T., Santarelli F.J. (1994). Shale Testing and Capillary Phenomena. *Int. J. Rock. Mech. Min. Sci. & Geomech. Abstr.*. Vol. 31(5). 411 – 427
75) Scully J. (1973). Landslides in the Pierre Shale in central South Dakota. Final Report to U.S. Federal Highway Admin. State study No. 635(67).
76) Sinclair S.R, Brooker E.W. (1967). The Shear Strength of Edmonton Shale. Poc. Of Geotechnical Conf., Oslo 1: 295 – 299
77) Skopec R.A. (1991). Revised core handling recommendations. API RP27/40. API Working Group draft report. 45 pages.
78) Steiger R.P. (1993). Advanced Triaxial Swelling Tests on Preserved Shale Cores. *Int. J. Rock. Mech. Min. Sci. & Geomech. Abstr.*. Vol. 30(7). 681 – 685
79) Stroman W.R., Feese A.H. (1984). Engineering properties of clay shales: Report 5: strength and deformation properties of Pepper and Del Rio clay shales from Waco Dam. US Army Engineer Waterways Exper. Station, Vicksburg, Miss
80) Tan, T.S., Lee, F.H., Chong, P.T., Tanaka, H. (2002). Effect of Sampling Disturbance on Properties of Singapore clay. *Journal of Geotechnical and Geoenvironmental Engineering*, Vol. 128(11): 898 – 906
81) Tanaka, H., Sharma, P., Tsuchida, T., Tanaka, M. (1996). Comparative Study on Sample Quality Using Several Types of Samplers. *Soils and Foundations*, Vol. 36(2): 57 – 68
82) Tare U.A., Mese A.I., Mody F.K. (2001). Time dependent impact of water-based drilling fluids on shale properties. *Rock Mechanics in the National Interest*, Elsworth, Tinucci & Heasley (eds.), 107 – 112
83) The Earth Technology Corporation (TETC). (1990). Geomechanical characterization of the Eagle Ford Shale at the Superconducting Super Collider Site. SSC Geotechnical Report GR-66 and GR-68, prepared for RTK Joint Venture.

84) Thomson S. (1970). Riverbank Stability at the University of Alberta, Edmonton. Can. Geot. J. 7: 157 – 168

85) Townsend F.C., Gilbert P.A. (1974). Engineering properties of clay shales; report 2: residual shear strength and classification indexes of clay shales. U.S. army Engineer Waterways Experiment Station, Vicksburg, Miss.

86) Vallejo L.E., Murphy A.S. (2001). Influence of pore wall roughness on the slaking of shales. *Rock Mechanics in the National Interest,* Elsworth, Tinucci & Heasley (eds), 93 – 98

87) Vaughan P. R., Chandler R. J., Apted J. P., Maguire W. M., Sandroni S. S. (1993). Sampling Disturbance with Particular Reference to Its Effect on Stiff Clays. *Proc. Wroth Memorial Symp.,* Oxford, 685-708

88) Vaughan P.R. (1997). Engineering behavior of weak rocks: Some answers and some questions. *Geotechnical Engineering of Hard Soils – Soft Rocks,* 1741 – 1765

89) Wolter K.E. (2003). TN 2003-46. Petrophysical Analysis of Drill Cores from the Opalinus Clay Formation of the Mont Terri Rock Laboratory.

90) Yamaguchi H., Miura Y., Kuroshima I., Fukuda M. (1993). Triaxial shear behavior of tertiary mudstone crushed by slaking. *Geotechnical Engineering of Hard Soils – Soft Rocks,* 871 – 881